

DENISE SILVA DE MOURA

**Gravimetric and magnetic modelling of the Ceará Plateau, Brazilian  
Equatorial Margin**

**Corrected Version**

Thesis submitted to *Instituto Oceanográfico, Universidade de São Paulo*, in partial fulfilment of the requirements for the degree of Master of Sciences in Oceanography, with emphasis in Geological Oceanography.

Advisor: Prof. Dr. Luigi Jovane

Co-advisor: Prof. Dr. Eder Cassola  
Molina

São Paulo

2018

Moura, Denise Silva de

M929g Gravimetric and magnetic modelling of the Ceará Plateau, Brazilian Equatorial Margin / Denise Silva de Moura. 2018

112 f. ; 30 cm

Thesis (Master) – Instituto Oceanográfico at Universidade de São Paulo.

Advisor: Prof. Dr. Luigi Jovane

Co-advisor: Prof. Dr. Eder Cassola Molina

1. Ceara Plateau 2. Gravimetric modelling 3. Magnetic modelling 4. Marine geophysics 5. Brazilian Equatorial Margin I. Jovane, Luigi (advisor) II. Molina, Eder Cassola III. Title.

UNIVERSIDADE DE SÃO PAULO  
INSTITUTO OCEANOGRÁFICO

Gravimetric and magnetic modelling of the Ceará Plateau, Brazilian  
Equatorial Margin

by

Denise Silva de Moura

Thesis submitted to *Instituto Oceanográfico, Universidade de São Paulo*,  
in partial fulfilment of the requirements for the degree of Master of Sciences in  
Oceanography, with emphasis in Geological Oceanography.

Evaluated in \_\_\_/\_\_\_/\_\_\_\_\_

---

Prof. Dr.

---

\_Grade

---

Prof. Dr.

---

\_Grade

---

Prof. Dr.

---

\_Grade

*“Ave, do mar Estrela,  
De Deus mãe bela,  
Sempre virgem, da morada  
Celeste, Feliz entrada.”*  
(Ave Maris Stella)

## CONTENTS

FIGURES .....	v
TABLES .....	xi
LIST OF ABBREVIATIONS AND ACRONYMS .....	xii
PREFACE .....	xiii
ACKNOWLEDGEMENTS.....	xiv
ABSTRACT.....	xvi
RESUMO.....	xvii
1. INTRODUCTION .....	1
2. OBJECTIVES.....	5
3. STUDY AREA .....	6
3.1 The Equatorial Margin.....	6
3.1.1 Tectonic synthesis .....	6
3.1.2 The BEM geomorphology .....	9
3.1.3 The Fracture Zones .....	9
3.1.4 The hotspot theory and the Fernando de Noronha hotspot.....	10
3.1.5 The Edge-Driven Convection .....	10
3.1.6 The African Equatorial Margin .....	13
3.2 The Potiguar Basin .....	16
3.2.1 The rift formation .....	16
3.2.2 The oceanic basin sediments .....	17
3.3 The Ceará Plateau .....	22
3.3.1 Ceará Plateau nomenclature .....	22
3.3.2 Geomorphology synthesis of the Ceará Plateau .....	22
4. MATERIALS AND METHODS .....	25
4.1 Available data .....	25
4.1.1 Equant Project.....	26
4.1.2 Bathymetry data .....	27

4.1.3 Gravity data .....	28
4.1.4 Magnetic data.....	29
4.1.5 Seismic data .....	30
4.1.6 The gravimetric and geomagnetic global models .....	31
4.2 Gravimetric data processing .....	33
4.2.1 The gravimetric anomalies .....	33
4.2.2 The regional-residual separation .....	36
4.2.3 The Bouguer anomaly .....	37
4.2.4 The isostatic compensation .....	40
4.2.5 The 2D gravity modelling .....	43
4.2.6 Parameters of the gravity 2D modelling .....	43
4.3 Geomagnetic data processing .....	45
4.3.1 The geomagnetic field sources .....	45
4.3.2 The geomagnetic anomalies .....	48
4.3.3 The Pole and the Equator reductions.....	49
4.3.4 Magnetic anomalies analyses .....	51
4.3.5 The magnetized layer modelling .....	56
5. RESULTS .....	59
5.1 Analyses of the gravimetric data .....	59
5.1.1 The gravimetric modelling .....	59
5.1.2 The basement and the Mohorovičić surfaces according to the gravity modelling .....	63
5.2 Analysis of the magnetic data.....	66
5.2.1 The magnetic model .....	66
6. DISCUSSION.....	68
6.1 Comparison between the gravimetric and magnetic anomalies .....	68
6.1.1 The gravity and magnetic anomalies source.....	68
6.1.2 The Bouguer anomaly and the TDR of the RTP .....	69
6.2 The gravity models .....	70
6.2.1 The crustal model .....	70

6.2.2 The gravity modelling for continental crust instead of oceanic crust .....	70
6.3 The COB and the transitional crust .....	72
6.3.1 The Equant profiles compared to the predicted edge anomalies .....	72
6.3.2 The estimated position of the COB .....	74
6.4 The magnetic models .....	75
6.4.1 The magnetic modelling from the basement .....	75
6.5 Considerations about the Ceará Plateau formation.....	76
6.4 The Iracema Guyot .....	77
7. CONCLUSIONS .....	78
REFERENCES .....	79

## FIGURES

Figure 1: Brazilian Equatorial Margin topobathymetric map. Red rectangle indicates the study area. Bathymetric contour each 1000 m.

Figure 2: Perspective view of the study area. Bathymetry 3D with 10x vertical exaggeration of the SRTM15PLUS data (modified from <<http://portal.gplates.org/cesium/?view=topo15>>).

Figure 3: Reconstruction of the Equatorial Atlantic Ocean rupture with the principal continental lineaments, the cratons and the continental basins (CASTRO et al., 2012). The black rectangle delimits the figure 11.

Figure 4: Simplified seismo-tectonic map of the Borborema Province (Modified from OLIVEIRA et al., 2015).

Figure 5: Regional heat flow map of the Equatorial Atlantic Ocean, derived from the spherical harmonic expansion to degree 36 (HAMZA et al., 2008).

Figure 6: Geoid height in the Borborema region (SANDWELL and SMITH, 1997 apud OLIVEIRA, 2008).

Figure 7: Correlation between surface wave tomography and geoid height residual (figure 4 minus 3 km upward continuation). Tomography data from global model CU\_SRT1.0 developed with the method created by Barmin et al. (2001) and applied by the authors of: <http://ciei.colorado.edu/~nshapiro/MODEL/> (OLIVEIRA, 2008).

Figure 8: A simplified model for the evolution of transform margins based on the example of Ivory Coast and Ghana margins (MASCLE et al., 1996). (A) an intra-continental active transform fault, creating a thinned crust and sedimentary cover, (B) a continent-ocean active transform fault contrast and (C) and inactive continent-ocean transform fault. (1) divergence; (2) transform motion between continental and (3) oceanic crust; (4) continental crust; (5) thinned continental crust; (6) oceanic crust; (7) ridge axis; (8) marginal ridge.

Figure 9: Schematic illustration of the evolution of the transform margin between the African and South American continents from Late Cretaceous through early Eocene times. A) Syntransform, intracontinental basin stage. Sedimentation during the late Albian was dominated by continental and lacustrine environments in pull apart basins developed by transcurrent shear between the South American



and African continental blocks. B) Marginal ridge emergence and initiation of subsidence in the Deep Ivorian Basin (late Albian to Coniacian). C) Submergence of the marginal ridge and formation of the Deep Ivorian Basin (late Coniacian to early Eocene) followed by passage of the oceanic spreading ridge (MASCLE et al., 1998).

Figure 10: A 2-D gravity model for Liberia sector of the West African Transform Margin. The densities are in  $\text{g/cm}^3$  (JILINSKI et al., 2013). The 70 km dashed line is the COB position determined by the ODP crew (MASCLE et al., 1998).

Figure 11: Geologic regional map of the onshore Potiguar Rift Basin (CASTRO et al., 2012). The area of the map is delimited in figure 3.

Figure 12: Faciology of the continental platform in the Northeast Brazilian Region, evidencing the presence of biological sedimentation and calcareous algae. These sediments were remobilized from the intern platform during a regressive event and formed aeolian carbonate-rich deposits. Red rectangle indicates the study area. Modified from Meireles et al. (2005).

Figure 13: Potiguar Basin stratigraphic chart (PESSOA NETO et al., 2007).

Figure 14: SW-NE profile of the Potiguar oceanic basin. It is located near to the Ceará Plateau and the scale indicates the COB 30 km far from the Continental Shelf (BERTANI et al., 1990).

Figure 15: Geomorphologic map of the Ceará Plateau created from the SRTM15PLUS bathymetric data.

Figure 16: Slope map of the Ceará Plateau created with the SRTM15PLUS bathymetric data. The declivity is in degrees. Grid interval of 15 seconds (approximately 450 m). Bathymetric contour each 500 m.

Figure 17: Distribution of the Equant data, the seismic profiles and the hole position into the region. The red, yellow and blue lines are the seismic profiles from Leplac Project, ANP and WesternGeco, respectively. The pink cross indicates the position of the ANP hole. Bathymetric contour each 500 m.

Figure 18: Bathymetric map and the localization of the data in the study area. Grid interval of 15 seconds (approximately 450 m). The red, yellow and blue lines are the seismic profiles from Leplac Project, ANP and WesternGeco, respectively. Bathymetric contour each 500 m.

Figure 19: Gravity anomaly map and the localization of the data in the study area. Grid interval of 30 seconds (approximately 900 m). The red, yellow and blue lines are the seismic profiles from Leplac Project, ANP and WesternGeco, respectively. Bathymetric contour each 500 m.

Figure 20: Magnetic anomaly map and the localization of the data in the study area. Grid interval of 30 seconds (approximately 900 m). The red, yellow and blue lines are the seismic profiles from Leplac Project, ANP and WesternGeco, respectively. Bathymetric contour each 500 m.

Figure 21: Interpreted seismic profile from Leplac Project, line 501 (JOVANE et al., 2016). Depth in seconds, TWT (Two-Way travel Time).

Figure 21: Interpreted seismic profile from ANP survey, line POT44 (JOVANE et al., 2016). Depth in seconds, TWT (Two-Way travel Time).

Figure 23: Interpreted seismic profile from WesternGeco, line 17. ANP round 11. Depth in meters.

Figure 24: Gravimetric Anomaly of the Brazilian Equatorial Margin and the main features of the BEM. Red rectangle indicates the study area. Topobathymetric isolines each 500 m.

Figure 25: Magnetic Anomaly of the Brazilian Equatorial Margin, 2 arcmin grid data from EMAG2 v2. Red rectangle indicates the study area. Topobathymetric isolines each 500 m and the main features of the BEM.

Figure 26: Bouguer anomaly map of the Ceará Plateau. Grid interval of 30 seconds (approximately 900 m). Bathymetric contour each 500 m.

Figure 27: Bouguer anomaly regional map (10 km upward continuation) of the Ceará Plateau. Grid interval of 30 seconds (approximately 900 m). Bathymetric contour each 500 m.

Figure 28: Bouguer anomaly residual map of the Ceará Plateau. Grid interval of 30 seconds (approximately 900 m). Bathymetric contour each 500 m.

Figure 29: Schematic free-air and Bouguer anomaly of a load (USSAMI et al., 2012).

Figure 30: Pratt and Airy models for isostatic compensation of topographic loads (EVANS and CROMPTON, 1946).

Figure 31: Scheme for the application of the Airy hypothesis at the Cear Plateau.  $w$  is the seawater;  $c$  is the oceanic crust;  $m$  is the mantle;  $d$  is the seawater column;  $h$  is the oceanic crust normal thickness;  $r$  is the Cear Plateau root.

Figure 32: Regional map of the study area with the calculated Magnetic Equator in 1987 (yellow line) and in 2017 (green line). Data provided by Sony Su Chen (INPE – personal communication).

Figure 33: Magnetic core field calculation for 1987 with the IGRF model (Data available in: <https://www.ngdc.noaa.gov/geomag-web/#igrfgrid>). Regional removed from the observed data on Equant I Project. Grid interval of 30 seconds (approximately 900 m). Bathymetric contour each 500 m.

Figure 34: 3-D perspective cartoon of oceanic crust (JOHNSON et al., 1997 apud GEE and KENT, 2007) showing spreading centers separated by a transform fault and the theoretical profile recorded by a marine magnetometer. The three main layers of the oceanic crust are illustrated, also the Curie limit as the red area.

Figure 35: Magnetic anomaly created by a dipole in different magnetic latitudes at the Magnetic South hemisphere. The  $l=0$  indicates the anomaly over the Magnetic Equator and the  $l=90^\circ$  over the Magnetic Pole. (Modified from USSAMI, 2008).

Figure 36: Magnetic anomalies. a) Total magnetic field. b) Magnetic anomaly. c) Magnetic anomaly reduced to the Equator. d) Magnetic anomaly reduced to the Pole. Grid interval of 20 seconds (approximately 620 m). Bathymetric contour each 500 m.

Figure 37: Magnetic anomalies filters. a) Magnetic anomaly RTP. b) First derivate in  $y$  of the magnetic anomaly. c) 1VD of the magnetic anomaly. d) Signum transform of the magnetic anomaly. Grid interval of 20 seconds (approximately 620 m). Bathymetric contour each 500 m.

Figure 38: ASA of the magnetic anomaly of the Cear Plateau. Grid interval of 20 seconds (approximately 620 m). Bathymetric contour each 500 m.

Figure 39: Other techniques to enhance the magnetic anomalies. a) Magnetic tilt derivative or tilt angle (TDR). b) Tilt angle of the horizontal derivative (TAGH). Grid interval of 20 seconds (approximately 620 m). Bathymetric contour each 500m.

Figure 40: Age grid for the oceanic crust at the Equatorial Margin. Bathymetric contour each 1000 m. Grid interval of 30 seconds (approximately 900 m).

Figure 41: Magnetic polarity map for the oceanic crust at the Equatorial Margin. Bathymetric contour each 1000 m. Grid interval of 30 seconds (approximately 900 m).

Figure 42: Modelled magnetic anomalies for the oceanic crust around the Ceará Plateau. Magnetized constant layer thickness of 1 km and magnetization of 5 A/m. Grid interval of 30 seconds (approximately 900 m). Same colour palette used in the magnetic anomaly map (figure 16 and 31b).

Figure 43: Gravimetric model of the profile 2 (S-N) with 2.5x vertical exaggeration. Densities in  $\text{g/cm}^3$ . The density is  $3.2 \text{ g/cm}^3$  below 26 km depth.

Figure 44: Gravimetric model of the profile 4 (S-N) with 2.5x vertical exaggeration. Densities in  $\text{g/cm}^3$ . The density is  $3.2 \text{ g/cm}^3$  below 26 km depth.

Figure 45: Gravimetric model of the profile 5 (S-N) with 2.8x vertical exaggeration. Densities in  $\text{g/cm}^3$ . The density is  $3.2 \text{ g/cm}^3$  below 26 km depth.

Figure 46: Gravimetric model of the profile 6 (S-N) with 2.6x vertical exaggeration. Densities in  $\text{g/cm}^3$ . The density is  $3.2 \text{ g/cm}^3$  below 26 km depth.

Figure 47: Gravimetric model of the profile 7 (S-N) with 2.8x vertical exaggeration. Densities in  $\text{g/cm}^3$ . The density is  $3.2 \text{ g/cm}^3$  below 26 km depth.

Figure 48: Gravimetric model of the profile 8 (S-N) with 2.5x vertical exaggeration. Densities in  $\text{g/cm}^3$ . The density is  $3.2 \text{ g/cm}^3$  below 26 km depth.

Figure 49: Gravimetric model of the profile 9 (S-N) with 1.9x vertical exaggeration. Densities in  $\text{g/cm}^3$ . The density is  $3.2 \text{ g/cm}^3$  below 26 km depth.

Figure 50: Basement of the Ceará Plateau area from the gravity 2D model. The red and the yellow lines are the COB and the limit between the thinned continental crust and the transitional crust, respectively. Grid interval of 15 seconds (approximately 450 m). Bathymetric contour each 500 m.

Figure 51: Sediment thickness of the Ceará Plateau area from the gravity 2D model. The red and the yellow lines are the COB and the limit between the thinned continental crust and the transitional crust, respectively. Grid interval of 15 seconds (approximately 450 m). Bathymetric contour each 500 m.

Figure 52: Mohorovičić discontinuity of the Ceará Plateau area from the gravity 2D model. The red and the yellow lines are the COB and the limit between the thinned continental crust and the transitional crust, respectively. Grid interval of 15 seconds (approximately 450 m). Bathymetric contour each 500 m.

Figure 53: Crust thickness of the Ceará Plateau area from the gravity 2D model. The red and the yellow lines are the COB and the limit between the thinned continental crust and the transitional crust, respectively. Grid interval of 15 seconds (approximately 450 m). Bathymetric contour each 500 m.

Figure 54: Residual anomaly map: the magnetic anomaly (figure 20) minus the theoretical magnetic anomaly (figure 42). Grid interval of 30 seconds (approximately 900 m). Bathymetric contour each 500 m.

Figure 55: Modelled magnetic anomaly calculated with 2 km layer above the basement surface. Grid interval of 30 seconds (approximately 900 m). Bathymetric contour each 500 m.

Figure 56: Residual anomaly map: the magnetic anomaly (figure 16) minus the modelled magnetic anomaly (figure 38). Grid interval of 30 seconds (approximately 900 m). Bathymetric contour each 500 m.

Figure 57: Comparison map: magnetic anomalies grid reduced to the Equator (figure 36c) and Bouguer residual anomalies (figure 28) contour in white lines. Grid interval of 20 seconds (approximately 620 m). Bathymetric contour each 1000 m.

Figure 58: Bouguer residual anomaly map grid (figure 28) with the TDR of the RTP contour (figure 39). The TDR lines are disposed mostly around the high Bouguer residual anomalies, mainly the tilt angle zero (black lines), which indicates the sources boundary. The red line indicates the position of the COB. Grid interval of 30 seconds (approximately 900 m). Bathymetric contour each 500.

Figure 59: Gravimetric model of the profile 2 for only continental crust (S-N), with 2x vertical exaggeration. Densities in  $\text{g/cm}^3$ . The density is  $3.2 \text{ g/cm}^3$  below 26 km depth. Transitional crust with 11 km thickness at the thinner region.

Figure 60: Gravimetric model of the profile 7 for only continental crust (S-N), with 2x vertical exaggeration. Densities in  $\text{g/cm}^3$ . The density is  $3.2 \text{ g/cm}^3$  below 26 km depth. Transitional crust with 11 km thickness at the thinner region, Ceará Plateau root with 20 km.

Figure 61: Profiles from Equant II with the COB position. Bathymetric (blue), free-air anomaly (yellow), Bouguer residual anomaly (purple), RTP (red) lines profiles (2-9). The blue rectangles are the COB estimative.

Figure 62: Magnetic anomalies comparison. a) Magnetic anomaly from Equant I data. b) Magnetic anomaly modelled with the basement.

## TABLES

Table 1: Geomorphologic parameters for the Cear Plateau.

Table 2: Variables in the gravity equations.

Table 3: Density values used in gravity models.

**LIST OF ABBREVIATIONS AND ACRONYMS**

ANP	Agência Nacional do Petróleo / Oil National Agency - Brazil
ASA	Analytic Signal Amplitude
BEM	Brazilian Equatorial Margin
COB	Continent-Ocean Boundary
EDC	Edge-Driven Convection
FZ	Fracture Zone
IGRF	International Geomagnetic Reference Field
NGDC	National Geophysical Data Center
ODP	Oceanic Drilling Program
RTE	Reduction to the Equator
RTP	Reduction to the Pole
TAGH	Tilt Angle of the Total Horizontal Derivative
TDR	Magnetic Tilt Derivative or Tilt Angle

## **PREFACE**

This Master Thesis was developed at the Department of Physical, Chemical and Geological Oceanography, Oceanographic Institute of the University of São Paulo (Brazil), as part of the requirements for the Master's degree, under supervision of Prof. Dr. Luigi Jovane (IO-USP) and co-supervision of Prof. Dr. Eder Cassola Molina (IAG-USP). The study is about the Ceará Plateau, a seamount located in the oceanic area of the Ceará State, Brazil. It presents the results derived from an integrated analysis of gravimetric and magnetic data, seismic profiles, geological data and preliminary works.

The author was funded by CNPq, process 130194/2016-6, CAPES/DS and by FAPESP, process 2016/15854-3. This study is part of the “Paleoceanografia da Margem Equatorial Brasileira” Project, supported by CAPES since 2014.



## ACKNOWLEDGEMENTS

Agradeço primeiramente à Deus, que muito além deste trabalho, me dá a vida, espero que por meio dela eu possa sempre Te honrar. À minha mãe Maria, a quem confiei tudo, e continua sendo a medianeira de tantas alegrias.

Gostaria muito de agradecer aos meus orientadores, que me receberam tão bem e me indicaram o caminho quando precisava mais. Dr. Luigi Jovane, obrigada pela confiança e pelo seu entusiasmo em tudo o que faz, me ajudou a gostar ainda mais do meu trabalho; obrigada também pelo ambiente que me proporcionou no CORE (Centro Oceanográfico de Registros Estratigráficos), o convívio nesse laboratório me ajudou muito, me fez compreender melhor como a ciência é produzida e como eu poderia me encaixar nesse processo. Obrigada Dr. Eder Cassola Molina, suas indicações fizeram esse projeto possível, não tenho dúvidas disso; também sua atenção me deu ânimo e vontade de continuar, mesmo quando os resultados não andavam bem ou quando minha saúde não colaborava.

Durante esses dois anos presenciei uma bela parceria entre os institutos da USP: IO, IAG e IGc. Esse contato me ajudou muito durante o projeto e minha formação como um todo, gostaria de agradecer àqueles que estavam diretamente e indiretamente envolvidos. Obrigada ao IO por me acolher tão prontamente, incluo aqui não só os pesquisadores e alunos, mas também os funcionários, que facilitam muito nosso trabalho. Ao IAG sempre serei grata, foi minha primeira casa nessa universidade e continua me auxiliando muito; em especial, gostaria de agradecer ao geofísico Roberto Zanon, sua ajuda não só tornou essas parcerias possíveis, mas colaborou no desenvolvimento do meu mestrado. Obrigada também ao IGc pela disposição durante os projetos entre os institutos, que foram de um ganho enorme.

Obrigada aos professores da pós-graduação que me ensinaram uma nova área na geofísica, o conhecimento de vocês me fez gostar ainda mais da geofísica marinha e tectônica global. Meus especiais agradecimentos aos professores Dr. Benjamim Bley, Dra. Isabel Montoya e ao Dr. Michel Mahiques, vocês foram os primeiros revisores desse trabalho. Também gostaria de agradecer à Dr. Leila

Marques, obrigada pela atenção e ajuda, não apenas durante o estágio PAE, mas em todo o mestrado.

Este trabalho contou fundamentalmente com a ajuda de muitos amigos, tantos que felizmente é difícil agradecer a todos em particular. Em especial gostaria de agradecer às revisões e atenção da Dr. Yára Regina Marangoni, fico feliz por essa parceria não ter se acabado na graduação e espero futuras colaborações. Agradeço também às sugestões do Dr. André Negrão, elas tiveram muita relevância nos resultados finais, assim como as conversas com o Dr. Marcelo Sperle, muito obrigada pela atenção e incentivo de vocês. Agradeço imensamente aos meus revisores de inglês favoritos, Caio e Ana, obrigada pela presença, amizade e também pela grande ajuda durante esse trabalho.

Obrigada à minha família, minha fortaleza, o incentivo de cada um me possibilita ter terminado esse trabalho, inclusive sem vocês não o haveria ao menos começado. Também agradeço à amizade e paciência dos meus amigos do SAAD, obrigada pela presença e pela clareza ao mostrarem que tudo o que fazemos precisa de um objetivo maior.

Por fim, agradeço àqueles que tornaram esse projeto possível financeiramente. Ao CNPq, processo 130194/2016-6, pelo financiamento da primeira etapa da pesquisa. À CAPES/DS por um mês de financiamento, necessário durante o andamento do processo. À FAPESP, processo 2016/15854-3, pelo financiamento da segunda etapa da pesquisa. E ao IO e à USP por todo o suporte durante esses dois anos.

## ABSTRACT

MOURA, Denise Silva de. **Gravimetric and magnetic modelling of the Ceará Plateau, Brazilian Equatorial Margin.** 2018. 112 p. Thesis (Master) – Oceanographic Institute, University of Sao Paulo, Sao Paulo.

The Brazilian Equatorial Margin is a transform passive margin with long fracture zones and several seamounts, including the Ceará Plateau, as the largest one. This is a very complex and poorly known area, with very few available research data. The geophysical approach was used to achieve a better understanding, and to guide further surveys. Gravity and magnetic data from the Equant I Project, seismic published lines and previous studies were applied to make several models and analyses. The gravity and the magnetic anomaly sources seemed to be the same, related to a denser and magnetized basement. It is estimated the basement surface between 800 and 6000 m and the Mohorovičić discontinuity, which is about 22-23 km below the Ceará Plateau. It is also presented and discussed the position of the continent-ocean boundary, recognized at approximately 40 km from the continental shelf, that locate the plateau at the oceanic crust. The area of the transitional crust, with an extension of 40-50 km, represents the altered continental crust, formed during the rift phase, previous to the Atlantic Ocean. The lack of data gives some limitation to the analysis, and add some uncertainties in the results, which are discussed along this thesis.

**Keywords:** Ceará Plateau; gravimetric modelling; magnetic modelling; marine geophysics; Brazilian Equatorial Margin; transform margin; continental-ocean boundary.

## RESUMO

MOURA, Denise Silva de. **Gravimetric and magnetic modelling of the Ceará Plateau, Brazilian Equatorial Margin.** 2018. 112 p. Dissertação (Mestrado) – Instituto Oceanográfico, Universidade de São Paulo, São Paulo.

A Margem Equatorial Brasileira é uma margem passiva transformante com longas zonas de fratura e diversos montes submarinos, incluindo o Platô do Ceará, o maior deles. Essa é uma área muito complexa e pouco conhecida, com poucos dados disponíveis. A abordagem geofísica foi utilizada para alcançar uma melhor compreensão da área e para guiar próximas pesquisas. Dados gravimétricos e magnéticos do Projeto Equant I, linhas sísmicas publicadas e estudos prévios foram aplicados para desenvolver os modelos e as análises. A fonte das anomalias gravimétricas e magnéticas pareceram ser as mesmas, relacionadas a um embasamento mais denso e magnetizado. É estimada a superfície do embasamento entre 800 e 6000 m e a descontinuidade de Mohorovičić, aproximadamente a 22-23 km abaixo do Platô do Ceará. Foi também apresentada e discutida a posição do limite crosta continental-oceânica, aproximadamente a 40 km da plataforma continental, colocando o platô na crosta oceânica. A área da crosta transicional, com uma extensão de 40-50 km, demarca uma crosta continental mais alterada, formada durante a fase rifte, anterior à abertura do Oceano Atlântico. A falta de dados limitou as análises, e certamente implicou em diversas incertezas nos resultados, que são discutidas durante esta dissertação.

**Palavras-chave:** Platô do Ceará; modelagem gravimétrica; modelagem magnética; geofísica marinha; Margem Equatorial Brasileira; margem transformante, limite crosta continental-oceânica.

## 1. INTRODUCTION

Studies about oceanic plateaus improve the knowledge about the crust and the Earth's interior, including its dynamic. It is known that the continental crust is formed by accretion of foreign terrains (RUDNICK, 1995). However, those continental terrains often include oceanic plateaus (OKAY, 2000; KOIZUMI and ISHIWATARI, 2006; MARTINS et al., 2009).

Today, these structures have also economic interests, since they are the source of some ores, as phosphates, polymetallic crusts and represent a particular and unique bioecological system.

Oceanic plateaus are anomalous crustal structures in comparison with normal oceanic crust (MOONEY, 2007). This definition highlights the principal characteristic of an oceanic plateau, which is its difference from the surrounding crust. Usually, the formation of this structure is related to magmatic events, hence, they were defined by Donnelly (1973) as oceanic flood basalt provinces.

Volcanic origin or not, the formation of a large structure as a plateau is generally explained by tectonic events. They could be related to intraplate volcanic activity (COFFIN et al., 1990), large igneous provinces (LIPs) (COFFIN and ELDHOLM, 1994), continental breakups (BASILE et al., 2013; SYMONDS et al., 1998), ridge volcanic spreading (GENTE et al., 2003), hotspot tracks and plume interaction (RÉVILLON et al., 2000), drowned atolls (CHASE, 1971) and many other events, some of them of uncertain origin (TAYLOR, 2006).

The Atlantic rifting created two different margins in Brazil. The East Brazilian margin, evolved into a passive margin, due to the orthogonal crustal extension (CHANG et al., 1992). In contrast, the North Brazilian Equatorial margin was formed during the strike-slip motion between Brazil and Africa, resulting in complex shear-dominated basins (GORINI, 1977; ZALAN, 1984; AZEVEDO, 1986; SZATMARI et al., 1987; MASCLE et al., 1988; GUIRAUD and MAURIN, 1992).

The North Brazilian Equatorial margin, or just Brazilian Equatorial Margin (BEM), where the Ceará Plateau is located, was formed during the

Equatorial Atlantic Ocean opening. The rifting phase occurred during the early Barremian to Aptian, and the first crust probably accreted during the late Aptian (BASILE et al., 2005). Since the breakup, the opening is slow with an average rate of about 2.5 cm/y. It gives to this region very rare characteristics as its long transform fracture zones: (1) the Chain, (2) the Romanche and (3) the Saint Paul ones. Figure 1 shows the BEM topobathymetric data with 15 arc-sec resolution by SRTM15PLUS (Shuttle Radar Topography Mission) (OLSON et al., 2014).

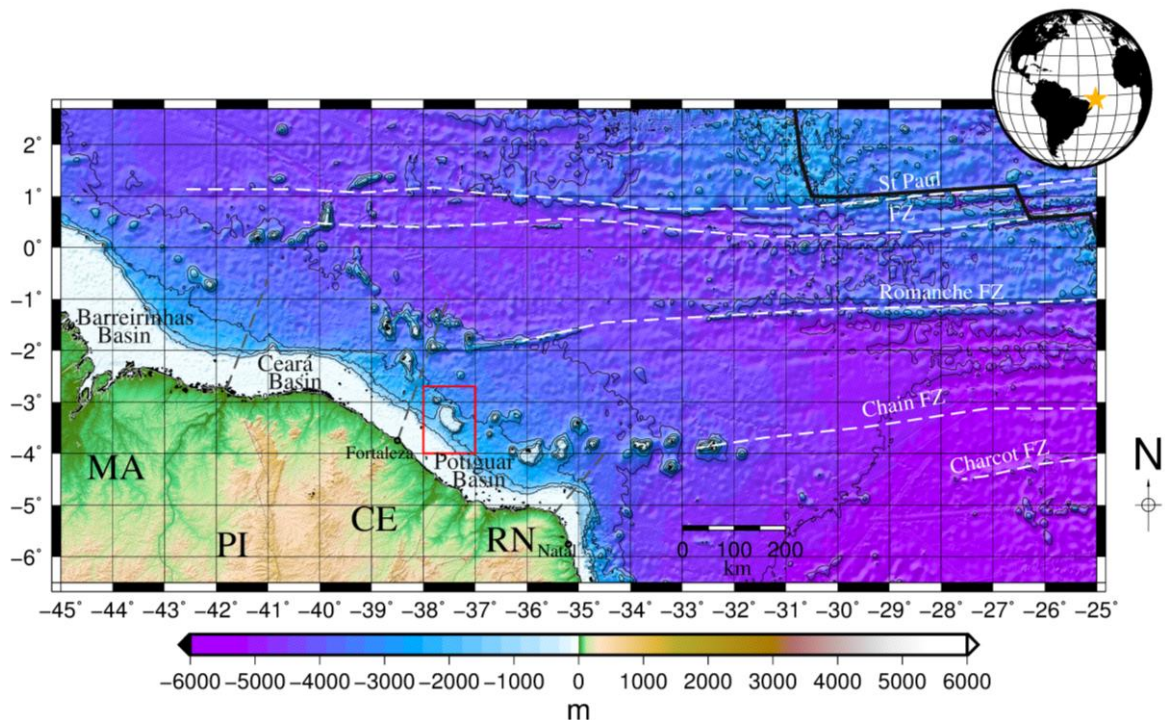


**Figure 1:** Brazilian Equatorial Margin topobathymetric map. Red rectangle indicates the study area. Bathymetric contour each 1000 m.

It is possible to find different research approaches about the BEM. They focus on bathymetric, gravimetric and magnetic data (MOLINA, 1996; CASTRO et al., 2012), tectonic formation (MIZUSAKI et al., 2002; CASTRO and BEZERRA, 2015; Mohriak and Rosendahl, 2003), neotectonic (Oliveira et al., 2015) and others, as reported in some available reviews (SOARES JR. et al., 2011; NÓBREGA, 2011).

The BEM has many islands, plateaus and seamounts, although they are poorly known. There is almost no information about the age, tectonic history and composition of the majority of them, including the Ceará Plateau.

The largest seamount of the BEM, the Ceará Plateau, is defined as a plateau by the GEBCO (General Bathymetric Chart of the Oceans) gazetteer (the visualization of the global undersea feature names is available at: <https://www.ngdc.noaa.gov/gazetteer/>). Its morphology is known through bathymetric data and previous definitions (FAINSTEIN and MILLIMAN, 1979). The plateau is 100 km away from Fortaleza city, Ceará State, into the Potiguar Basin (figure 1). It is located between the continental and the oceanic crust, next to the continental slope. Its area is about 850 km<sup>2</sup>, the shape is irregular with a flat top relief at a water depth of around 300 m, indicating an ancient sediment deposit, as shown in figure 2 with a 3D view of the SRTM15PLUS by GPlates Project (MÜLLER et al., 2016).

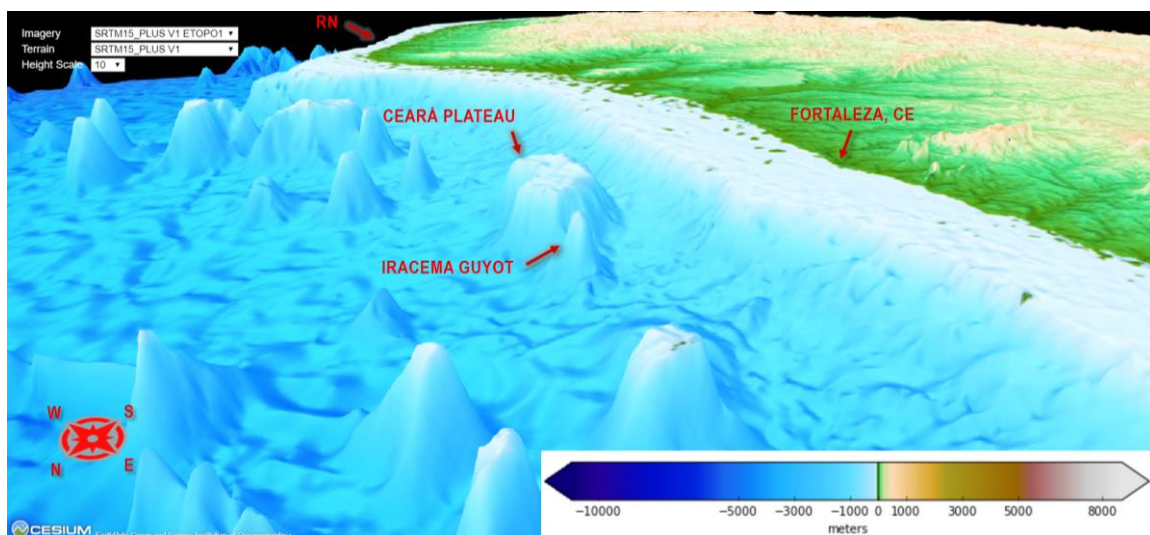


**Figure 2:** Perspective view of the study area. Bathymetry 3D with 10x vertical exaggeration of the SRTM15PLUS data (modified from <http://portal.gplates.org/cesium/?view=topo15>).

Geophysical data are used to assist the studies in remote areas due to the lower price of the acquisition comparing to geologic sample approaches. They help oceanographic studies offering general views of the regions, for example, about the density, inner structure and oceanic crust age, through gravimetric, seismic and magnetic data, respectively.

Marine gravity surveys are used to analyze the behavior of the oceanic crust and the offshore continental crust. Some tectonic processes, as the formation of sedimentary basins, the distribution of the sediments and the thermal subsidence of the crust are objectives for those surveys. For example, Constantino and Molina (2015) estimated the Santos Basin basement depth based on gravimetric data, with comparison with results from seismic line showed a good agreement.

Marine geomagnetic surveys in offshore continental areas are similar to those in the onshore areas, because the anomalies are related to geology and structural features. Along the oceanic crust the magnetic anomalies are commonly used to date the oceanic crust because the oceanographic surveys compare the magnetic anomalies to geomagnetic polarity timescales, as the Cande and Kent (1995) one. This pattern was observed firstly by Vine and Matthews (1963) and Morley and Larochelle (1964).

Nevertheless, combined, the gravity and magnetic methods have produced many contributions for the tectonic and dynamic studies and facilitated the exploration of the seafloor. Castro et al. (2012), for example, studied the origin of the Potiguar basin based on gravity and magnetic information.

Our study aims to comprehend better the Ceará Plateau region by correlating the gravity and magnetic anomalies with a crustal model. The continental and the oceanic crust generally have distinct physical characteristics, as density and magnetic susceptibility. This allows the gravimetric and magnetic studies associated with the interpreted seismic profiles and published literature, to distinguish between them.

Also, this study aims to provide subsidies for a possible drilling cruise carried by the IODP (International Ocean Discovery Program) along the BEM.



## 2. OBJECTIVES

The main objective of this study is to build up a crustal model using potential methods for the region where the Ceará Plateau is located. In order to achieve this objective, it is necessary to test whether the physical properties estimated using magnetometry and gravimetry, specially the density and magnetization of the oceanic crust or the continental crust are compatible with the models.

In order to reach the main objective, it is very important to accomplish these specific objectives:

- Describe and compare the gravimetric and magnetic data in a map view.
- Correlate the available data and the limitations of each method, to list the parameters of the 2D model.
- Define a crustal/geological 2D model, through the gravimetric anomaly, integrating the magnetic, seismic and core data.
- Through the 2D model, define the position of the COB in the area.
- Also through the 2D model, define the region of the transitional crust, a continental crust modified by many igneous intrusions.

The interpretation of the models should cooperate to achieve a better understanding about the evolution of the BEM, considering tectonic and sedimentary processes.

### **3. STUDY AREA**

#### **3.1 The Equatorial Margin**

##### **3.1.1 Tectonic synthesis**

At the end of Paleozoic Era, around 300 Ma ago, a collision between the North America and the N-NW of the Gondwana raised the Quachitas mountains in the Central America and the Apalaches in the U.S.A. (AZEVEDO, 1991, MACDONALD et al.,2003). The consequence was the closure of the Iapetus Ocean and the Pangea formation. During this period, the subduction of South America and the Pangea tafrogenesis were already underway (SZATMARI et al., 1987; MATOS, 2000).

According to McHone (2000), about 200 Ma ago ( $200\pm 4$  Ma:  $40\text{Ar}/39\text{Ar}$ ) a magmatic event characterized as a LIP occurred in the Pangea supercontinent, covering almost  $7 \times 10^6$  km<sup>2</sup>, this event is named CAMP, Central Atlantic Magmatic Province. It is considered the cause of the Pangea's rupture and, consequently, of all the following tectonic processes, as the Atlantic Ocean opening (DEMIN et al., 2003; WHALEN, 2015).

During the stretching phase in the Equatorial Atlantic, between the Jurassic and the beginning of Cretaceous, sediments have been depositing in the Marajó, Potiguar and Benue Rift Basins (MATOS, 1999 apud NÓBREGA, 2011; MATOS, 1992; NÓBREGA et al., 2005). The rifting phase started in the Neocomian (CASTRO and BEZERRA, 2015) reactivating some NE Precambrian lineaments (MATOS, 1992; SOUTO FILHO et al., 2000). The first oceanic crust (figure 3) was formed during the Early Aptian (BASILE et al., 2005), when an almost instant extension happened, forming NW-SE trends and sedimentary strike-slip basins with rotated blocks.

Between Albian-Cenomanian, the transtensional deformation became a deep-water deformation, delimiting the lithospheric boundary between Brazil and Africa, which was controlled by the transform faults. The NW-SE and EW main directions orientated the spreading (MATOS, 1992). Some authors consider that

the rotation poles between South America and Africa plates have changed in consecutive times since Aptian (MATOS, 2000), others explain the Atlantic opening with only one rotation pole (MOULIN, 2003; SOARES JR, 2008).

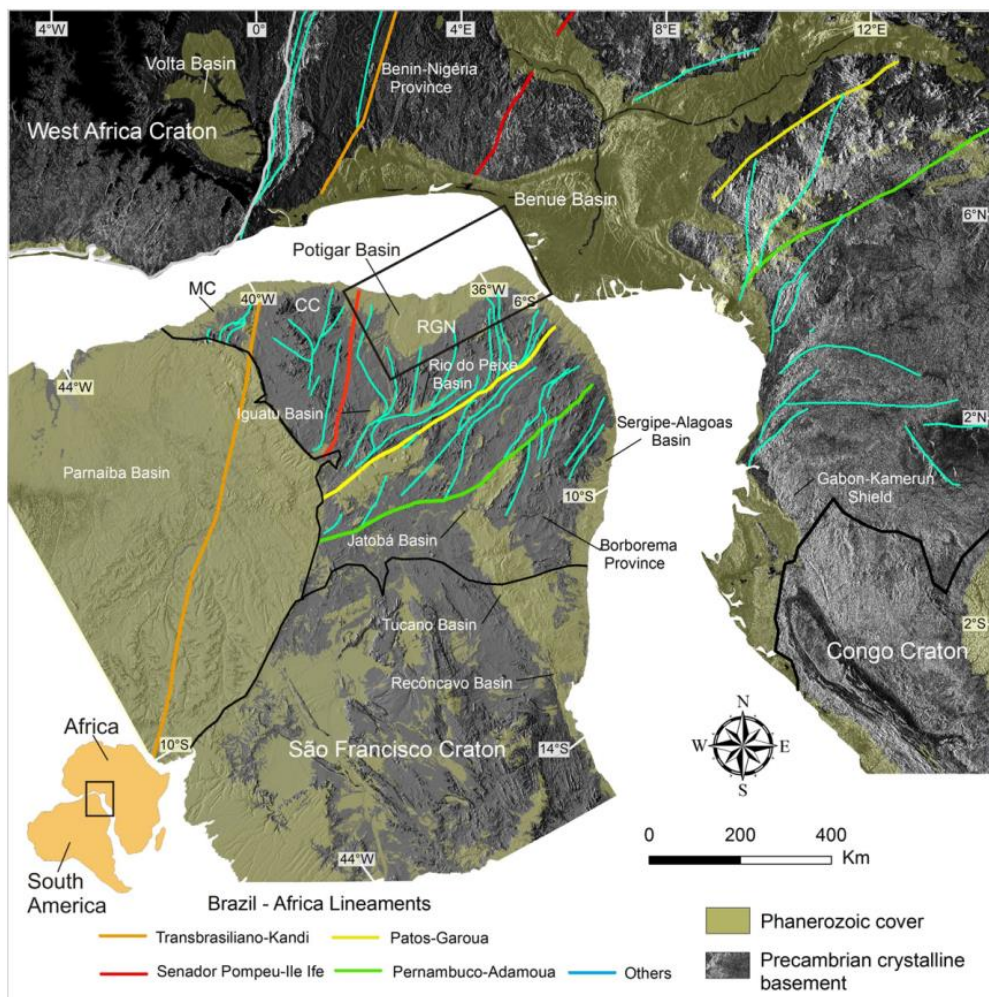


**Figure 3:** Reconstruction of the Equatorial Atlantic Ocean rupture with the principal continental lineaments, the cratons and the continental basins (CASTRO et al., 2012). The black rectangle delimits the figure 11.

Currently, the BEM is one of the most seismic regions at Brazil, even far away from the plate boundary. Considering that large lateral density variations create stresses (STEIN et al., 1989), and the transform margin has an uneven topography, seismic movements are expected to release the stresses, balancing the forces. Not only the topography, but the crustal thickness models can be used to explain this high seismic activity incidence, since the thinnest crust of the Rio Grande do Norte State and the isostatic compensation could be responsible by the

plate movements (AGURTO-DETZEL et al., 2015; ASSUMPÇÃO et al., 2013). The direction stresses are related to the Mid Atlantic Ridge (FERREIRA et al., 1998; LIMA et al., 1997) (figure 4). The Borborema Province is also a region with thermal anomalies, related to an upper Moho, mantle heterogeneities and recent magmatism (HAMZA et al., 2008) (figure 5).

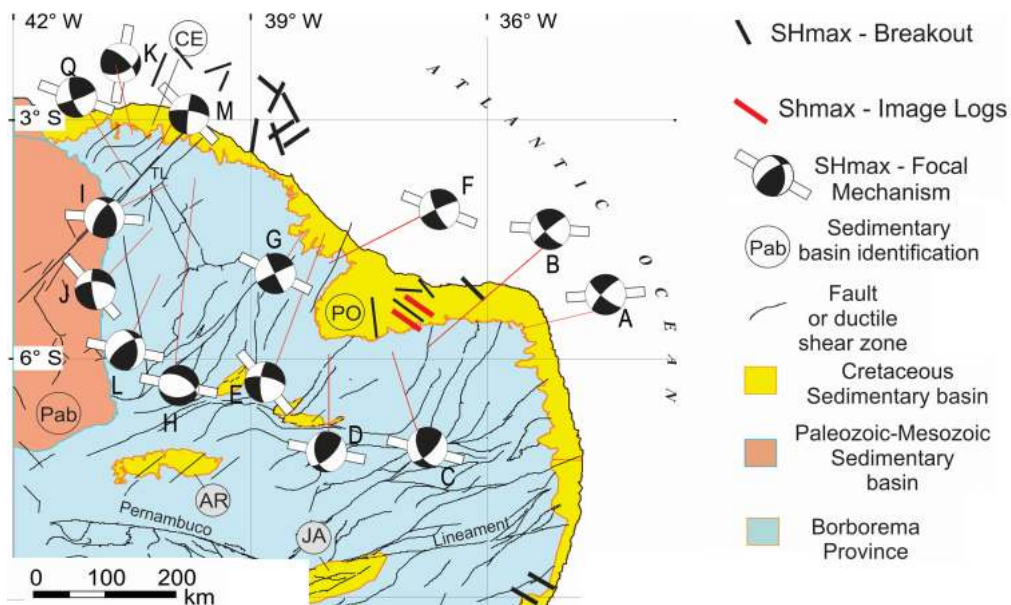


**Figure 4:** Simplified seismo-tectonic map of the Borborema Province (Modified from OLIVEIRA et al, 2015).

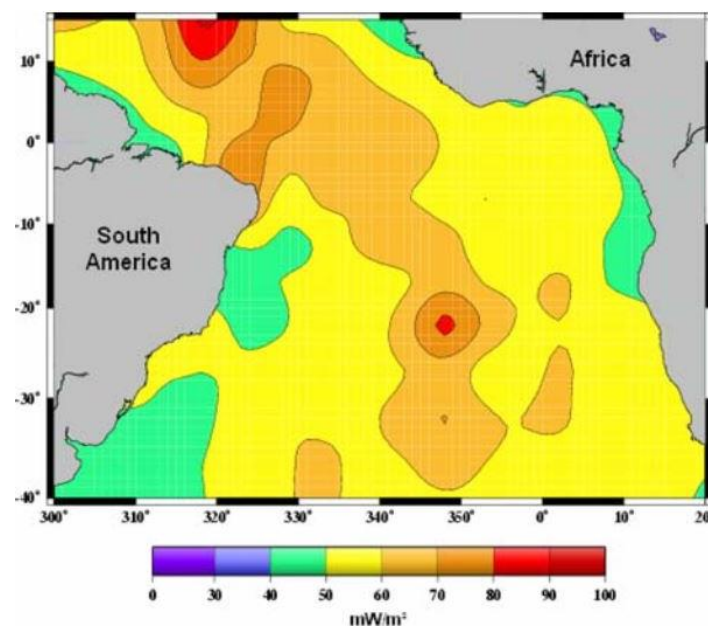


**Figure 5:** Regional heat flow map of the Equatorial Atlantic Ocean, derived from the spherical harmonic expansion to degree 36 (HAMZA et al., 2008).

### **3.1.2 The BEM geomorphology**

The Brazilian Continental Margin has attributes of a classic passive margin, with physiographic, tectonic-magmatic and sedimentary elements well defined (VITAL et al., 2005). It is parted in three regions: North, Northeast-East and South (ZEMBRUSCKI et al., 1979). The BEM mostly comprehend in the North part, it differs from the others since its relief is dominantly tectonic and volcanic dependent, related to the fracture zones, becoming complex and heterogeneous (CASTRO et al., 2010).

According to the tectonic classification, the margin was named transforming passive margin by Nóbrega (2011). Hydrodynamically, the BEM is classified as mixed to tide dominated (TABOSA, 2006).

The coastline is defined by dunes, beach ridges and cliffs. Silveira (1964) classified the region as Northeast semi-arid coast, i.e., few river supplies, coastal plain with small arcade lagoon-barrier systems, mangroves along lagoons and estuary borders, sandy barriers with unstable beach ridges due to NE strong winds, such as the dunes of the Lençois Maranhenses (SOUZA et al., 2005).

### **3.1.3 The Fracture Zones**

The Equatorial Atlantic fracture zones (FZ) are represented by very long highs and valleys, complexly related, with hundreds of kilometers, almost linear, easily spotted in bathymetric and gravimetric maps (figure 1 and 19). The bathymetric differences are explained by oceanic crust age differences, due to the thermal subsidence (NÓBREGA, 2011; MOHRIAK et al., 2003).

The scarps expose ultramafic rocks, some samples dredged along FZ have been related with ultrabasic rock diapirs highly serpentized, along the most deformed zones in the BEM FZ (GORINI, 1981; BONATTI, 1973; BONATTI and HONNOREZ, 1976). There are many volcanic seamounts at the BEM and two volcanic islands: the Rocas Atoll and the Fernando de Noronha Island. There is also a non-volcanic island, the St. Peter and St. Paul Archipelago, from where samples have been classified as ultramafic rocks, mostly serpentized peridotites

from the mantle (CAMPOS et al., 2003; GORINI, 1981; SICHEL, 2001 apud NÓBREGA, 2011), being the unique case of this kind of island (MAIA et al., 2016). It is an evidence of the BEM complexity.

### **3.1.4 The hotspot theory and the Fernando de Noronha hotspot**

The hotspot theory (ANDERSON, 1962; WILSON, 1963; MORGAN, 1971) became very popular after long lasting studies related to the Hawaii-Emperor seamount trail located in the North Pacific and, to other studies, such as the Louisville seamount trail formed by intraplate magmatism, located in the South Pacific (KOPPERS et al., 2010).

According to Morgan (1983) and Misuzaki et al. (2002), the formation of the Fernando de Noronha Island, the Rocas Atoll and part of the seamounts of the BEM is related to a hotspot, the Fernando de Noronha hotspot (DAVIES, 1988; SLEEP, 1990; STEINBERGER, 2000). Nevertheless, Courtillot et al. (2003) have not classified the Fernando de Noronha hotspot as formed by a deep plume, after considering criteria as: track line presence, buoyancy flux, reliability and  $^3\text{He}/^4\text{He}$ .

### **3.1.5 The Edge-Driven Convection**

The alternative source of a hotspot was defined by King and Anderson (1998) as the Edge-Driven Convection (EDC). A small scale convective instability that is the origin of the intraplate magmatism, i.e., a magmatism formed in a shallower region compared to the conventional hotspot theory. The instability is created by the variation in lithospheric thickness, as at a continent-ocean lithospheric boundary (VOGT, 1991 apud KING and ANDERSON, 1998).

The Fernando de Noronha hotspot was analyzed by King (2007) as a probable EDC. This hypothesis was adopted by Oliveira (2008) in his study about the Brazilian Equatorial Margin. It was also motivated by the geoid height high anomaly and the negative anomaly in the surface wave tomography of the BEM and especially around the Borborema region (figures 6 and 7). These anomalies



are indicative of a thinner crust at the area, other studies also have pointed this condition (ASSUMPCÃO et al., 2013; HAMZA et al., 2008).

Therefore, the BEM seamounts formation remains undefined, and the presented theories are: the deep hotspot source for magmatism (RIVALENTI et al., 2000; MORGAN et al., 1983), the shallow hotspot, or Edge-Driven Convection (KING and ANDERSON, 1995; 1998) and the tectonic formation influenced by the FZ (ALMEIDA, 2006; BONATTI et al., 1994; SIBUET, 1978).

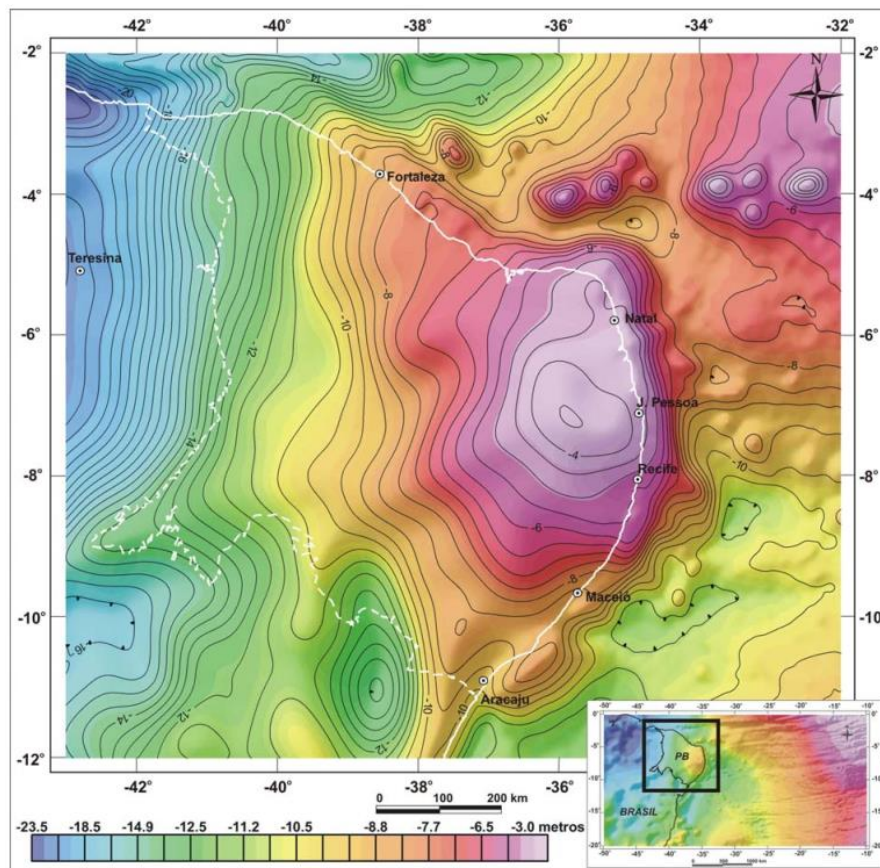


**Figure 6:** Geoid height in the Borborema region (SANDWELL and SMITH ,1997 apud OLIVEIRA, 2008).

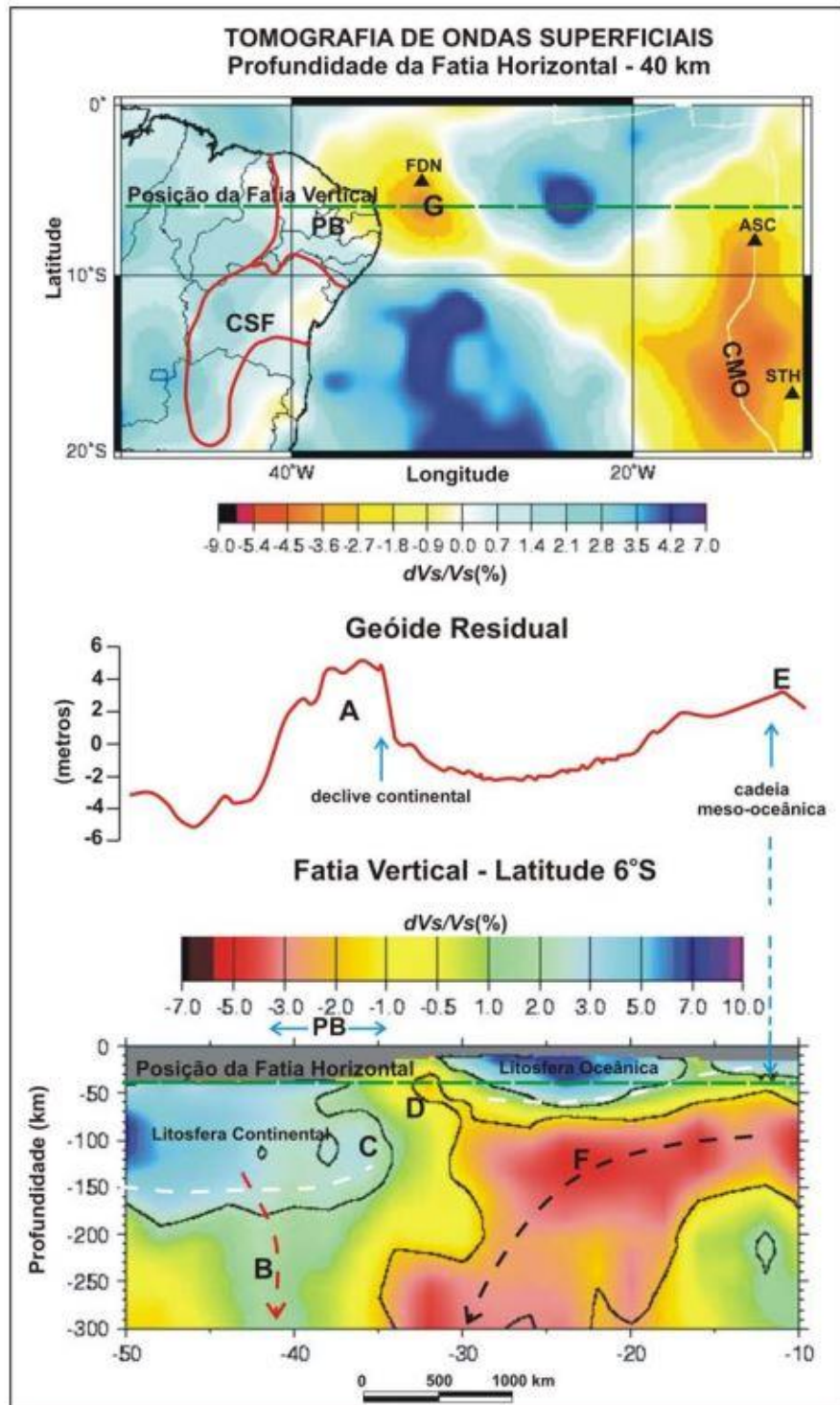


**Figure 7:** Correlation between surface wave tomography and geoid height residual (figure 4 minus 3 km upward continuation). Tomography data from global model CU\_SRT1.0 developed with the method created by Barmin et al. (2001) and applied by the authors of: <http://ciei.colorado.edu/~nshapiro/MODEL/> (OLIVEIRA, 2008).



### 3.1.6 The African Equatorial Margin

The Cotê d'Ivoire-Ghana transform margin, Brazilian Equatorial conjugate margin, was drilled in 1996 by an ODP scientific cruise. One of the objectives of that study was to better understand the evolution of transform continental margins (MASCLE et al., 1996). The sites were located along the continent-ocean boundary (COB), above the Romanche FZ.

Mascle and Blarez (1987) have schematized three main stages for the evolution of a transform margin: During phase A, with the rapid subsidence caused by the stretching of the continental crust, the Ivorian and Benin sedimentary basins and the Ghanaian shelf were formed, on the African side, and the Barreirinhas, Ceará and Potiguar basins on the Brazilian side. Phase B includes the creation of the first oceanic crust in the Equatorial Atlantic. During this event the thermal gradient was very strong between the cold continental crust and the hot oceanic lithosphere, resulting in a marginal ridge uplift in the order of 1 km, with 20 km of horizontal influence. The final stage of the evolution, C, starts with the thermal subsidence of the transform margins (BASILE et al., 1992, 1993), therefore, as further away the oceanic crust was from the ridge, it was colder and deeper. These stages can be seen on figure 8.

Between phases A and B, the South of the Atlantic Ocean crust was being formed. Apatite fission track indicates the first heating event about  $110 \pm 4$  Ma (MASCLE et al., 1998). It is important to mention that in the Equatorial margin the opening have not started as a divergent margin, but as a transform margin (figure 9). The ridge was perpendicular to the continental crust in the African and in the Brazilian side. After phase C the margin became more similar to a divergent margin, and the ridge was more parallel with the continent than before.

The sediments of the African plate, collected during the ODP cruise, have the average densities around  $2 \text{ g/cm}^3$ . The densities increase with the depth, starting with 1.6 until  $2.5 \text{ g/cm}^3$ .

Jilinski et al. (2013) proposed a method to demarcate the COB position and the area of the transitional crust, they applied it to the African Transform Margin,

and used a gravity model to support it (figure 10). The 2D gravity modelling is very similar to the one used in this study to present the geological structure of the BEM. They used seismic lines to create the profile, and it was in good agreement with the ODP interpretations (MASCLE et al., 1998).

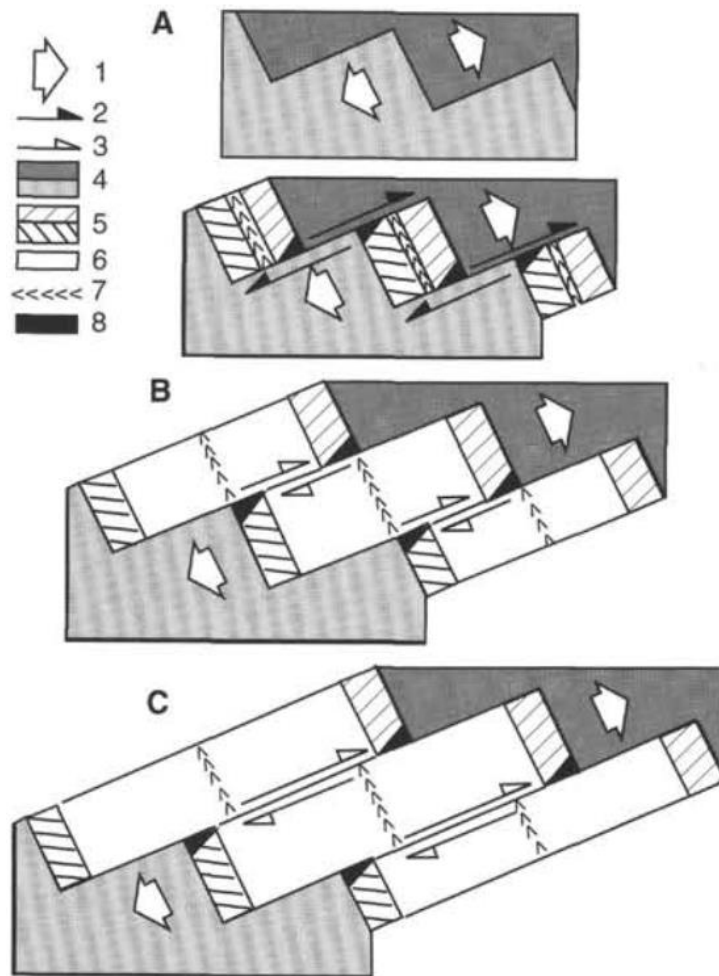


**Figure 8:** A simplified model for the evolution of transform margins based on the example of Ivory Coast and Ghana margins (MASCLE et al., 1996). (A) an intra-continental active transform fault, creating a thinned crust and sedimentary cover, (B) a continent-ocean active transform fault contrast and (C) and inactive continent-ocean transform fault. (1) divergence; (2) transform motion between continental and (3) oceanic crust; (4) continental crust; (5) thinned continental crust; (6) oceanic crust; (7) ridge axis; (8) marginal ridge.

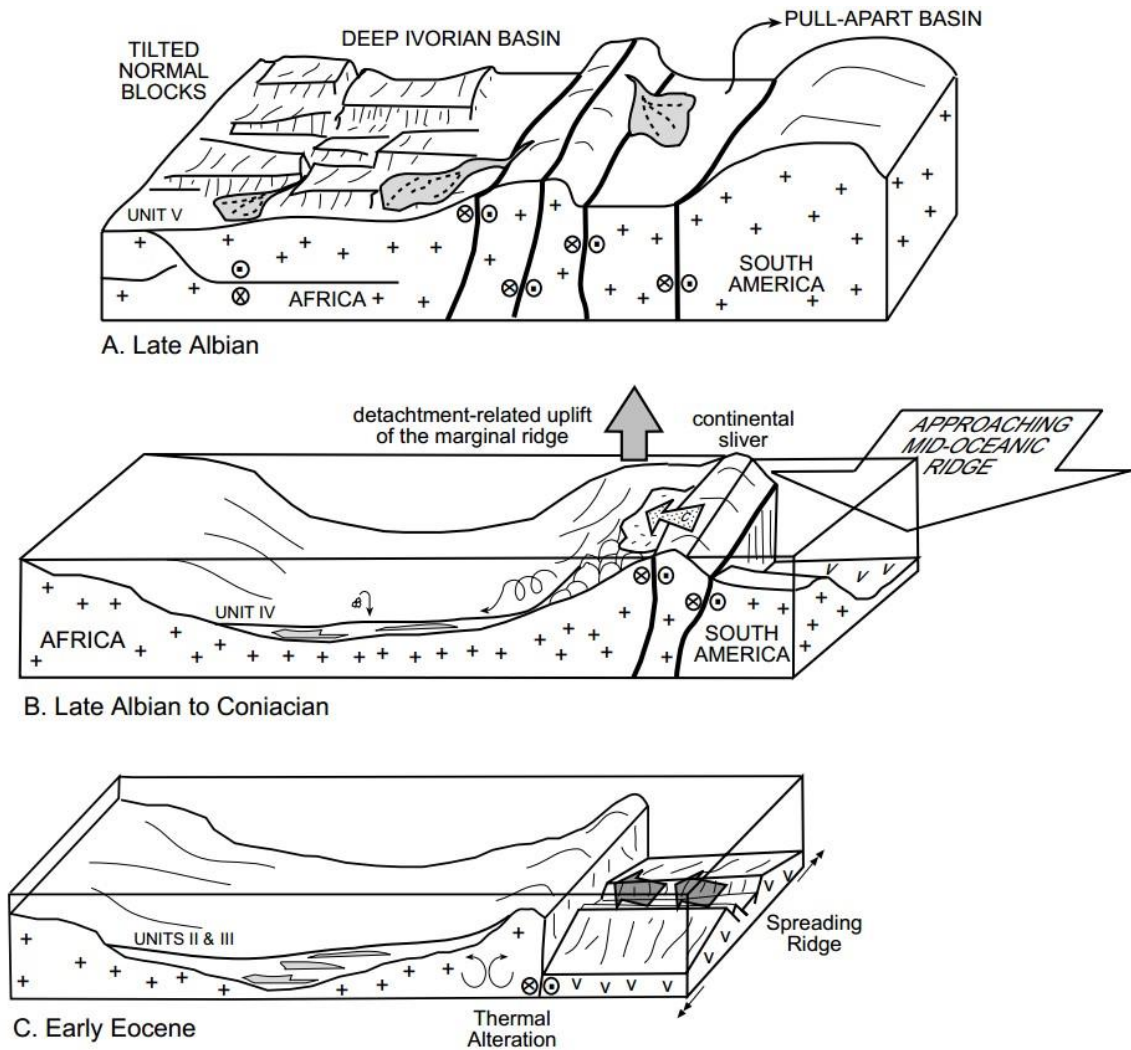


**Figure 9:** Schematic illustration of the evolution of the transform margin between the African and South American continents from Late Cretaceous through early Eocene times. A) Syntransform, intracontinental basin stage. Sedimentation during the late Albian was dominated by continental and lacustrine environments in pull apart basins developed by transcurrent shear between the South American and African continental blocks. B) Marginal ridge emergence and initiation of subsidence in the Deep Ivorian Basin (late Albian to Coniacian). C) Submergence of the marginal ridge and formation of the Deep Ivorian Basin (late Coniacian to early Eocene) followed by passage of the oceanic spreading ridge (MASCLE et al., 1998).

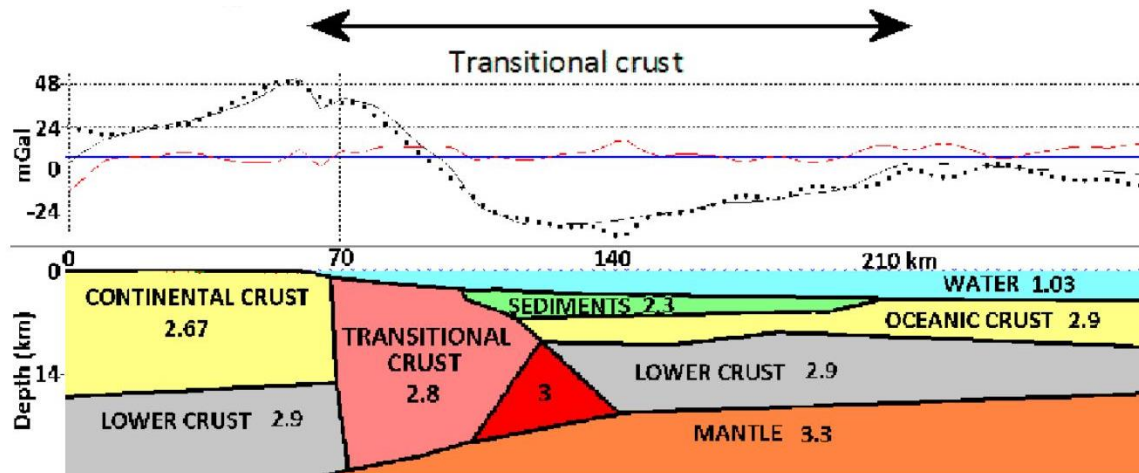


**Figure 10:** A 2-D gravity model for Liberia sector of the West African Transform Margin. The densities are in  $\text{g/cm}^3$  (JILINSKI et al., 2013). The 70 km dashed line is the boundary between the continental extended crust and the transitional crust determined by the ODP crew (MASCLE et al., 1998).

## 3.2 The Potiguar Basin

### 3.2.1 The rift formation

The Potiguar Rift Basin is about 6 km depth and  $2 \times 10^5 \text{ km}^2$  in area, mostly submerse, limited by the Fortaleza high in the west and the Touros high in the south. It is a rift aborted during the Cretaceous in the Brazilian Northeast continental margin (figure 11). This rift basin is one of the main tectonic structures formed before the Pangea breakup, between the South American and the African continents (CASTRO et al., 2012).

Neoproterozoic shear zones have an important role in the rifting process of the Neocomian Potiguar Basin in the Brazilian Northeast. During the early Cretaceous, the NW-SE extension promoted the development of a range of intracratonic basins in the Borborema Province, mostly, reactivating previous NE-SW weak zones (BRITO NEVES et al., 1984).

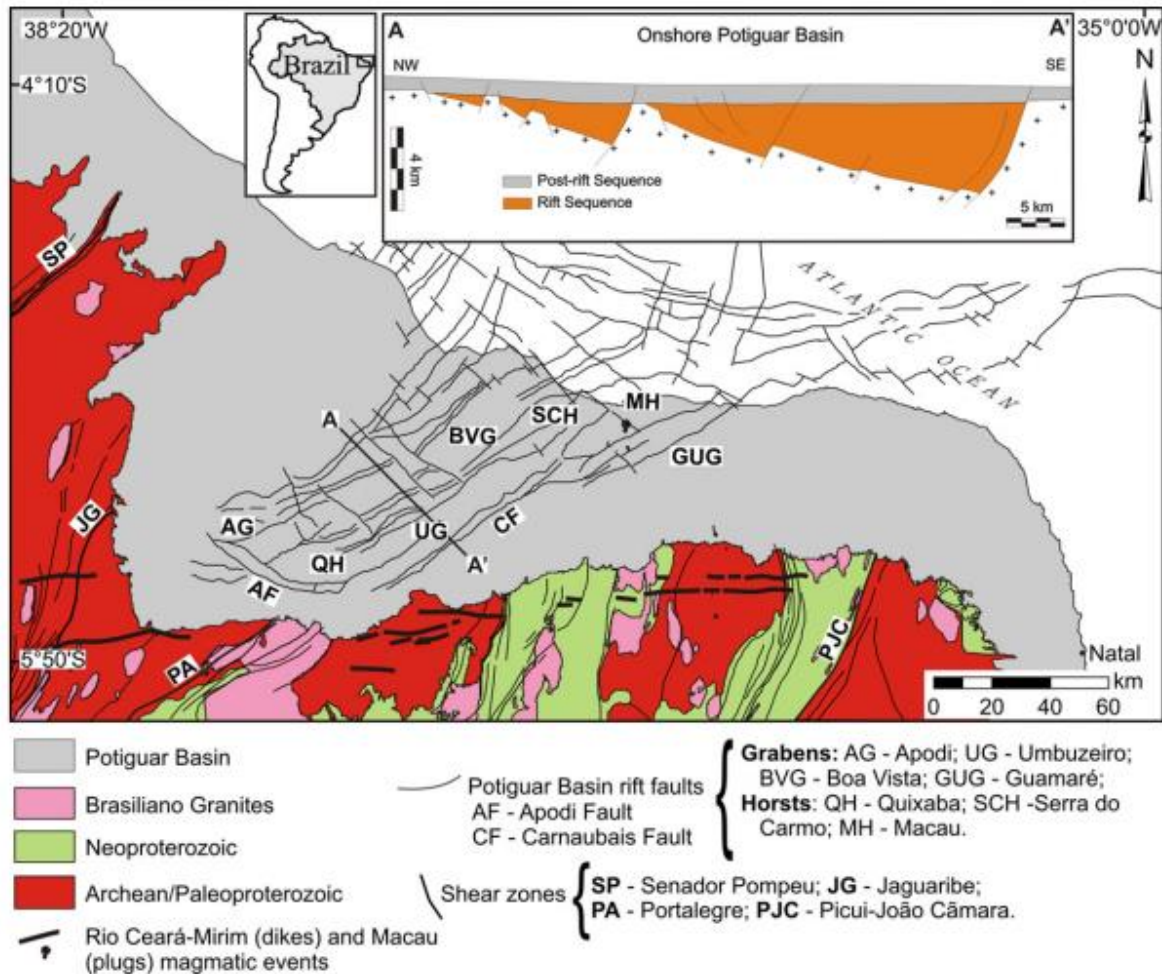


**Figure 11:** Geologic regional map of the onshore Potiguar Rift Basin (CASTRO et al., 2012). The area of the map is delimited in figure 3.

### 3.2.2 The oceanic basin sediments

The marine sedimentation reflects the source, the climate, the drainage and the tectonic environment. Due to the Equatorial tropical weather and the little terrigenous sedimentation, this narrow (about 60 km in the Ceará State) and shallow (mean under 50 m) continental platform is one of the few areas in the world where a stable and open platform is covered mostly by biogenic carbonate sediments (SOUZA et al., 2005).

The sediment source is, almost exclusively, reworking in situ of previous deposits and biologic contributions (VITAL et al., 2005). Figure 12 presents a surface distribution of the sediments in the Ceará State platform (MEIRELES et

al., 2005), evidencing the influence of the carbonate sedimentation near to the Ceará Plateau area.

Contrasting with other tropical platforms, the corals, the ooids and different forms of carbonates are virtually absent. The carbonate sediments are controlled by recent coral algae (SOUZA et al., 2005).

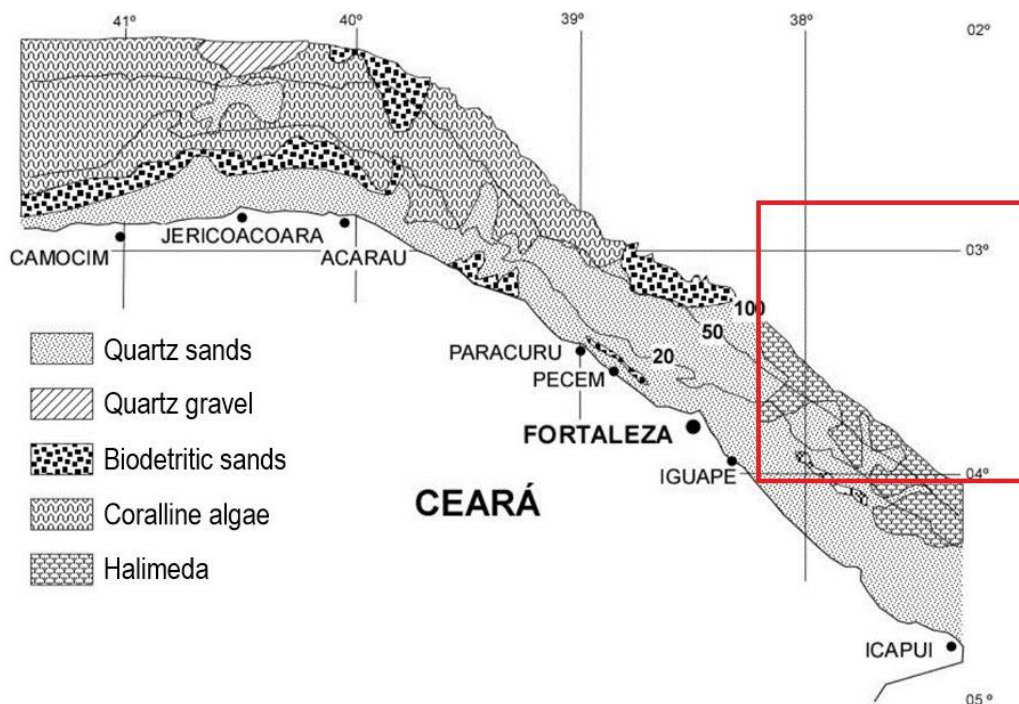


**Figure 12:** Faciologic of the continental platform in the Northeast Brazilian Region, evidencing the presence of biological sedimentation and calcareous algae. These sediments were remobilized from the intern platform during a regressive event and formed aeolian carbonate-rich deposits. Red rectangle indicates the study area. Modified from Meireles et al. (2005).

Besides the sedimentary source, it is important to highlight the ocean currents, influenced by the weather and the drainage. After all, in the sea, they are the main cause for the sediment movements along the water column. Between the source and the continental platform, the clastic sediments must cross many costal environments, which are traps for the sediments, as estuaries, bays, lagoons, deltas and tide plains, that hinders the sediments from reaching the ocean basin. Once sediments arrive at the platform, they are also dependent on hydrodynamic



processes, as waves, tides, oceanic and density currents, carrying some material to the deep ocean (SOUZA et al., 2005), and some to the seamounts located after the continental slope, as the Ceará Plateau.

Along the BEM, the surface ocean current is named North Brazilian or Guianas. It has a SE-NW flow, and it is characterized by an oxygenated and salter water, influenced by the trade winds, which increases its velocity during the winter (OLIVEIRA, 2007).

The tectonic environment is also important for the formation of sedimentary basins. The transform margin is characterized by an abrupt transition between the continent and the ocean, i.e., short platforms and a steep slope (BASILE et al., 2013). Magmatic events during the sedimentation change the condition and the form of the basins. High seismic activity also reworks the sediments making the scarps even more unstable.

The stratigraphic chart of the Potiguar Basin shows the predominance of each sediment type accordingly to its position, from the coast until deep waters (figure 13). It presents the evolution of the margin sediments while the Equatorial Atlantic Ocean was forming. A SW-NE profile of this basin (figure 14) provides a complementary view of the sediment distribution and the basement format.

The sediments are associated to four main sequences: rift, transitional, transgressive and regressive phases. The first one corresponds to a rift tectonic evolution described by a fluvial/lacustrine system during Valanginian/Aptian. The transitional phase has an Aptian/Albian lagoon system. The transgressive marine sequences started with a fluvial/marine system during the Albian/Campanian. The last phase is a marine regressive mega sequence of passive margin, it begun in Campanian (SOUZA, 1982, BERTANI et al., 1990 apud TABOSA, 2006). The sedimentation is related to the tectonic evolution presented in 3.1.6 in this study.





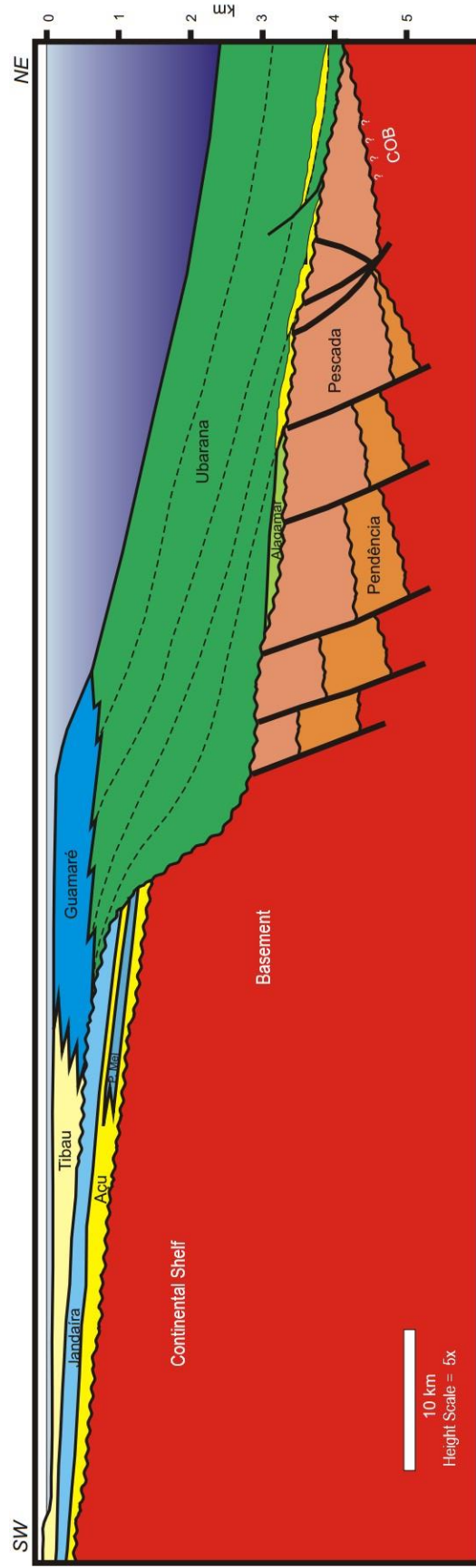


**Figure 14:** SW-NE profile of the Potiguar oceanic basin. It is located near to the Ceará Plateau and the scale indicates the COB 30 km far from the Continental Shelf (BERTANI et al., 1990).

### **3.3 The Ceará Plateau**

#### **3.3.1 The Ceará Plateau nomenclature**

The seamount studied in this work does not have a consensual classification in the literature. There are some divergences. In the REMAC (Reconhecimento global da Margem Continental Brasileira / Recognition of the Brazilian Continental Margin) Project reports (1979), it is named guyot, in other words, the formation was defined as volcanic, followed by an erosional phase, responsible for creating a flat surface and, then, a subsidence phase, descending the structure. However, the non-conic shape differs from the guyot definition, which demands a ratio between the length and the width less than 2, implying that the formation is more complex than that.

Due to the undefined formation, the structure is usually named as Ceará Plateau, for example, in the GEBCO gazetteer (the visualization of the global undersea feature names is available: <https://www.ngdc.noaa.gov/gazetteer/>). The word plateau is defined by the International Hydrographic Organization (2008) as a flat or almost flat elevation, with an area proportionately reasonable to the size and an abrupt fall along one or many of its sides.

Also, this region is sometimes called by the local fishermen Banco Aracati (Aracati bank).

#### **3.3.2 Geomorphologic synthesis of the Ceará Plateau**

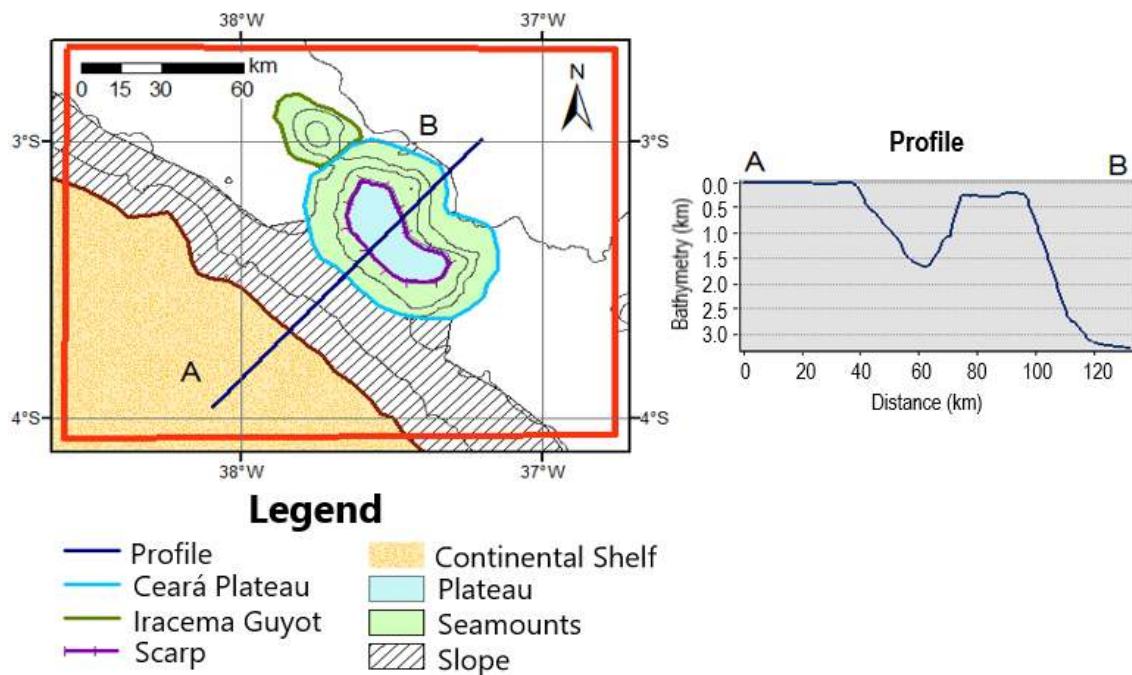
The Ceará Plateau, as the name definition proposes, is a seamount with a reasonable flat top and an abrupt fall along its sides. The average slope angle is 15°. A simple geomorphologic map with these structures is presented in figure 15. The geomorphologic dimensions analyzed in the map are presented in table 1.

The slope map (figure 16) highlights the flat top and the abrupt inclination around it. The inclination of the Ceará Plateau and the Iracema Guyot are higher

than the slope itself. This specific geomorphology is characteristic of a biogenic building, but it cannot be conclusive without samples.

Due to the high slope angle of the plateau, turbidite systems and canyons are probably distributed along their scarps. Similar structures were observed in the continental slope of the Rio Grande do Norte State by ALMEIDA et al. (2015), although the resolution of the data used in this study was not sufficient to detect them.

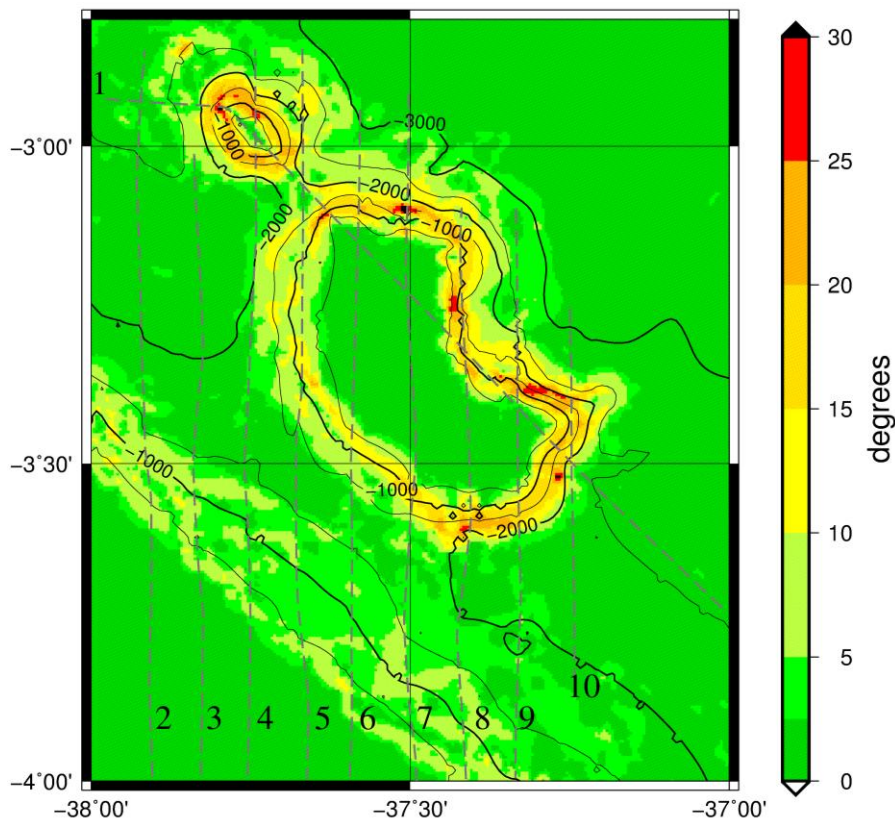
Slope anomalies on the northeast of the plateau indicate the deposition of local rework sedimentation, named contourite drifts, sediments eroded and deposited by the background currents (HERNÁNDEZ-MOLINA et al., 2006.).



**Figure 15:** Geomorphologic map of the Ceará Plateau created from the SRTM15PLUS bathymetric data.

**Table 1:** Geomorphologic parameters for the Ceará Plateau.

Description	Value
Plateau area	850 km <sup>2</sup>
Average plateau length	45 km
Average plateau width	16 km
Distance (plateau and continental shelf)	45 km
Average continental shelf length	70 km
Average plateau depth	300 m
Minimum plateau depth	170 m
Average continental shelf depth	50 m

**Figure 16:** Slope map of the Ceará Plateau created with the SRTM15PLUS bathymetric data. The declivity is in degrees. Grid interval of 15 seconds (approximately 450 m). Bathymetric contour each 500 m.

## 4. MATERIALS AND METHODS

### 4.1 Available data

The geophysical and geological data used in this study are from previous surveys. They include: bathymetry, gravity and magnetic data from track lines of the Equant I project (NESS et al., 1989), the interval along the data is about 800 m and 9 km between the profiles; 15x15 arcsec elevation grid SRTM15PLUS (OLSON et al., 2014); 15x15 arcsec satellite radar altimeter free-air gravity anomaly grid (SANDWELL et al., 2014); 2x2 minute geomagnetic anomaly grid EMAG2 model (MAUS et al., 2009); published interpreted seismic reflection profiles (JOVANE et al., 2016 and available in: <[http://www.brasil-rounds.gov.br/arquivos/Seminarios\\_r11/tec\\_ambiental/Bacia\\_Potiguar.pdf](http://www.brasil-rounds.gov.br/arquivos/Seminarios_r11/tec_ambiental/Bacia_Potiguar.pdf)>).

The maps with the data, ship tracks and the location of the published profiles are created using the GMT – Generic Mapping Tools (WESSEL and SMITH, 1998) open software at the Mercator projection. GMT is used to interpolate, reduce and manage the data. The Oasis Montaj software is also used to treat some data. The GravMag software is used to do the gravity modelling. A FORTRAN routine developed by Maia et al. (2005) and based in Blakely (1996) is used to do the magnetic modelling.

The ship tracks, the seismic lines location and the position of the CES-112 ANP (Agência Nacional do Petróleo / Oil National Agency – Brazil) hole are presented in figure 17.

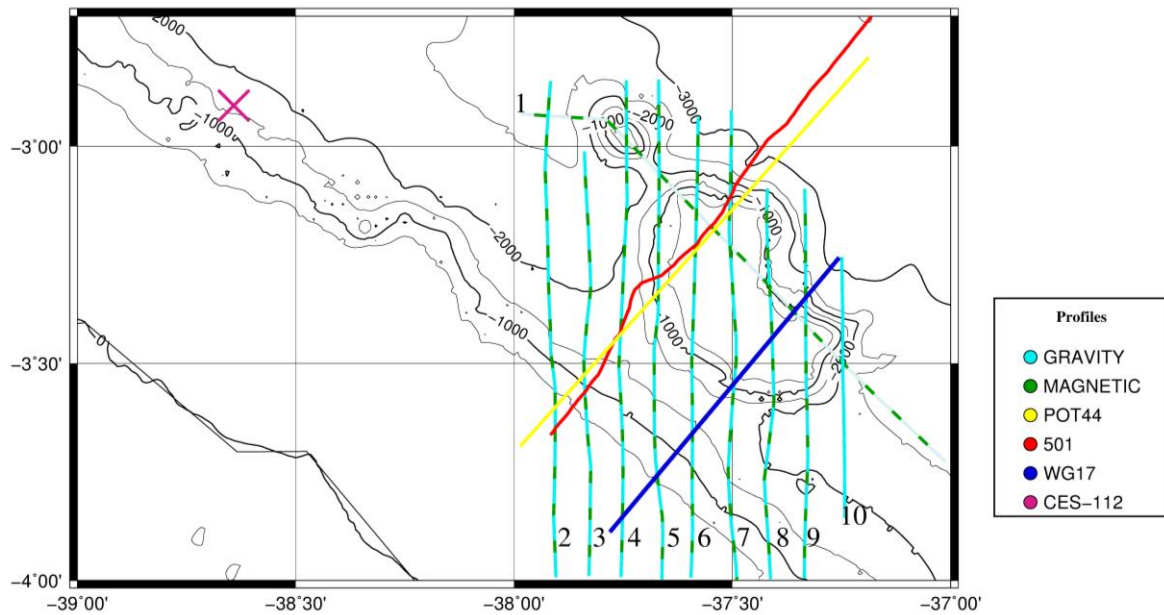


**Figure 17:** Distribution of the Equant data, the seismic profiles and the hole position into the region. The red, yellow and blue lines are the seismic profiles from Leplac Project, ANP and WesternGeco, respectively. The pink cross indicates the position of the ANP hole. Bathymetric contour each 500 m.

#### 4.1.1 Equant Project

The Equant Project was elaborated to study the North and Northeast of the Brazilian coast (NESS et al., 1989). It had two phases, both carried by the Oregon State University and aboard of the oceanographic ship Prof. W. Besnard, owned and operated by the University of São Paulo.

The data acquired in this study correspond to the first phase of the Equant Project, the Equant I. This phase was carried out during August 27 to October 10, 1987, along the Brazilian Equatorial Margin, motivating the name Equant (Equatorial Atlantic). The profiles are between Maranhão and Rio Grande do Norte states. This study uses 10 profiles from Equant project (figure 17).



### 4.1.2 Bathymetry data

The bathymetry data from the Equant I cruise add up to a total of 44,204 data points in 10 profiles. It is a 12 kHz single-beam bathymetric data collected along all the tracks. The bathymetric data precision is about 19 m (NESS et al., 1989). The Equant bathymetry data are used to make the reductions and corrections in the gravity and magnetic data, and for the modelling. In order to create the maps, it is used the global model SRTM15PLUS, an estimated seafloor topography with 15 arcsec resolution (OLSON et al., 2014), developed by the NOAA (National Oceanic and Atmospheric Administration – U.S.A.) (figure 18).

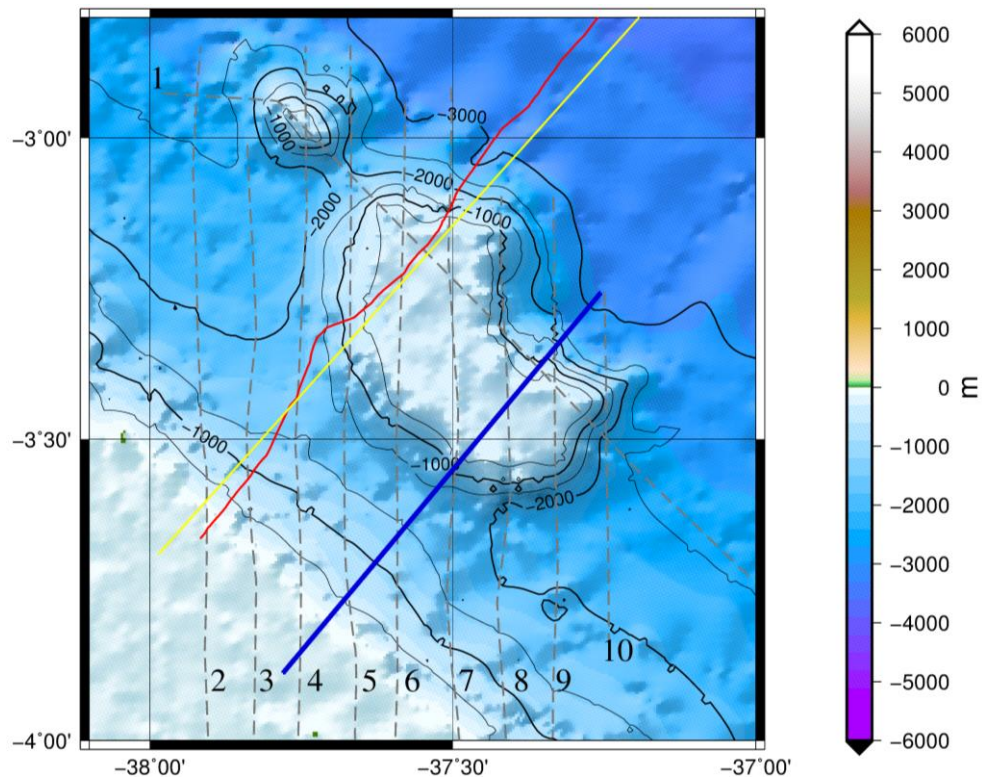


**Figure 18:** Bathymetric map and the localization of the data in the study area. Grid interval of 15 seconds (approximately 450 m). The red, yellow and blue lines are the seismic profiles from Leplac Project, ANP and WesternGeco, respectively. Bathymetric contour each 500 m.

### 4.1.3 Gravity data

The gravity data used in this study are from ship profiles collected during the Equant I project (figure 19). There is a total of 31,068 gravimetric data points. The gravity data was collected by an adapted LaCoste & Romberg gravimeter, S-42. The Equant I data is already corrected for latitude, drifting of the equipment and the Eötvös effect. The mean gravimetric data precision is about 2.9 mGal (NESS et al., 1989).

Marques et al. (1992) compared the Equant I and II data with the anomaly calculated by satellite altimetry computed for 2 years, or 44 cycles of the GEOSAT satellite, and did not find any resolution discrepancy. Comparing the global model calculated by Sandwell et al. (2014) with the Equant I data, the differences are also not substantial.

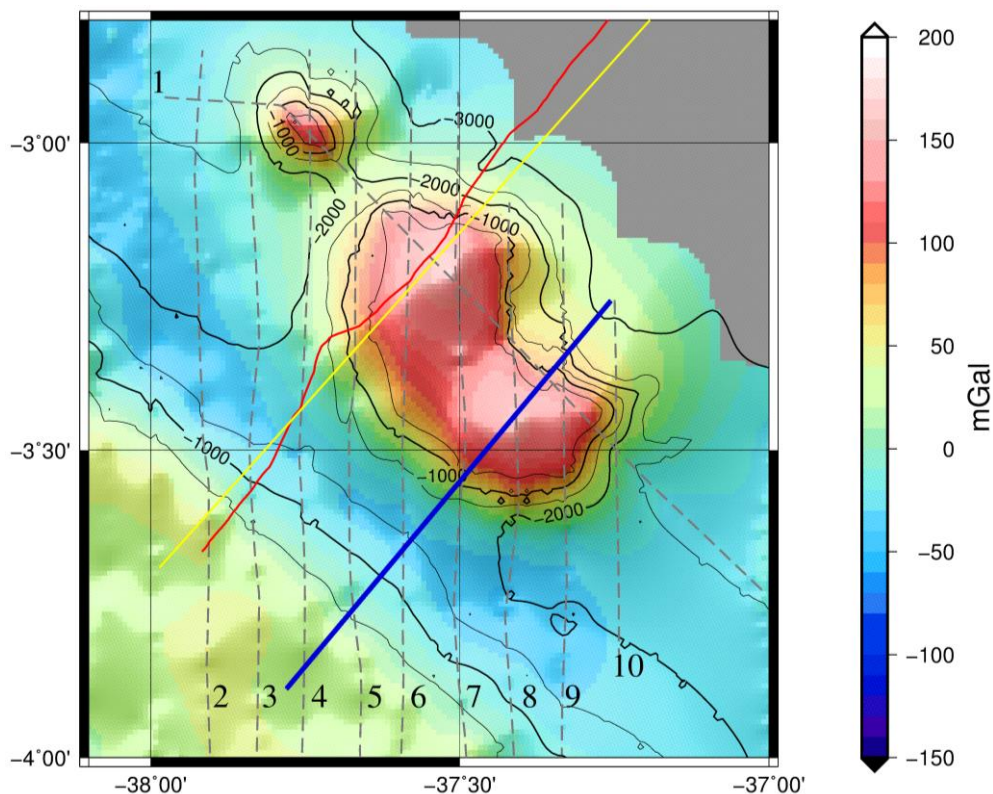


**Figure 19:** Free-air gravity anomaly map and the localization of the data in the study area. Grid interval of 30 seconds (approximately 900 m). The red, yellow and blue lines are the seismic profiles from Leplac Project, ANP and WesternGeco, respectively. Bathymetric contour each 500 m.



#### 4.1.4 Magnetic data

The magnetic residual anomalies used in this study are from the Equant I cruise as well (figure 16). There is a total of 9,250 data points. The magnetic total field and the magnetic anomalies data were downloaded from the NGDC site (<https://maps.ngdc.noaa.gov/viewers/geophysics/>) (National Geophysical Data Center – U.S.A.).

The magnetic data used in this study is already processed, i.e., corrected from usual variations and fluctuations, as the diurnal variation and instrument spikes. The core field and the secular variations with the IGRF – 1985 model (International Geomagnetic Reference Field) are also removed. The magnetic data precision is about 18 nT (NESS et al., 1989). It resulted in the residual magnetic anomaly, due predominantly to structures present in the crust (figure 20).

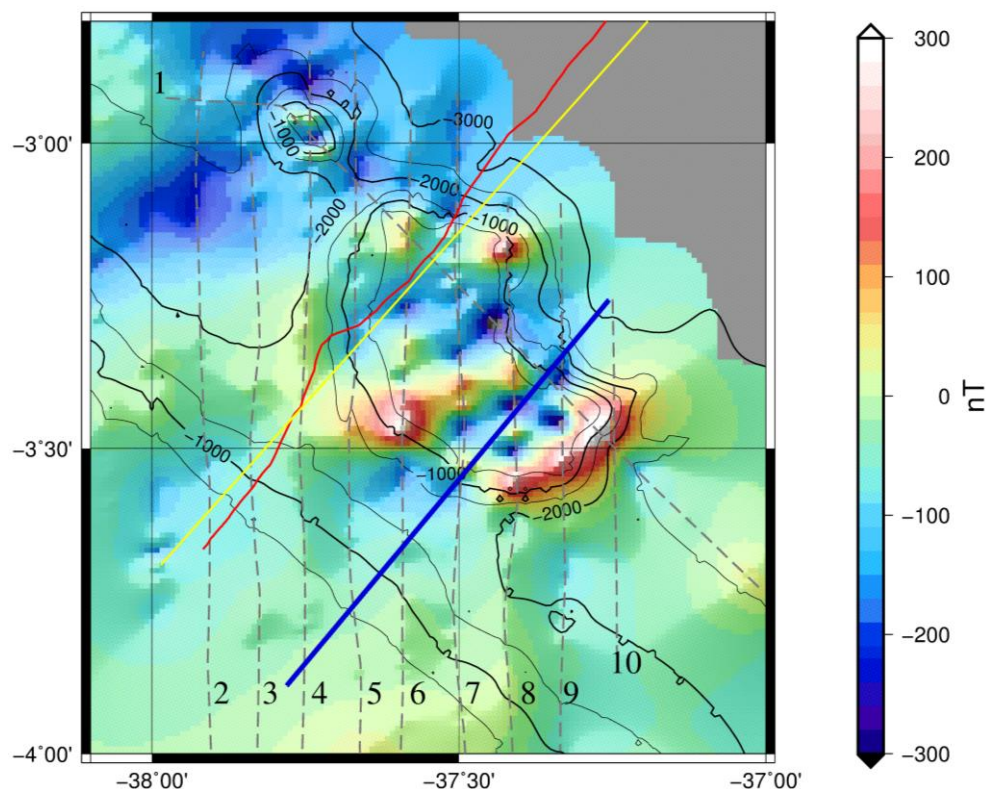


**Figure 20:** Magnetic anomaly map and the localization of the data in the study area. Grid interval of 30 seconds (approximately 900 m). The red, yellow and blue lines are the seismic profiles from Leplac Project, ANP and WesternGeco, respectively. Bathymetric contour each 500 m.

### 4.1.5 Seismic data

The published seismic profiles crossing the Ceará Plateau were published by Jovane et al. (2016). The data were collected during the Leplac Project (Levantamento da Plataforma Continental / Survey of the Continental Shelf), profile 501 (figure 21), and from ANP surveys, pot44 (figure 22).

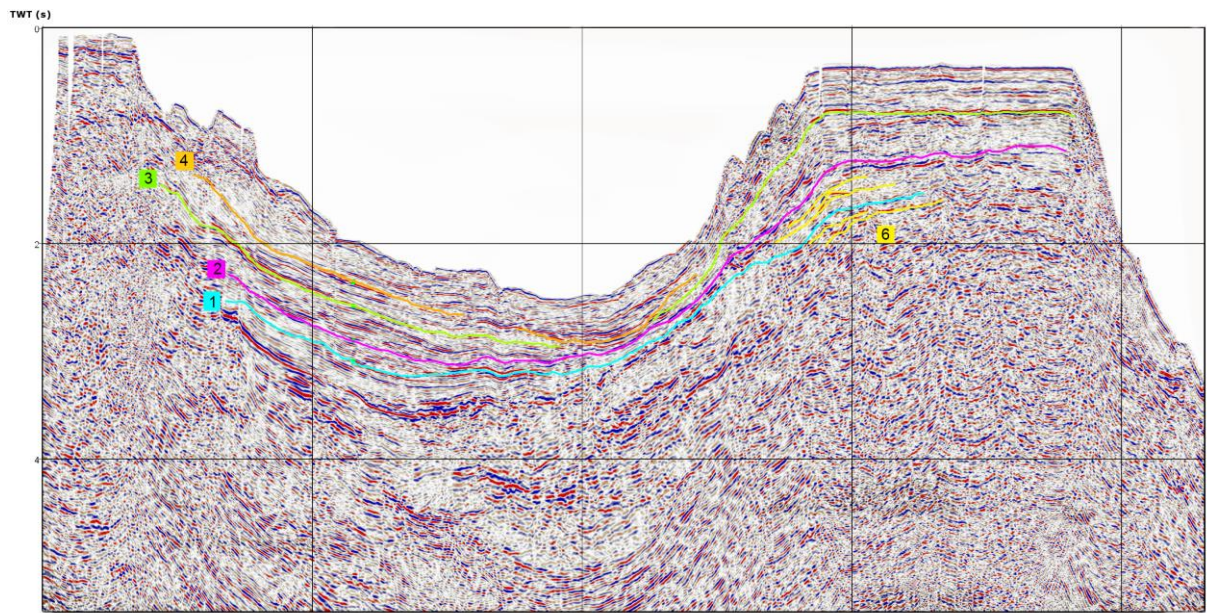


**Figure 21:** Interpreted seismic profile from Leplac Project, line 501 (JOVANE et al., 2016). Depth in seconds, TWT (Two-Way travel Time).

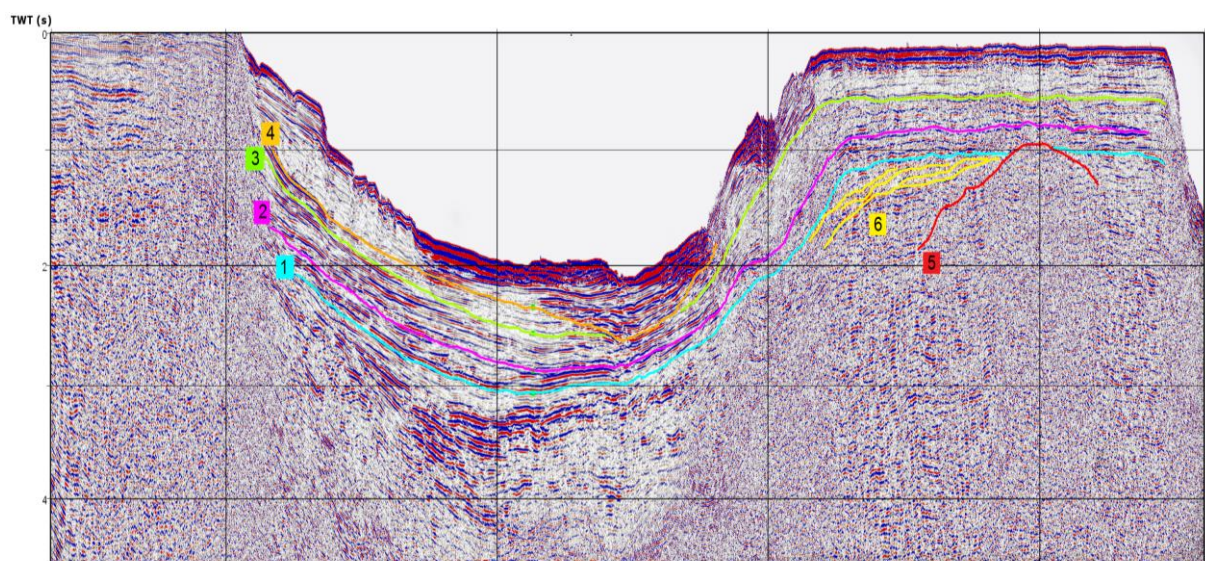


**Figure 22:** Interpreted seismic profile from ANP survey, line POT44 (JOVANE et al., 2016). Depth in seconds, TWT (Two-Way travel Time).



Seven interpreted seismic lines from WesternGeco (available in: [http://www.brasil-rounds.gov.br/arquivos/Seminarios\\_r11/tec\\_ambiental/Bacia\\_Potiguar.pdf](http://www.brasil-rounds.gov.br/arquivos/Seminarios_r11/tec_ambiental/Bacia_Potiguar.pdf)) were available on ANP website to characterize some exploratory blocks that were sold in ANP round 11. The line 17 is presented in figure 23.

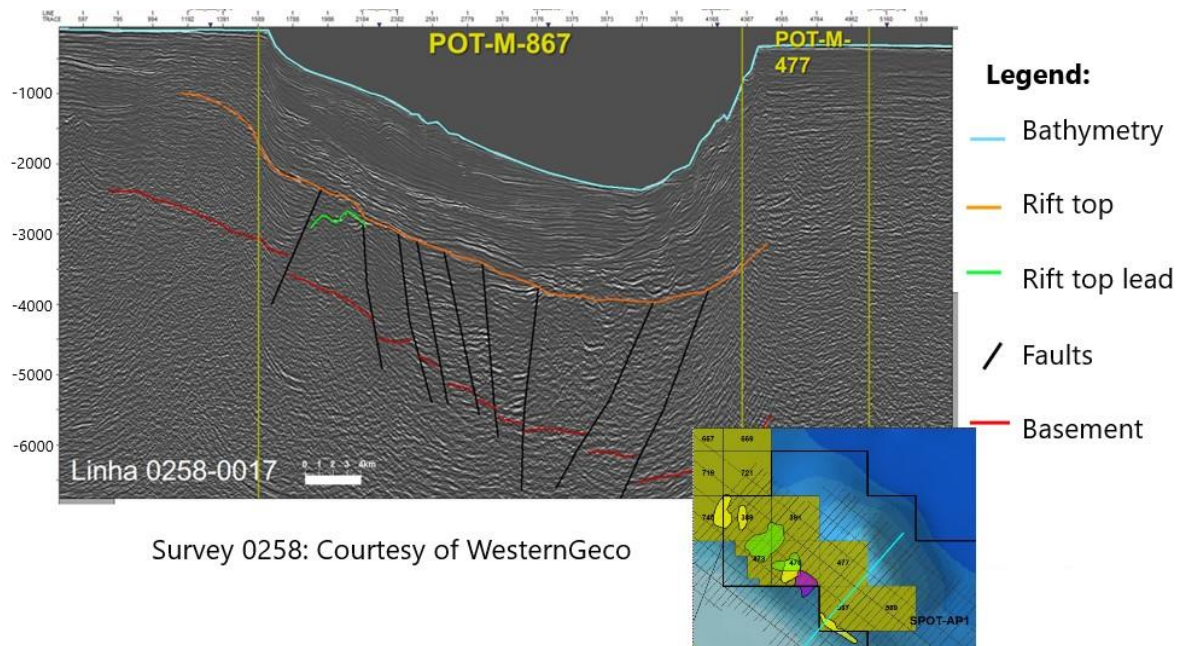


**Figure 23:** Interpreted seismic profile from WesternGeco, line 17. ANP round 11. Depth in meters.

#### 4.1.6 The gravimetric and geomagnetic global models

There are multiple global models for the gravimetric and geomagnetic fields. They are calculated with predicted physical models, satellite data, and some of them also use land, aeromagnetic and marine observed data.

The gravimetric model used in this study is composed by the ocean free-air anomalies with 1-minute grid data from Sandwell et al. (2014), and the land free-air anomaly is from EGM2008 (PAVLIS et al., 2008) (figure 24). This global model is one of the most recent global models. Its accuracy is about 2 mGal, as result of an altimeter derived gravity field.

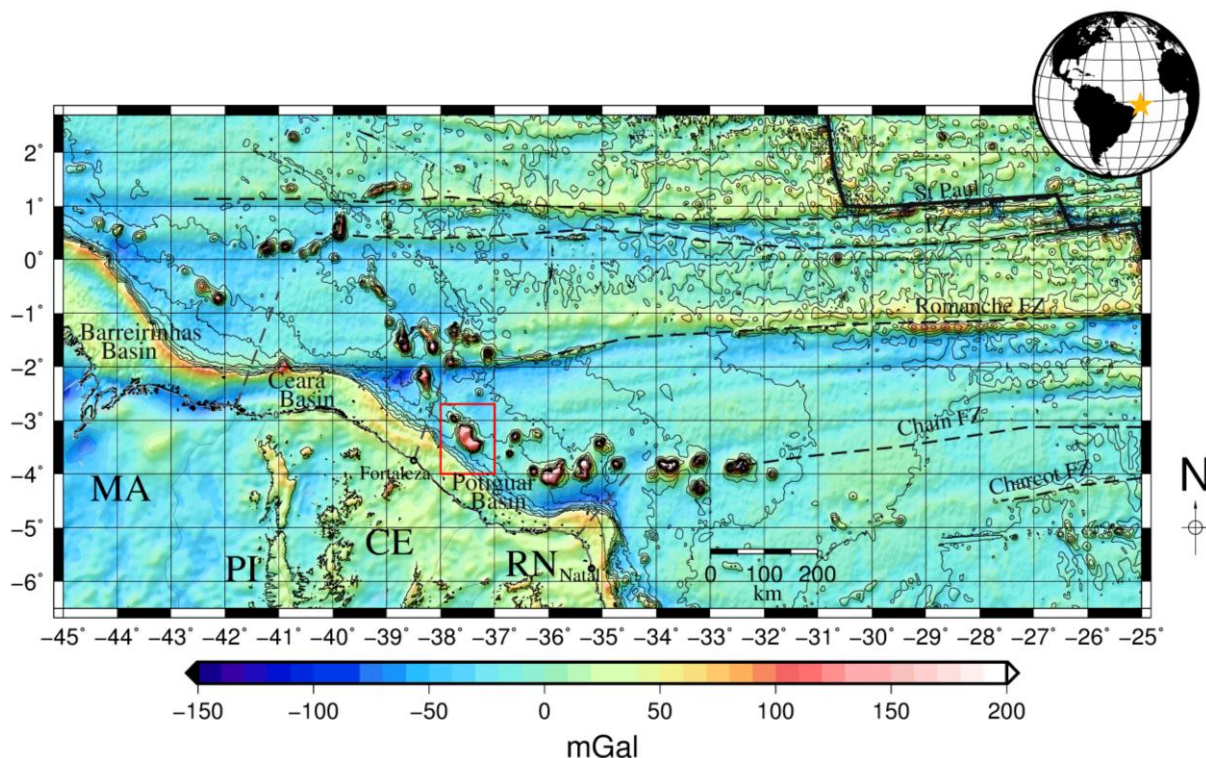


**Figure 24:** Gravimetric Anomaly of the Brazilian Equatorial Margin and the main features of the BEM. The red rectangle indicates the study area. Topobathymetric isolines each 500 m.

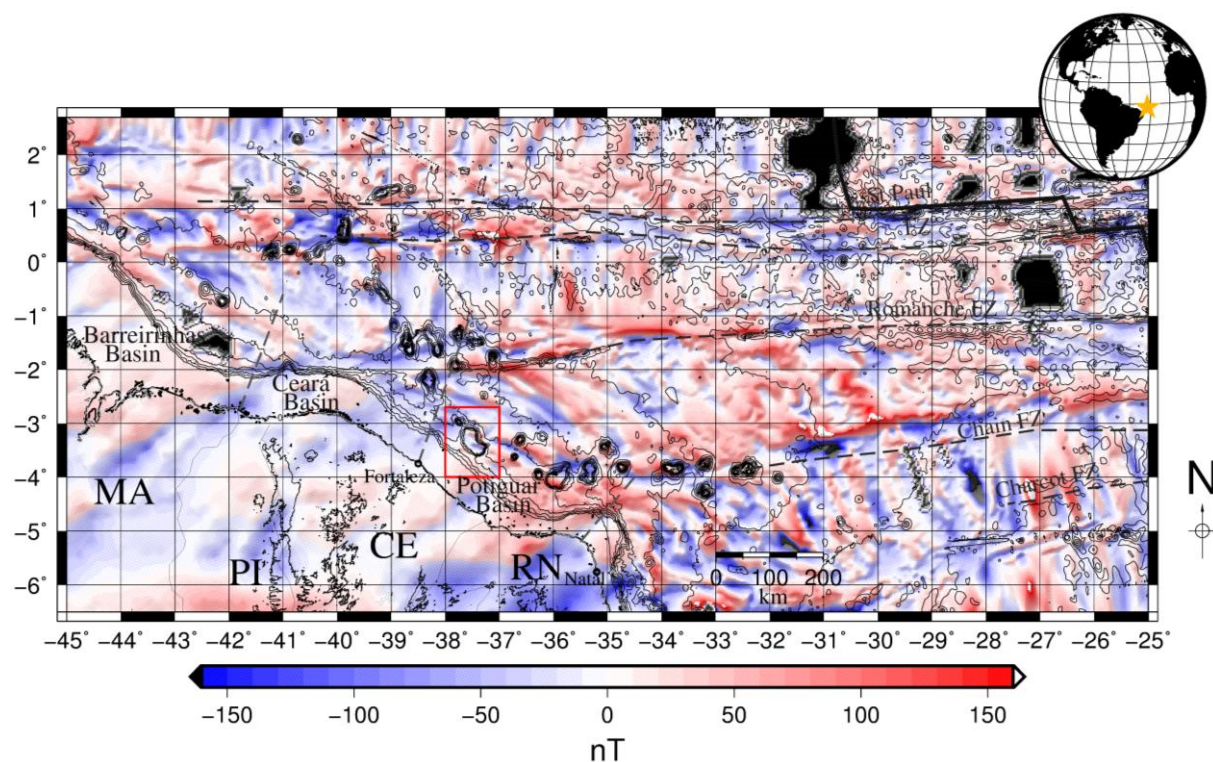


**Figure 25:** Magnetic Anomaly of the Brazilian Equatorial Margin, 2 arcmin grid data from EMAG2 v2. The red rectangle indicates the study area. Topobathymetric isolines each 500 m and the main features of the BEM.

The geomagnetic models are separated by the source of the field. The choice of the model depends on the objective of each study. It can be the main field, as the given by the IGRF (<https://www.ngdc.noaa.gov/IAGA/vmod/igrf.html>), used to correct the data in this study, an ionospheric field, and a grid with the anomalies from the crust, as the EMAG2 v2 (MAUS et al., 2009) (figure 25), used in this study. It is a model with 2-minute grid calculated 4 km above the mean sea level. On the ocean floor it is possible to identify some positive and negative anomalies, related to the geomagnetic pole reversal during the geological time.

## **4.2 Gravimetric data processing**

### **4.2.1 The gravimetric anomalies**

Gravity and magnetic methods are commonly referred to as potential field methods because the measurements involve a function of the observed field potential, either the terrestrial gravity or magnetic field, at the observation site. These methods provide subsurface information through the physical properties of the Earth. (HINZE et al., 2013).

The gravity method involves measurements of very small variations in the Earth's gravitational field, of the order of a few parts per million or lower, caused by lateral density variations. Gravity observations include the combined effects of instrumental, surface, terrain, and planetary sources in addition to the subsurface mass variations, that are the objective of an exploration gravity survey (HINZE et al., 2013).

The drifting correction: The first procedure with the gravity data is the correction of the drifting of the equipment. It is calculated with the differences between the start and the end of the survey, and it is related to the changes in the mechanic system of the gravimeter. The drifting of the Equant I was previous calculated with the gravimeter base tie made at Fortaleza.



The Eötvös correction: The movement direction of the ship implies in variations of the acceleration, which also needs to be removed from the data. This is called the Eötvös effect (eq. 1) explained by Dehlinger (1978). The Eötvös corrections were previously calculated in the available data from final 1 minute navigation samples.

The theoretical gravity correction: The theoretical gravity ( $\gamma$ ) is applied to remove the effect of the variation of the gravity acceleration with different latitudes, which modifies the gravity acceleration (SILVA, 1986 apud CASTRO, 1990). It is calculated assuming a conceptual model that describes the gravity at the observation site. The difference between the observed and the theoretical values is the gravity anomaly. The theoretical gravity corrections in this study were previously calculated using the IAGS 1967 formula (eq. 2) (NESS et al., 1989).

The free-air anomaly: In order to interpret the data some reductions of the gravity anomaly must be done. The free-air anomaly is the most basic of the anomalies used in geologic studies because unlike other anomalies no assumptions are made about the Earth's masses. The free-air correction removes the influence of the different altitudes, and each meter causes a 0.3086 mGal difference (eq. 3). Marine surveys, although, are already on the mean sea level, then, the gravity anomaly after the theoretical gravity removal is in fact the free-air anomaly. The first three corrections, drifting, Eötvös and theoretical gravity anomaly were made by the Equant I group.

The Bouguer anomaly: The second common reduction is the Bouguer correction. It removes from the free-air anomaly the gravity effect of a semi-infinite horizontal slab of the material with thickness  $H$  (eq. 4), in marine surveys this  $H$  is the bathymetry. The density used is the difference between the continental crust and the water densities, both values are international determined values, so it is possible to correlate different studies. The result is an anomaly that highlights the lateral density variations.

The variables of the three equations are listed in table 2.

$$E_C = (7.5 V \cos \alpha \sin \varphi + 0.004V^2) \quad (1)$$

$$\gamma_{1976} = (1 + 0.0053024 \sin^2 \alpha + 0.0000059 \sin^2 2\alpha) \quad (2)$$

$$g_{FA} = g - \gamma + 0.3086H \quad (3)$$

$$g_B = g_{FA} - 2\pi G\rho H \quad (4)$$

**Table 2:** Variables in the gravity equations.

Variable	Description
$E_C$	Eötvös correction (mGal)
$\alpha$	Latitude (°)
$\varphi$	Angle between the North and the vessel heading
$V$	Velocity of the vessel (knots)
$g_B$	Bouguer gravity anomaly (mGal)
$g_{FA}$	Free-air gravity anomaly (mGal)
$g$	Observed gravity (mGal)
$\gamma$	Theoretical gravity model (mGal)
$H$	Orthometric height (m)
$2\pi G\rho H$	Bouguer correction (mGal)
$0.3086H$	Free-air correction (mGal)
$G$	Gravitational constant = $6.67428(67) \times 10^{-11} \text{ m}^3 \text{ kg s}^2$
$\rho$	Density ( $\rho_C - \rho_W$ )
$\rho_C$	Crust density (2.67 g/cm <sup>3</sup> )
$\rho_W$	Sea water density (1.024 g/cm <sup>3</sup> )

### 4.2.2 The regional-residual separation

After the observed data are reduced to the anomaly form, only the effects of unknown subsurface mass variations remain, that are liable to a process that isolates or enhances the anomalies of interest in the particular survey. This step is called regional-residual separation. Isolation and enhancement procedures effectively serve as filters to minimize the effect of short-wavelength noise and long-wavelength regional anomalies upon the anomalies of interest.

Oceanic gravity surveys commonly use free-air anomalies to analyze and to model the geologic structures, while land surveys use the Bouguer anomalies (HINZE et al., 2013).

Once the free-air anomaly interpretation requires some strategies in order to define a model compatible with the observed data, the regional-residual separation seems to serve as a tool to highlight and individualize the anomalies of interest. This procedure is very discussed in gravimetry, because it is not exclusive. There are several methods to estimate the regional trend and the choice depends on the interpreter, so the geologic overview helps a lot with it.

The common methods to do the regional calculation are: the frequency filters to remove the shallowest sources, as for example, the upward continuation (JACOBSEN, 1987), and the polynomial adjustment through profiles and trend surfaces with the least square method.

The Ceará Plateau is a large structure, which is able to create a gravimetric anomaly with high wavelength, hindering the regional calculations on the anomaly grid by upward continuations or frequency filters. Also, it is located in a complex region, near to the COB, which has itself a density difference. Therefore, this study does not remove the regional component of the free-air anomaly. It considered the deep structures as well the shallow ones to make the models. It is the same procedure adopted in a previous study (CASTRO, 1990).



### 4.2.3 The Bouguer anomaly

The Equant I data are already reduced to the free-air anomaly. The calculation of the Bouguer anomaly is done using the equation 4 (figure 26). In continental areas the Bouguer correction is calculated with the mean density of the crust,  $2.67 \text{ g/cm}^3$ . The Bouguer anomaly in this work is not used to model, but it is a useful tool to help the interpretation.

Offshore surveys use the difference between the mean crust density and the seawater density to calculate the Bouguer anomaly. By using the bathymetry, the effect of the Bouguer slab, that is removed from the data with this approach, gives to the oceans large positive values, because the anomalies include the effect of filling the ocean with rock (DEHLINGER, 1978).

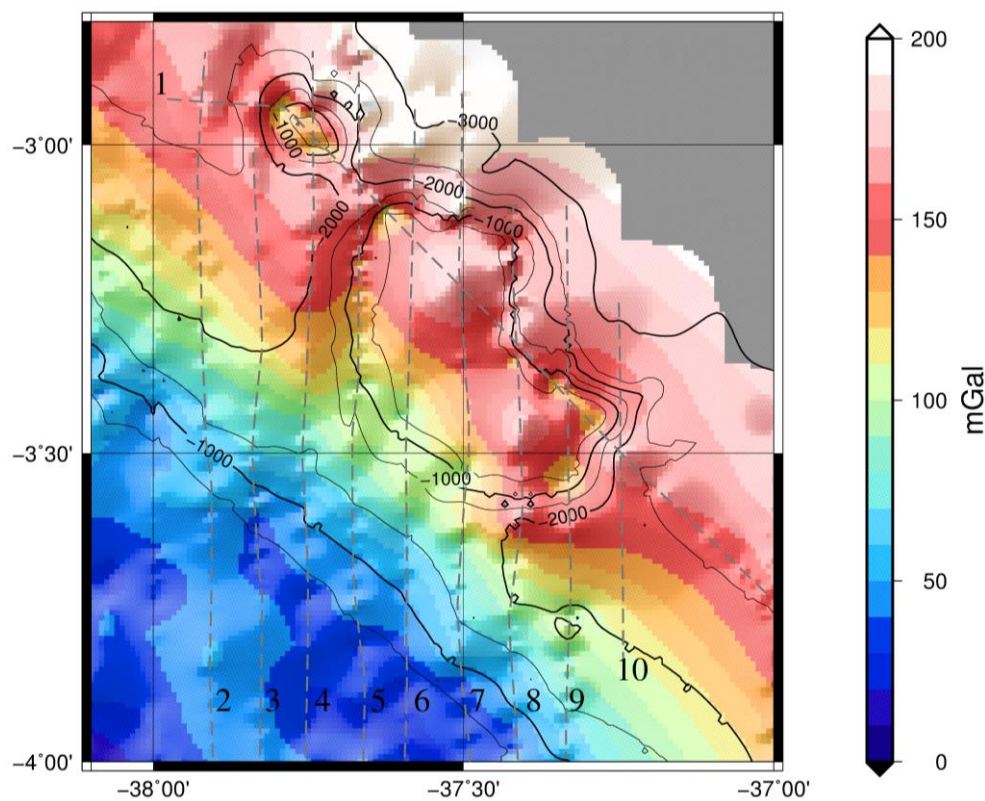


**Figure 26:** Bouguer anomaly map of the Ceará Plateau. Grid interval of 30 seconds (approximately 900 m). Bathymetric contour each 500 m.

Although the regional-residual separation has not been applied in the free-air anomaly, it has been used to interpret the Bouguer anomaly. The long wavelength related to the mantle, or the Mohorovičić discontinuity, is apparently removed as the regional component (figure 27). The regional grid is calculated by the software Oasis Montaj using a 10 km upward filter. The residual Bouguer anomaly map (figure 28) enhances the two positive anomalies inside the Plateau, and the negative anomaly of the Iracema Guyot and around the Plateau, indicative of the presence of a root or sediments, or both. The specific negative Bouguer anomaly is usually present in seamounts, caused by the flexure of the lithosphere (figure 29).

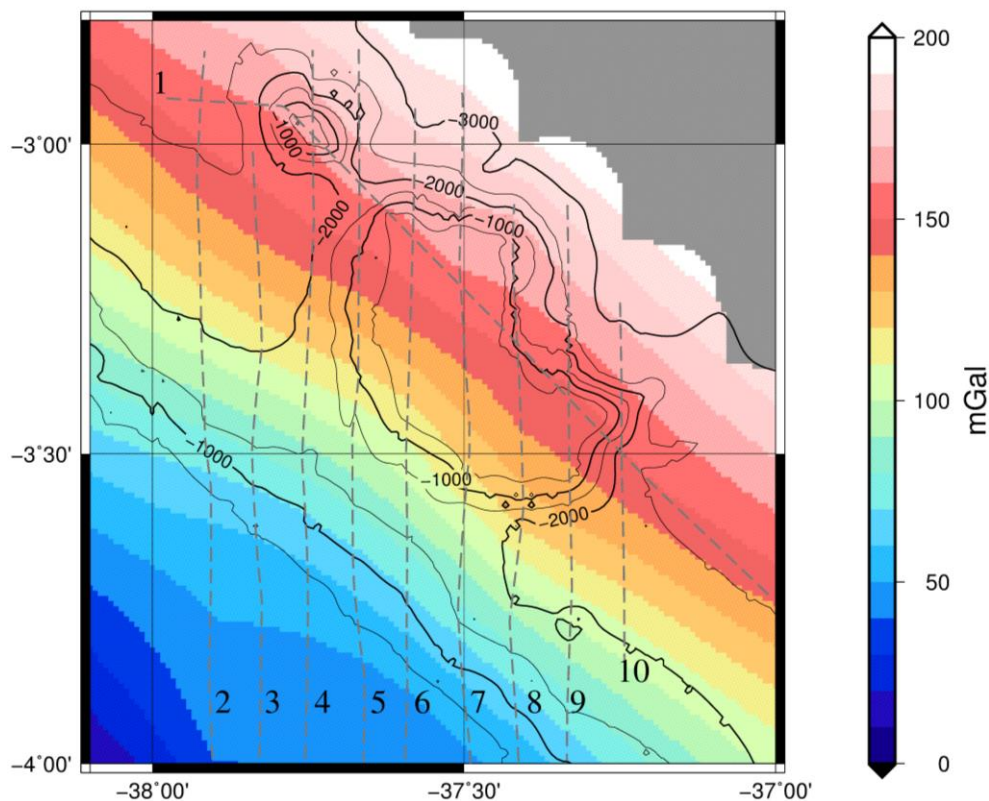


**Figure 27:** Regional Bouguer anomaly map (10 km upward continuation) of the Ceará Plateau. Grid interval of 30 seconds (approximately 900 m). Bathymetric contour each 500 m.

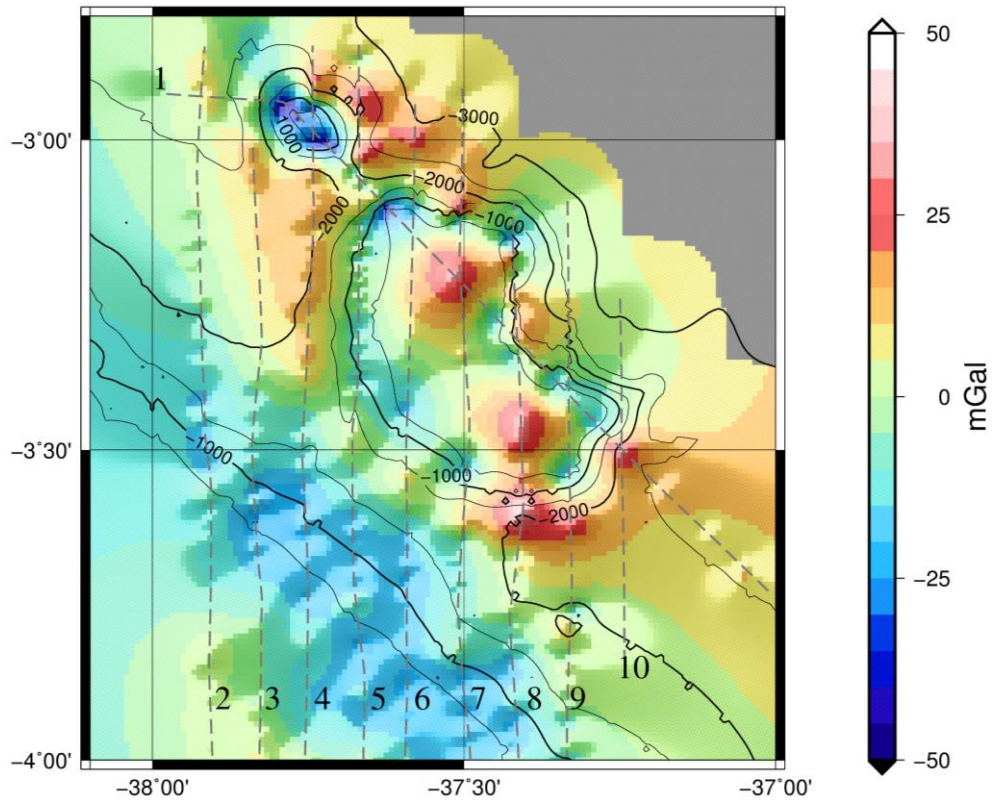


**Figure 28:** Residual Bouguer anomaly map of the Ceará Plateau. Grid interval of 30 seconds (approximately 900 m). Bathymetric contour each 500 m.

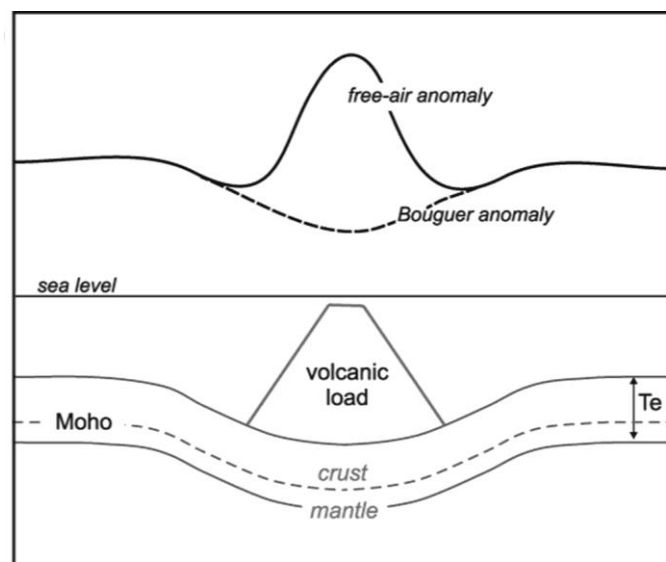


**Figure 29:** Schematic free-air and Bouguer anomaly of a load (USSAMI et al., 2012).

#### 4.2.4 The isostatic compensation

The isostasy explains how the topographic variations and loads are sustained by the lithosphere. The word isostasy means “equal standing”, i.e., it is the equilibrium condition to which the Earth’s crust and mantle tend to. It is a very debated theme until nowadays. Some hypotheses have been proposed to calculate the physical response of the loads at the Earth.

The Pratt hypothesis: To calculate the attraction of the Himalaya, Pratt (1854 apud WATTS, 2001) had proposed that the Earth is rigid, and the density varies laterally under each load (figure 30b) and it is enough to sustain it. So, the compensation is achieved locally.

The Airy hypothesis: One year later Airy (1855 apud WATTS 2001) proposed another way for the masses equilibrium. He proposed that there is a variation on the compensation level instead of lateral density variations (figure 30a). This hypothesis assumes that the crust has no rigidity, so the compensation of the load pressure is also local.

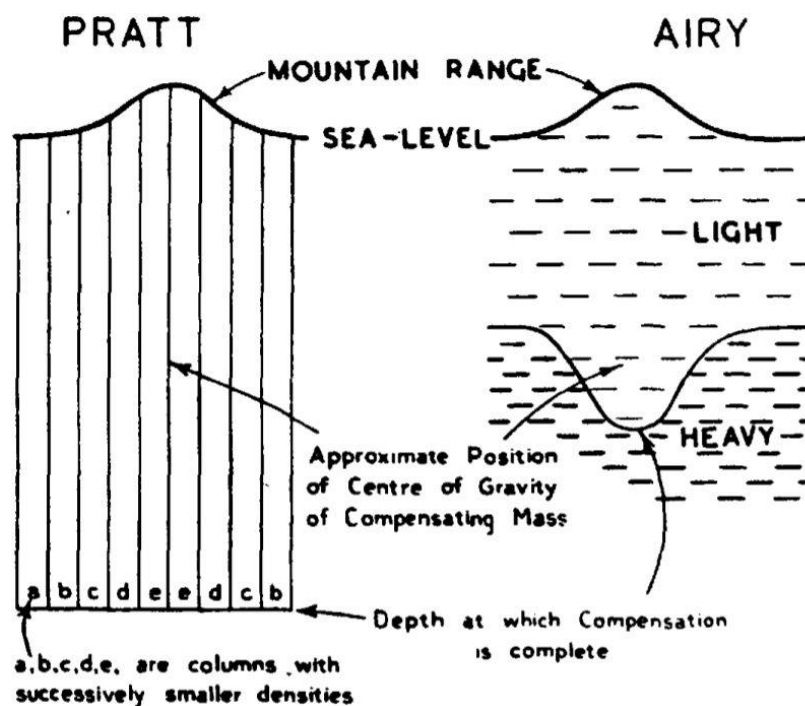


**Figure 30:** Pratt and Airy models for isostatic compensation of topographic loads (EVANS and CROMPTON, 1946).

Flexure: The flexural model considers that the compensation of the loads on the crust is not local, but regional. Vening Meinesz (1941 apud Watts 2001) suggested that the load creates a flexure on the crust dependent on the load weight and the rigidity of the crust. This model is solved considering the flexure of a thin elastic plate, as stated by equation 4, where the parameter that controls the lithosphere flexure, the flexural rigidity, is given by the relation 5.

$$D \frac{d^4 w}{dx^4} = V(x) - H \frac{d^2 w}{dx^2} \quad (4)$$

$$D = \frac{ETe^3}{12(1 - \nu^2)} \quad (5)$$

$D$  is the flexural rigidity;  $E$  is the Young's modulus, whose value is between 10 and 100 GPa for continental and oceanic crust;  $T_e$  is the effective elastic thickness;  $\nu$  is the Poisson's ratio, between 0.1 and 0.4;  $w$  is the plate deflection;  $V$  is the vertical force and  $H$  is the horizontal forces. If the flexural rigidity ( $D$ ) is zero, this model is equivalent to Airy's hypothesis.

Considering the Ceará Plateau as the load, it is possible to evaluate the maximum and minimum deflection. The maximum deflection can be estimated with the Airy model application. For the Ceará Plateau it is calculated with the eq. 6 (figure 31).

$$d \rho_w + h \rho_c + r \rho_m = (d + h + r) \rho_c \quad (6)$$

With  $d = 2000\text{m}$ ;  $h = 10000\text{m}$ ;  $\rho_w = 1024 \text{ kg/m}^3$ ;  $\rho_c = 2850 \text{ kg/m}^3$ ;  $\rho_m = 3300 \text{ kg/m}^3$ . The root thickness is equal 8100 m. The depth limit or the Mohorovičić discontinuity, considering the whole water column and the oceanic crust, is 25.5 km for the Airy hypothesis.

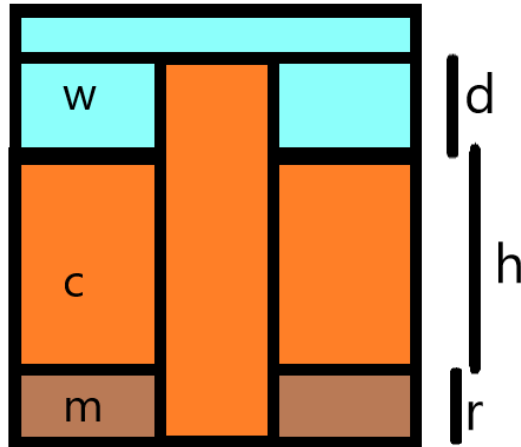


**Figure 31:** Scheme for the application of the Airy hypothesis at the Cear  Plateau.  $w$  is the seawater;  $c$  is the oceanic crust;  $m$  is the mantle;  $d$  is the seawater column;  $h$  is the oceanic crust normal thickness;  $r$  is the Cear  Plateau root.

The crustal thickness for the Potiguar Basin, according to Oliveira (2008), is near to 10 km for the Cear  Plateau region, 5 km in the east part of the Potiguar Basin. Assump o et al. (2013) also present an anomaly in the crustal thickness near the study area: it is lower than the surrounding area.

According to Watts et al. (2017), 10 km of oceanic crustal thickness creates a response on an order of 2.5x the height of the load. The Cear  Plateau is 2000 m high. Then, the root is expected to be 5000 m thick, according to this supposition. And this may be the minimum estimate for the root.

There is no specific and detailed study about the crustal thickness of the Cear  Plateau. Its age formation is also unknown, which made the estimation of the root more difficult. A root thickness variation between 5 km and 8 km is considered for this study.

#### 4.2.5 The 2D gravity modelling

The ship track data is better analyzed in profiles than in map surfaces, due to the sampling distribution. Seven profiles (figure 17): 2, 4, 5, 6, 7, 8 and 9, are used to create the gravimetric models. Due to the data distribution along the Ceará Plateau we can use the gravimetric and magnetic modelling.

The 2D forward models along these profiles are performed with the GRAVMAG software (PEDLEY et al., 1993 and updated by JONES, 2012). The software calculates the gravity effect for structures of infinite strike length and polygonal cross-section using the solution of Talwani et al. (1959).

#### 4.2.6 Parameters of the gravity 2D modelling

In order to model the continental and oceanic crust, it is necessary to analyze the physic limitations to avoid a geological unreachable model. The parameters calculated here or from previous studies are:

The mean thickness of the oceanic crust without a seamount: Assumpção et al. (2013) presented discrete values to the Mohorovičić discontinuity in the Ceará Basin in the order of 15 km, that is at the same distance from the continental shelf as the Ceará Plateau area. Castro et al. (1990) have also considered 15 km to his models for the Potiguar Basin.

The mean thickness of the oceanic crust below the Ceará Plateau: The Bouguer anomaly maps (figure 26 and 28) indicate lateral variations in density around the plateau and in the Iracema Guyot. As cited before, it can be an indicative of a root, a volume with lower density below the structure (figure 29) to compensate the load. As detailed in 4.2.4, the maximum root thickness considered is 8 km and the minimum is 5 km. Adding the whole water column and the oceanic crust, the depth of the root is estimated between 23 and 25 km.

The mean thickness of the continental crust: The thickness of the continental crust is the limit of the model, and below this depth it is assumed that the mantle is homogeneous, and its effect has already been removed by the normal gravity. The value considered is 26 km, as calculated by Oliveira (2008), considering the flexure of the lithosphere, for the same area. With gravity models for the North Brazilian Margin, Nóbrega (2008) indicates that this is the minimum value for the thickness near the COB, and it certainly increases quickly. Castro (1990) developed gravity models in the area with an upper continental crust of 10-15 km thickness and the total continental crust thickness of an order of 35 km, but he considered a larger area than the one used in this study.

The mean thickness of the sediments: The sediments thickness is analyzed in some seismic interpreted profiles from the 258 survey by WesternGeco (available in: [http://www.brasil-rounds.gov.br/arquivos/Seminarios\\_r11/tec\\_ambiental/Bacia\\_Potiguar.pdf](http://www.brasil-rounds.gov.br/arquivos/Seminarios_r11/tec_ambiental/Bacia_Potiguar.pdf)) (figure 23). The direction of the lines is NE-SW, while the Equant I profiles are N-S. The crossing points of the lines are analyzed and the thickness of the sediments in the same positions are used.

The mean sediment thickness above the gravimetric anomaly high: The sediment thickness above the gravimetric anomaly is estimated by the seismic lines (figures 21 and 22). The basement high is considered 1 second deep, in a two-way-time profile, considering the values presented by Hamilton (1971) for sound velocity in marine sediments. It is assumed a 1530 m/s velocity for the seawater and 1650 m/s for the sediments. The mean depth of the basement is 800 m, or 500 m sediment thickness, subtracting the 300 m water column. However, the seismic lines do not cross the maximum of the gravity anomaly that is about 3 km away. The approximated depth considered is 700 m and the sediment thickness 400 m.

The sediments density: The density for the sediments is estimated by a hole in the Ceará Basin, the 1CES-0112-CE, drilled in 1993 by ANP. The principal lithology are shale, marl, siltstone and sandstone. The measured densities varied



between 2 and 3.2 g/cm<sup>3</sup>. The average density is 2.2 g/cm<sup>3</sup>. These are the sediments densities assumed for the continental and oceanic sediment layers.

Crustal and mantle densities: The densities of the crust and the mantle for the Equatorial Margin are not unique. The Mohriak (1998) and Jilinsk et al. (2013) density estimates for gravity modelling and Nóbrega (2011) for time-depth conversion are used here. A 2.7 g/cm<sup>3</sup> density was assumed for the continental upper crust, 2.8 g/cm<sup>3</sup> for the continental lower crust, 2.8 g/cm<sup>3</sup> for the transitional crust, 2.85 g/cm<sup>3</sup> for the oceanic crust and 3.2 g/cm<sup>3</sup> for the mantle.

Expected geologic features: The modelling follows the Jilinks et al. (2013) gravity model for the African Equatorial Margin (figure 10), the Brazilian conjugate margin.

### **4.3 Geomagnetic data processing**

#### **4.3.1 The geomagnetic field sources**

The magnetic method is similar to the gravity method, since a planetary field is also measured, which is in this case, the Earth's magnetic field. As in the gravity method, the magnetic measurements include effects from a wide variety of sources, natural, as planetary, external and crustal, and man-made surface features, as well as instrumental, which vary spatially and temporally. These sources have a range of amplitudes and periods in the case of temporal variations and wavelengths in spatial contributions which can mask or at least distort magnetic effects from subsurface sources of interest in a survey.

The diurnal correction: The highly dynamic external fields due to the interaction with solar wind contributes with most of the remaining field. This effect is removed from the data by the diurnal variation in quiet days, collected by a shore-based magnetic base-station and Brazilian observatory data (NESS et al. 1989).

Solar storm days are hardly corrected, mainly in Equatorial areas. At this region the influence of the external components is stronger, because of the Equatorial Electrojet: tidal winds move the conducting ionosphere across the Earth's magnetic field lines and produce currents in the same system (FORBES, 1981). The Equant I survey was realized in 1987, and during this year the Magnetic Equator was closest to the Ceará Plateau than nowadays (figure 32). This proximity may have caused more spikes and interferences during the processing of the first data. The available magnetic anomalies are already corrected for daily variations. The low precision of 18 nT, reported by Ness et al. (1989), may be the result of those measuring conditions.

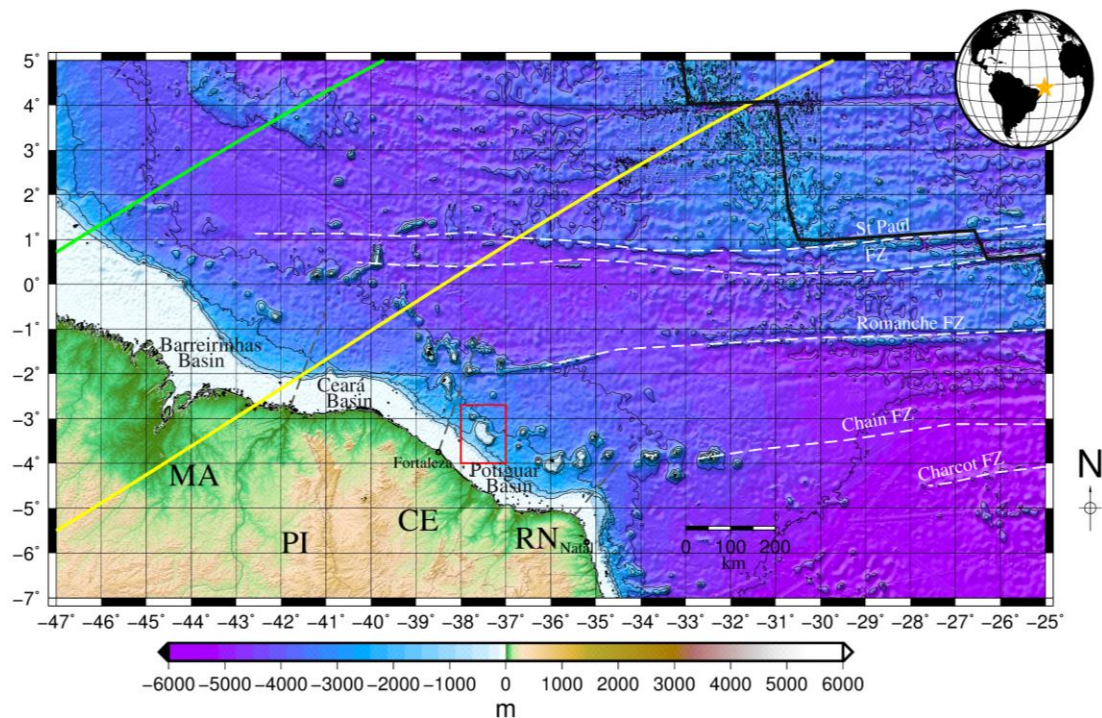


**Figure 32:** Regional map of the study area with the calculated Magnetic Equator in 1987 (yellow line) and in 2017 (green line). Data provided by Sony Su Chen (INPE – personal communication).

The IGRF correction: The main field of the Earth is generated by the movement of a conductive metallic liquid in the outer core of the Earth. It accounts for about 98% or more of the geomagnetic field (HINZE et al., 2013). Considering

the massive influence of the core field, in the treatment of the observed data, a model for this component should be removed, similarly to the gravimetric study.

Every half decade, since 1965, the IGRF (THÉBAULT et al., 2015) has been computed and internationally adopted, based on magnetic observatories and survey measurements. The IGRF models the secular variation of the main field. It should be applied considering the position and date of the survey. The core field and the secular variations have been removed from the data using the IGRF - 1985 correction (figure 33).

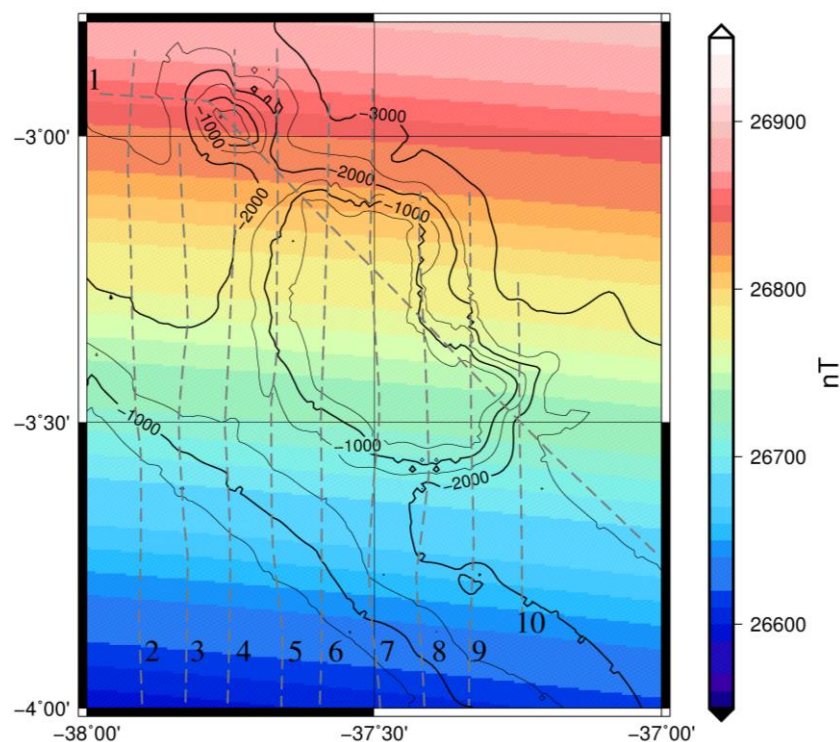


**Figure 33:** Magnetic core field calculation for 1987 with the IGRF model (Data available in: <https://www.ngdc.noaa.gov/geomag-web/#igrfgrid>). Regional removed from the observed data on Equant I Project. Grid interval of 30 seconds (approximately 900 m). Bathymetric contour each 500 m.

### 4.3.2 The geomagnetic anomalies

Superimposed to the main and external fields are the relatively minor static effects from subsurface magnetization contrasts that are of interest in exploration studies. The product of the diurnal correction and the IGRF correction is the magnetic anomaly, caused by objects of high magnetic susceptibility that become polarized or magnetized when they are present in the Earth's geomagnetic field (HINZE et al., 2013).

The magnetic anomalies are used to help to determine the compositional, structural and thermal properties, and thus the history of the Earth's crust. The magnetic anomalies observed at the surface are mostly caused by two different magnetization processes, the induced and the remanent magnetization. The first one is the result of the present magnetic field, while the remanent magnetization does not immediately disappear on the termination of the ambient magnetic field.

The most intense and stable remanent magnetization is the thermo-remanent magnetization (TRM) which is recorded upon a magmatic rock as it cools. The remanent magnetization is predominant at the oceanic crust, mainly the basalts layer. The geomagnetic field reverses through the time, and as its main component is dipolar, the remanent magnetization records these events in a linear pattern at the oceanic crust (figure 34), as strips of alternate polarities. As the ocean floor moves away from the mid ocean ridges and the geomagnetic field slowly changes with time the declination and the inclination of the field is registered in the basaltic layer as it cools off. This pattern was observed firstly by Vine and Matthews (1963) and Morley and Larochelle (1964). This special feature of the oceanic crust was a key issue in the formulation of the plate tectonic theory, suggesting the movement of the plates through time.

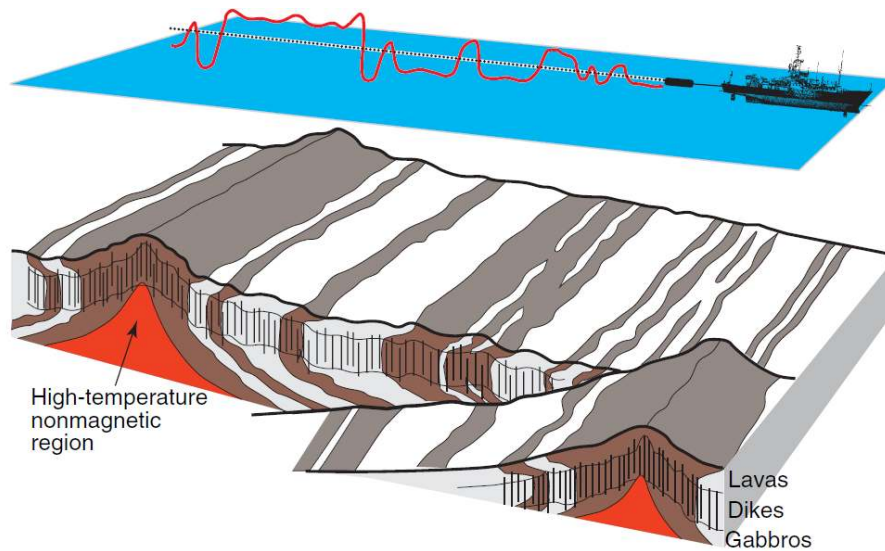


**Figure 34:** 3-D perspective cartoon of oceanic crust (JOHNSON et al., 1997 apud GEE and KENT, 2007) showing spreading centers separated by a transform fault and the theoretical profile recorded by a marine magnetometer. The three main layers of the oceanic crust are illustrated, also the Curie limit as the red area.

### 4.3.3 The Pole and the Equator reductions

The magnetic anomalies are dipolar; their shapes depend on various factors, as the magnetic latitude (figure 35). In order to centralize the anomaly over its source, it is possible to apply the reduction to the Pole (RTP), a mathematic filter that centralizes the anomaly highs over the sources. For places where the magnetic latitude is between  $+15^\circ$  to  $-15^\circ$  the Equator reduction (RTE) should be used. RTE is similar to RTP, but results in a negative anomaly above the source with a half-amplitude compared with RTP.

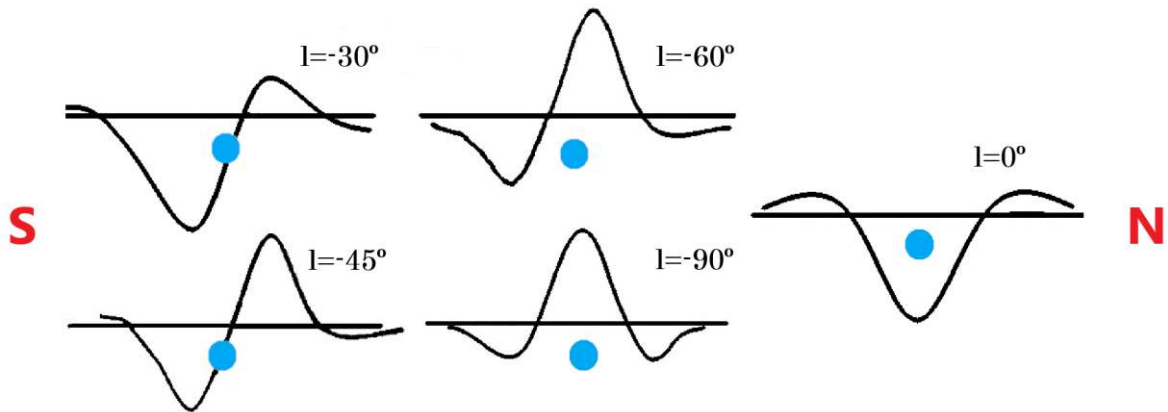


**Figure 35:** Magnetic anomaly created by a dipole in different magnetic latitudes at the Magnetic South hemisphere. The  $l=0$  indicates the anomaly over the Magnetic Equator and the  $l=90^\circ$  over the Magnetic Pole. (Modified from USSAMI, 2008).

The RTP centralizes the anomaly over the source, as in the latitude  $90^\circ$  in the figure 35. This study uses RTP to simplify the magnetic data analyses. In order to use this correction, it is necessary to consider that the predominant magnetization of the rocks is the induced magnetization, or the remanent magnetization with the same inclination and declination that the actual field. However, it presents numeric instabilities near to the Magnetic Equator, between magnetic latitudes of  $\pm 15^\circ$ , as it was the case for the Ceará Plateau during the Equant I expedition.

The RTE, in this case, is better, because it is more stable in these magnetic latitudes. The expected result is the same of dipole at the latitude  $0^\circ$  (figure 35). Both reductions are presented in this study (figure 36).



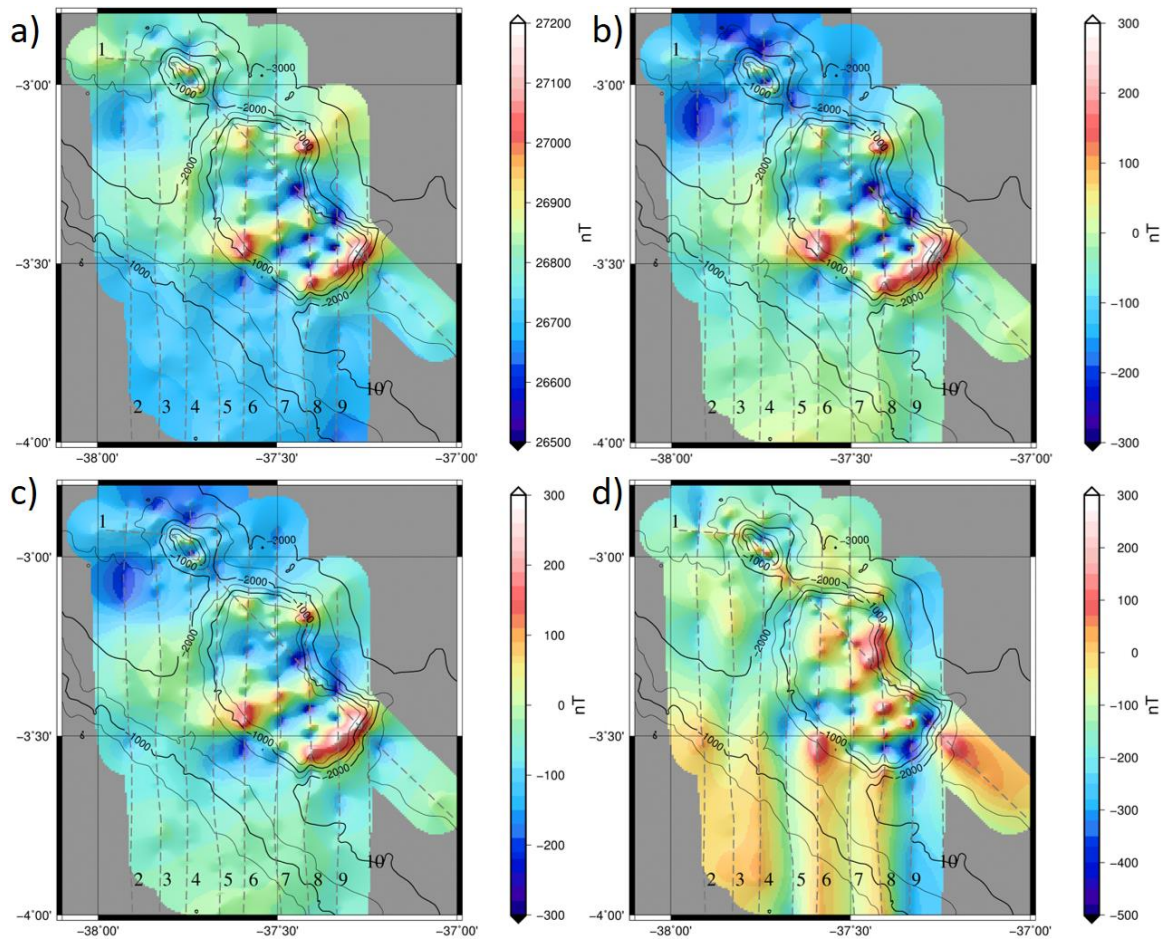


**Figure 36:** Magnetic anomalies. a) Total magnetic field. b) Magnetic anomaly. c) Magnetic anomaly reduced to the Equator. d) Magnetic anomaly reduced to the Pole. Grid interval of 20 seconds (approximately 620 m). Bathymetric contour each 500 m.

#### 4.3.4 Magnetic anomalies analyses

There are some methods to analyse the magnetic anomalies in order to determine the boundary and location of the source. On the magnetic anomalies of the Cear Plateau some techniques are used with the Oasis Montaj software:

The First-order Derivate of the magnetic anomaly in the y direction (figure 37b): This technique is helpful to estimate the source boundary. The first derivative is calculated in this study in the direction of the track lines to compare with the other methods, which centralizes the anomaly above the source. The calculation is made with eq. 7. The variable M is the magnetic anomaly.

$$FDy = \frac{\partial M}{\partial y} \quad (7)$$

The First Vertical Derivative of the RTP magnetic anomaly (figure 37c): The 1VD (first vertical derivative) is used to quantify the changes of the signal in the z direction. It is calculated with eq. 8 applied to the RTP. It is commonly used to enhance the shorter wavelength signal, highlighting the shallow sources.

$$1VD = \frac{\partial M}{\partial z} \quad (8)$$

Signum Transform of the RTP magnetic anomaly (figure 37d): The border of the sources can be identified by the point where the signal of the derivative changes from positive to negative or the other way around. In this study it is applied to the 1VD as the derivative function  $f$  on the eq. 9, as used by Souza and Ferreira (2012, 2013, 2015) and Oliveira et al. (2017). This technique defines the bodies which are the source of the magnetic anomalies.

$$ST = \begin{cases} \frac{f}{|f|} & f \neq 0 \\ -1 & f = 0 \end{cases} \quad (9)$$



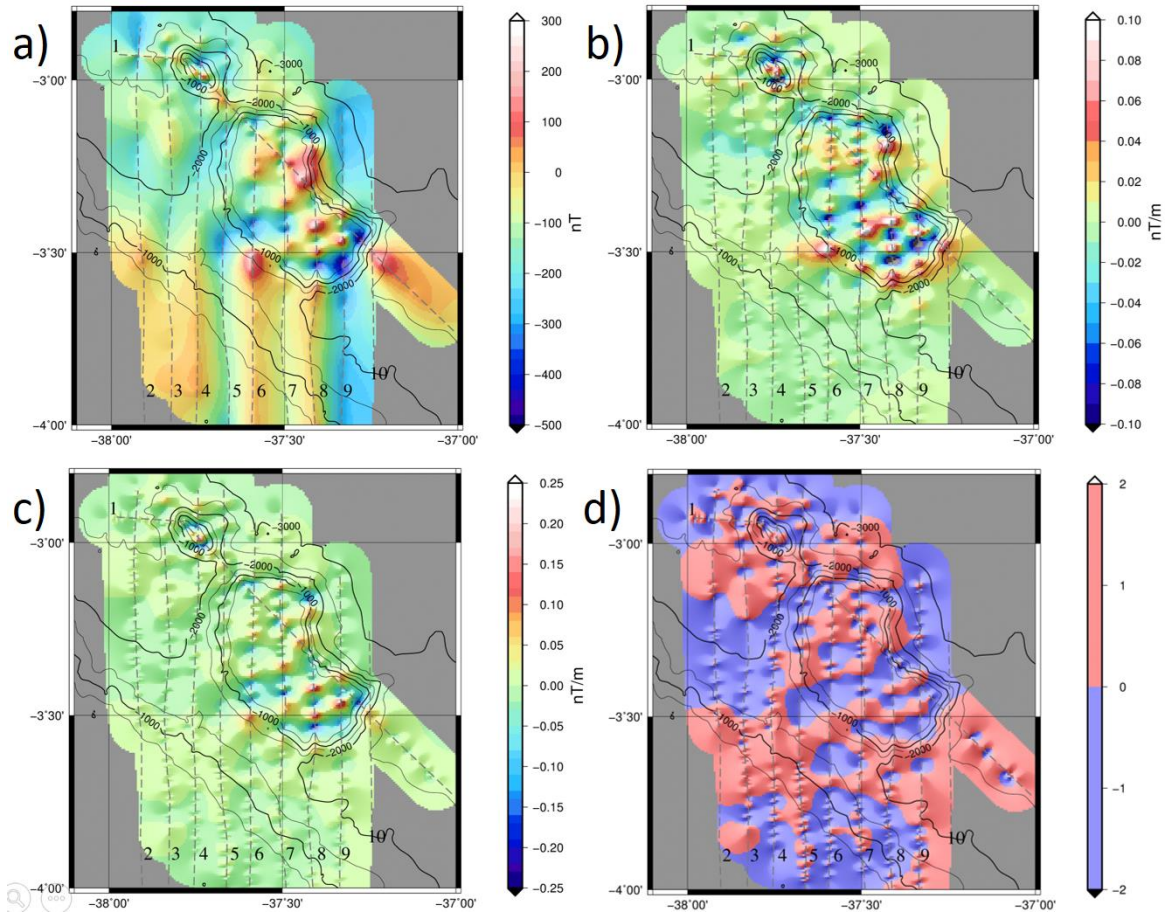


**Figure 37:** Magnetic anomalies filters. a) Magnetic anomaly RTP. b) First derivate in y of the magnetic anomaly. c) 1VD of the magnetic anomaly. d) Signum transform of the magnetic anomaly. Grid interval of 20 seconds (approximately 620 m). Bathymetric contour each 500 m.

Analytic Signal Amplitude (ASA) of the magnetic anomaly (figure 38): The method assumes that all causative bodies have uniform magnetization and a cross-section which can be represented by a polygon of either finite or infinite depth extent (NABIGHIAN, 1972; ROEST et al. 1992). The technique uses eq. 10. It is able to highlight the outlines of the sources, independently from the inclination and the declination of the magnetic field. The application of this method in the Ceará Plateau data highlights almost the whole structure, mainly the Southeast area.

$$ASA = \sqrt{\left(\frac{\partial M}{\partial x}\right)^2 + \left(\frac{\partial M}{\partial y}\right)^2 + \left(\frac{\partial M}{\partial z}\right)^2} \quad (10)$$

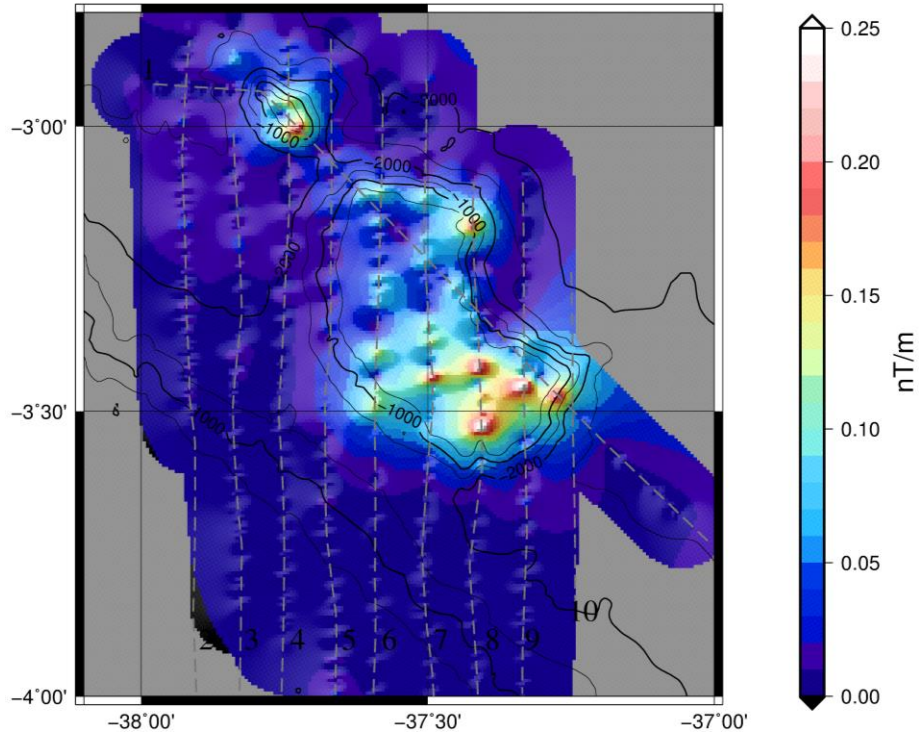


**Figure 38:** ASA of the magnetic anomaly of the Ceará Plateau. Grid interval of 20 seconds (approximately 620 m). Bathymetric contour each 500 m.

Magnetic Tilt Derivative or Tilt Angle (TDR) (figure 39a): The TDR is a useful transformation of potential field data for boundary detection (MILLER and SINGH, 1994). It is calculated with the eq. 11 applied to the RTP magnetic anomaly. This technique is not influenced by the depth of the source, so it is useful to highlight even the deep sources. The zero contour of the tilt is theoretically the outline of the body. In the figure 39a the zero is approximately the yellow contour.

$$\theta = \tan^{-1} \left( \frac{\partial M / \partial z}{\sqrt{\left(\frac{\partial M}{\partial x}\right)^2 + \left(\frac{\partial M}{\partial y}\right)^2}} \right) \quad (11)$$

Tilt Angle of the Total Horizontal Derivative (TAGH) (figure 39b): The Total Horizontal Derivative (THDR) eq. 12, is a useful and conventional derivative method to highlight the magnetic anomalies. Ferreira et al. (2013) proposed a technique to enhance the THDR using the TDR. The TAGH, eq. 13, ranges from  $+\pi/2$  to  $-\pi/2$ . The main attributes of this method are to provide maximal amplitudes on the source edges and equalize signals from shallow and deep sources (FERREIRA et al., 2013).

$$THDR = \sqrt{\left(\frac{\partial M}{\partial x}\right)^2 + \left(\frac{\partial M}{\partial y}\right)^2} \quad (12)$$

$$TAGH = \tan^{-1}\left(\frac{\frac{\partial THDR}{\partial z}}{\sqrt{\left(\frac{\partial THDR}{\partial x}\right)^2 + \left(\frac{\partial THDR}{\partial y}\right)^2}}\right) \quad (13)$$

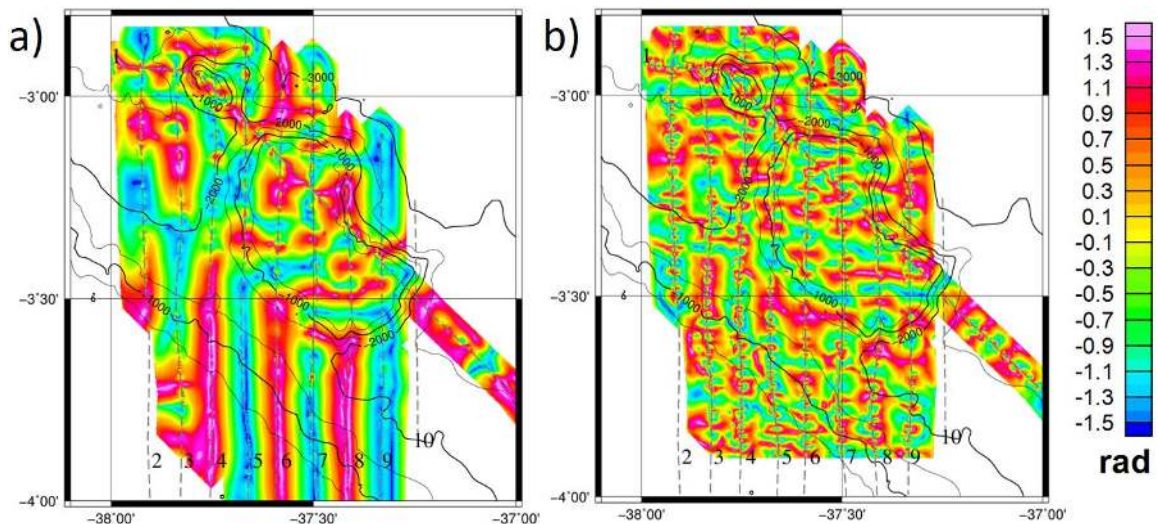


**Figure 39:** Other techniques to enhance the magnetic anomalies. a) Magnetic tilt derivative or tilt angle (TDR). b) Tilt angle of the horizontal derivative (TAGH). Grid interval of 20 seconds (approximately 620 m). Bathymetric contour each 500 m.

### 4.3.5 The magnetized layer modelling

There are several methods to model the gravity and the magnetic anomalies on Earth. The Ceará Plateau area is near to the Magnetic Equator (figure 32), which difficult the magnetic analyses, since in this region the intensity of the magnetic field is low, in 1987 during the survey, it was about 26770 nT (Calculated with the NGDC calculator: <https://www.ngdc.noaa.gov/geomag-web/#igrfwmm>).

It is adopted a magnetized layer modelling proposed by Maia et al. (2005) based on some sub-routines from Blakely (1996). Denise (2015) presented a application for this modelling to the Saint Peter and Saint Paul Archipelago.

The software needs the following parameters:

Magnetized layer thickness: The magnetic anomalies do not have deep sources because the rock magnetization needs a thermal stability. The limit for each rock is its Curie temperature; above it the thermal energy is stronger than the magnetic energy and the rocks cannot be magnetized. According to Tharimena et al. (2017) the average limit for a temperature of 500-600 °C in oceanic lithosphere with 120 Ma is about 30 km.

The layers of the oceanic crust are different, so their magnetization is not homogeneous. The first layer, extrusive or pillow lava layer is the main source of the magnetic anomalies, but the dyke and the gabbro layers also contribute with the magnetization (GEE and KENT, 2007). The mean thickness of the extrusive layer is about 500 m.

The crust around the Ceará Plateau is relatively old, and other magmatic sources as extrusive layers may be representative in the magnetic signal, so, it is considered a 1 km constant thickness layer for modelling. The top of the layer is considered the bathymetric surface.

Magnetization: For the estimation of the magnetization of the oceanic crust there is not a consensual methodology. There are no samples from the Ceará Plateau, so, it is decided to use published studies. Considering the Ceará Plateau was formed synchronously with the adjacent crust, values are chosen from a sample with similar age and position. The choice is a rock magnetized during the



Cretaceous Normal Superchron with 122 Ma, at the Pacific tectonic plate, located at 4°N with remanent magnetization of 5.9 A/m and the magnetization calculated at the Magnetic Equator of 4.2 A/m (global studies from JUARÉZ et al., 1998). Using those information, it is used 5 A/m for modelling the remanent magnetization.

Parameters of the magnetic field during the survey: The inclination and declination of the total magnetic field during the survey are calculated by the NGDC calculator (<https://www.ngdc.noaa.gov/geomag-web/#igrfwmm>):

$$\text{Inclination} = -7.2392^\circ$$

$$\text{Declination} = -21.4236^\circ$$

Age grid of the area: The estimated age for the oceanic crust is used from the NGDC data bank (MÜLLER et al., 2008) (figure 40).

Polarity grid of the area: The polarity inversions table used for the modelling is from Cande and Kent (1995) (figure 41).

The results from modelling are presented in figure 42. After the gravimetric modelling it was recalculated the magnetized layer modelling using the basement surface interpolated from the 2D gravity models.

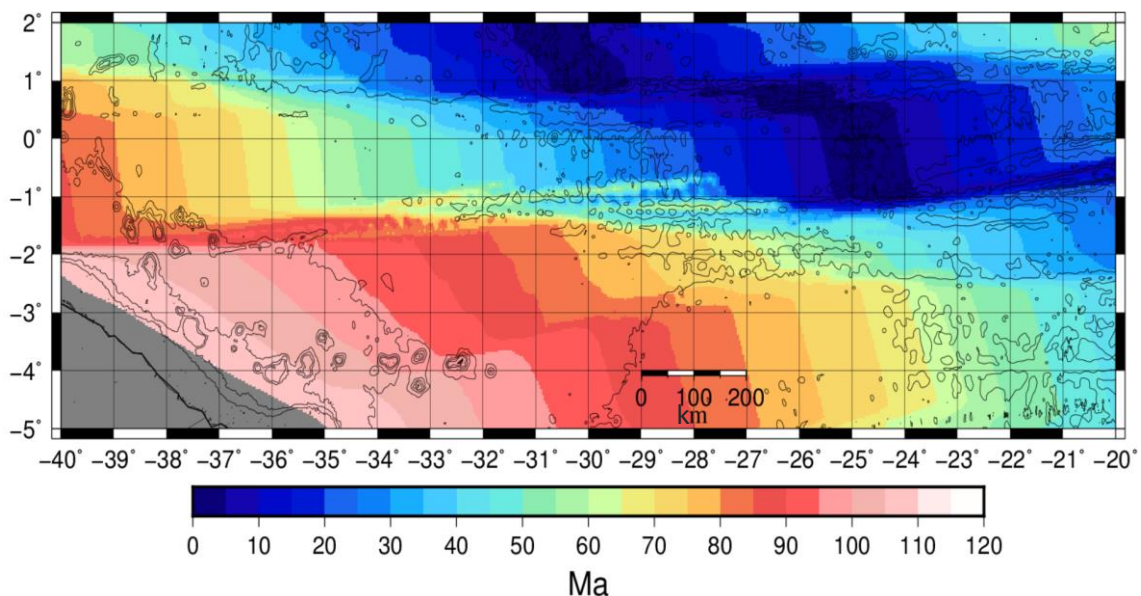


**Figure 40:** Age grid for the oceanic crust at the Equatorial Margin. Bathymetric contour each 1000 m. Grid interval of 30 seconds (approximately 900 m).

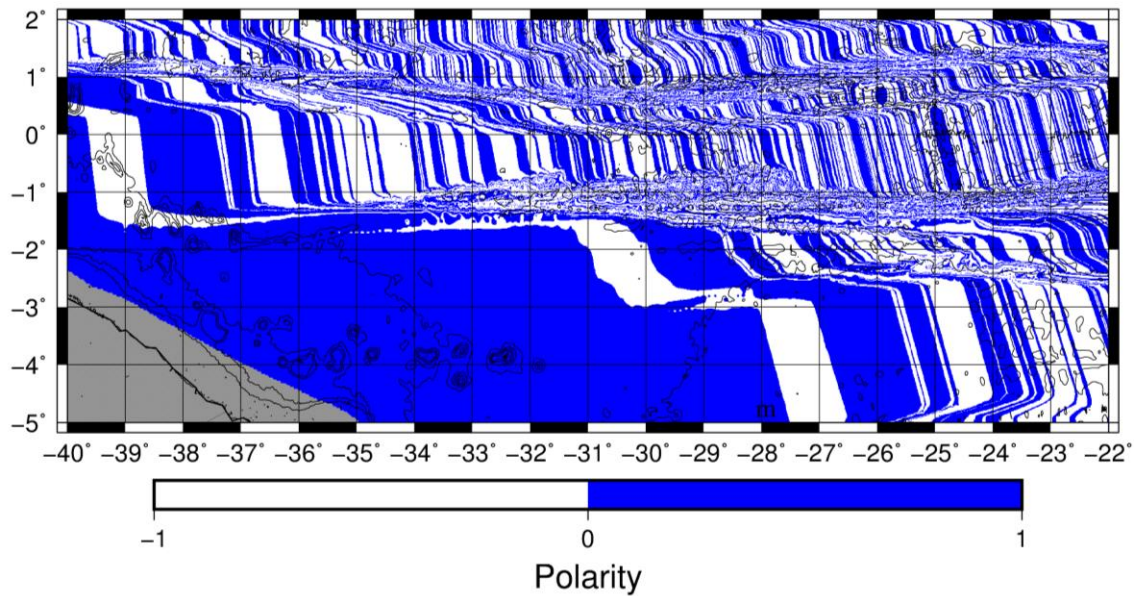


**Figure 41:** Magnetic polarity map for the oceanic crust at the Equatorial Margin. Bathymetric contour each 1000 m. Grid interval of 30 seconds (approximately 900 m).

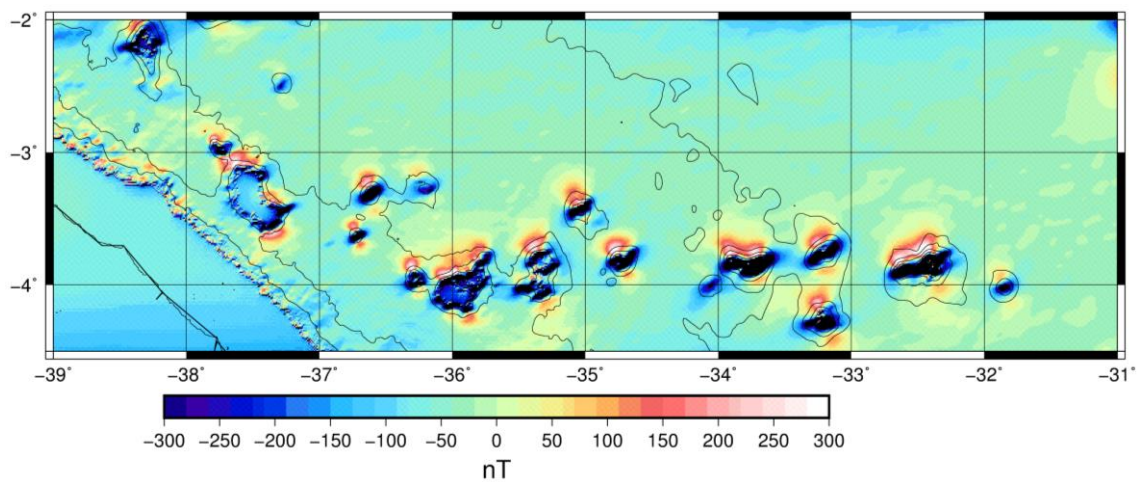


**Figure 42:** Modelled magnetic anomalies for the oceanic crust around the Ceará Plateau. Magnetized constant layer thickness of 1 km and magnetization of 5 A/m. Grid interval of 30 seconds (approximately 900 m). Same colour palette used in the magnetic anomaly map (figure 16 and 31b).

## 5. RESULTS

### 5.1 Analysis of the gravimetric data

#### 5.1.1 The gravimetric modelling

The 2D gravity modelling follows the parameters presented in 4.2.6. The seismic lines are very important to define the sediment thickness in different positions. The densities used are in table 3, and since the potential methods is quite ambiguous, the values choice could modify the thickness of the layers. This ambiguity is related to the correlation between the depth and the rock density or magnetization. The seven profiles modelled are presented in figures 43-49.

The geologic geometry used to model is based in Jikinski et al. (2013). The assumption that there is a transitional continental crust with higher density between the oceanic and the continental crust is widely accepted in rift margins as the Brazilian-African margin (MAGALHÃES, 2015; NÓBREGA, 2008). The high density is explained by the intrusive dykes that are formed during the initial stages of rifting (LIGI et al., 2011; KEIR et al., 2013). It is also accepted the idea that the mantle forms a denser region between the oceanic crust and the transitional crust (orange polygons with 3 g/cm<sup>3</sup>) as a response to the opening of the ocean, this tectonic behavior is presented by Péron-Pinvidic et al. (2017).

**Table 3:** Density values used in gravity models.

Geologic layer	Considered value (g/cm <sup>3</sup> )
Sediment	2.2
Upper continental crust	2.7
Lower continental crust	2.8
Transitional crust	2.8
Oceanic crust	2.85
Mantle	3.2
Mantle intrusion	3
Seawater	1.024

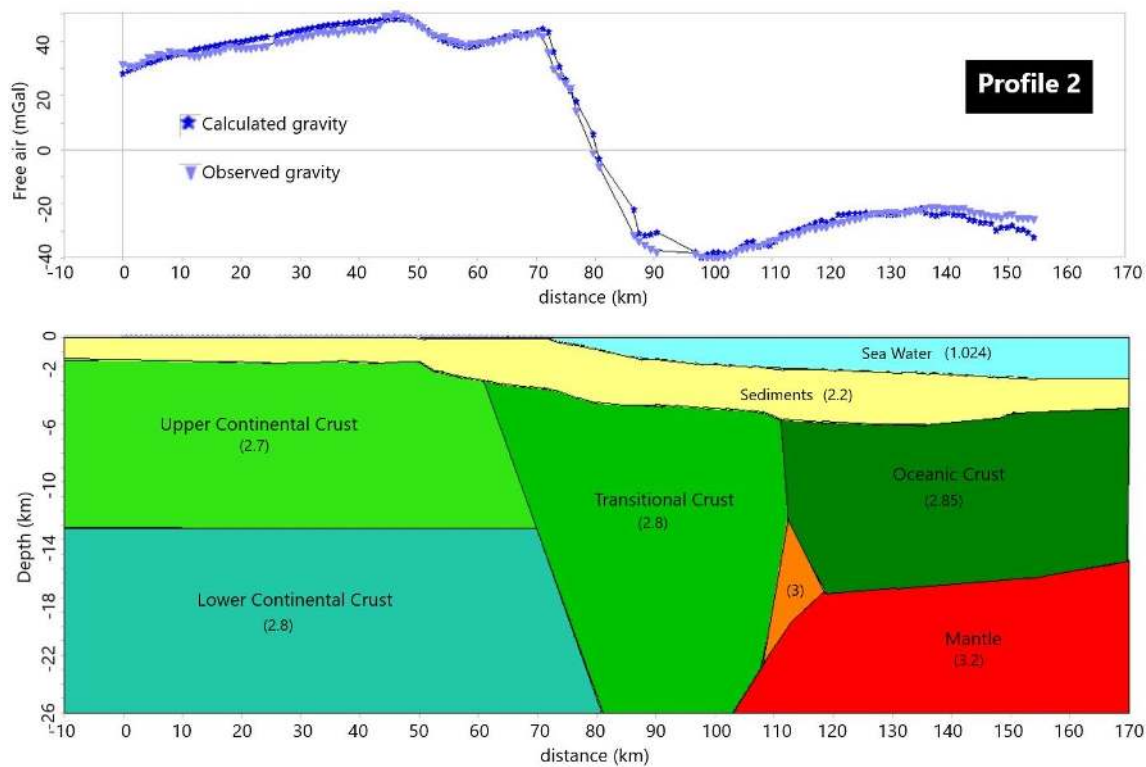


**Figure 43:** Gravimetric model of the profile 2 (S-N) with 2.5x vertical exaggeration. Densities in  $\text{g/cm}^3$ . The density is  $3.2 \text{ g/cm}^3$  below 26 km depth.

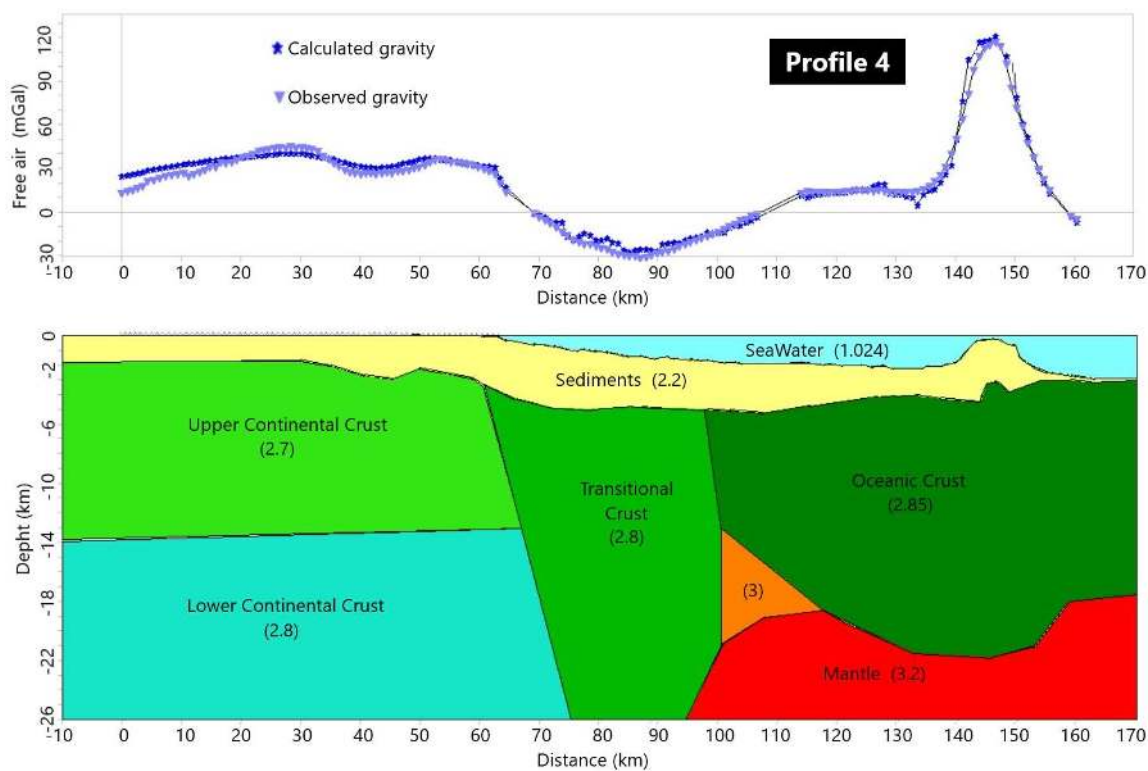


**Figure 44:** Gravimetric model of the profile 4 (S-N) with 2.5x vertical exaggeration. Densities in  $\text{g/cm}^3$ . The density is  $3.2 \text{ g/cm}^3$  below 26 km depth.



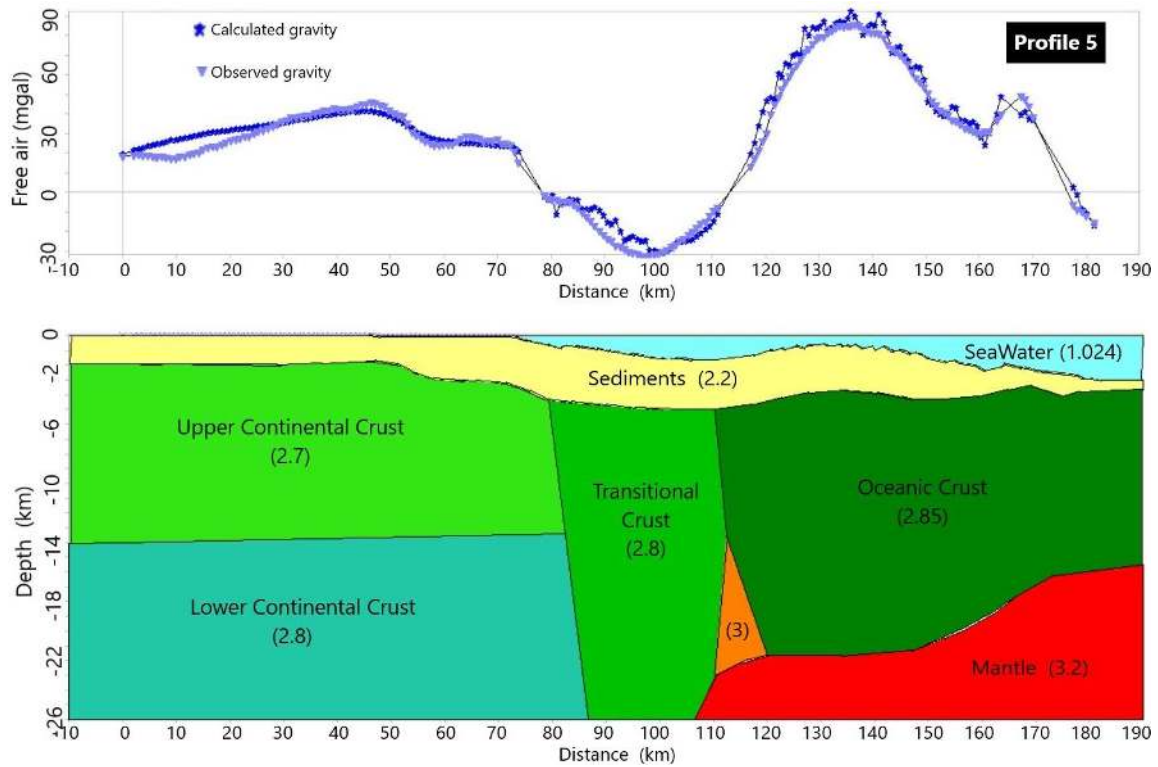


**Figure 45:** Gravimetric model of the profile 5 (S-N) with 2.8x vertical exaggeration. Densities in  $\text{g}/\text{cm}^3$ . The density is  $3.2 \text{ g}/\text{cm}^3$  below 26 km depth.

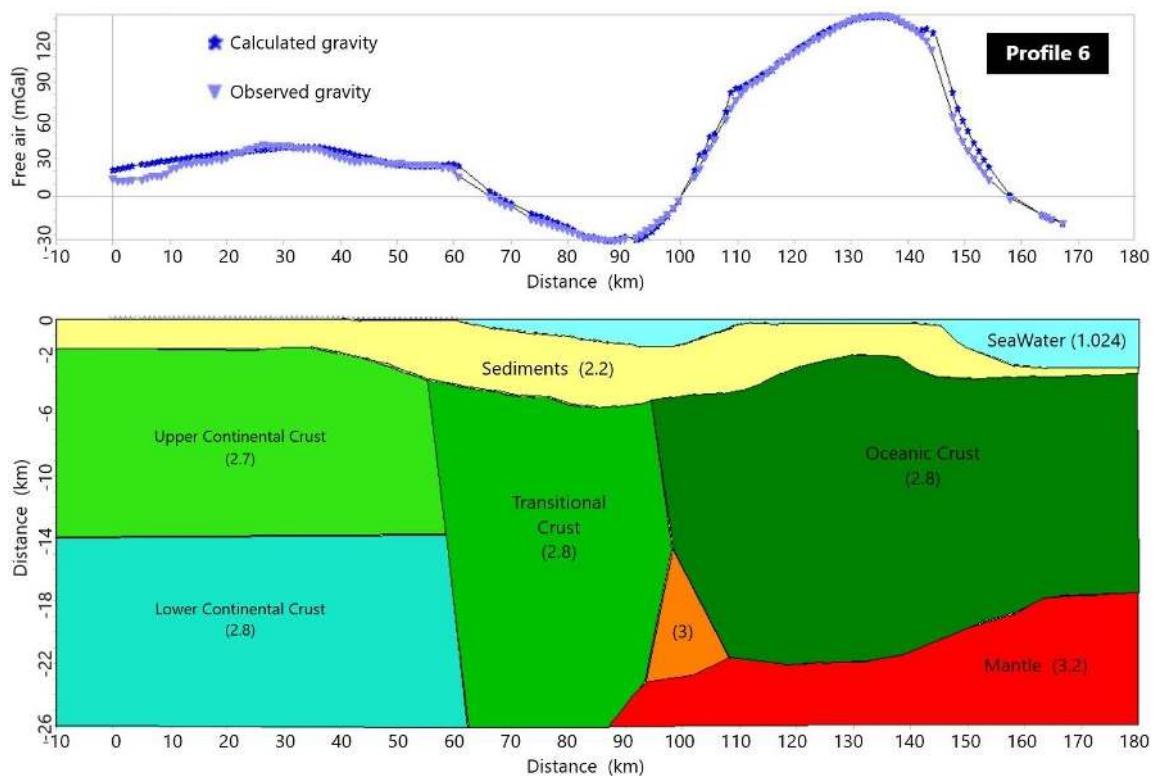


**Figure 46:** Gravimetric model of the profile 6 (S-N) with 2.6x vertical exaggeration. Densities in  $\text{g}/\text{cm}^3$ . The density is  $3.2 \text{ g}/\text{cm}^3$  below 26 km depth.

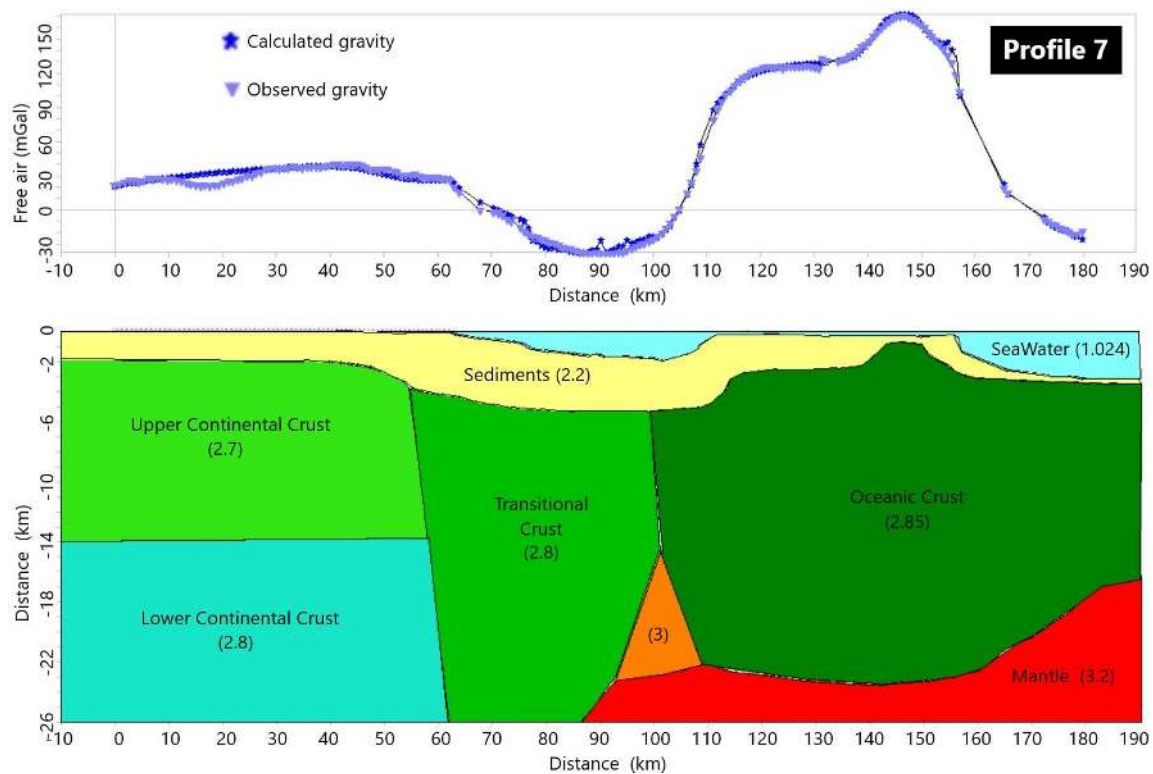


**Figure 47:** Gravimetric model of the profile 7 (S-N) with 2.8x vertical exaggeration. Densities in  $\text{g/cm}^3$ . The density is  $3.2 \text{ g/cm}^3$  below 26 km depth.

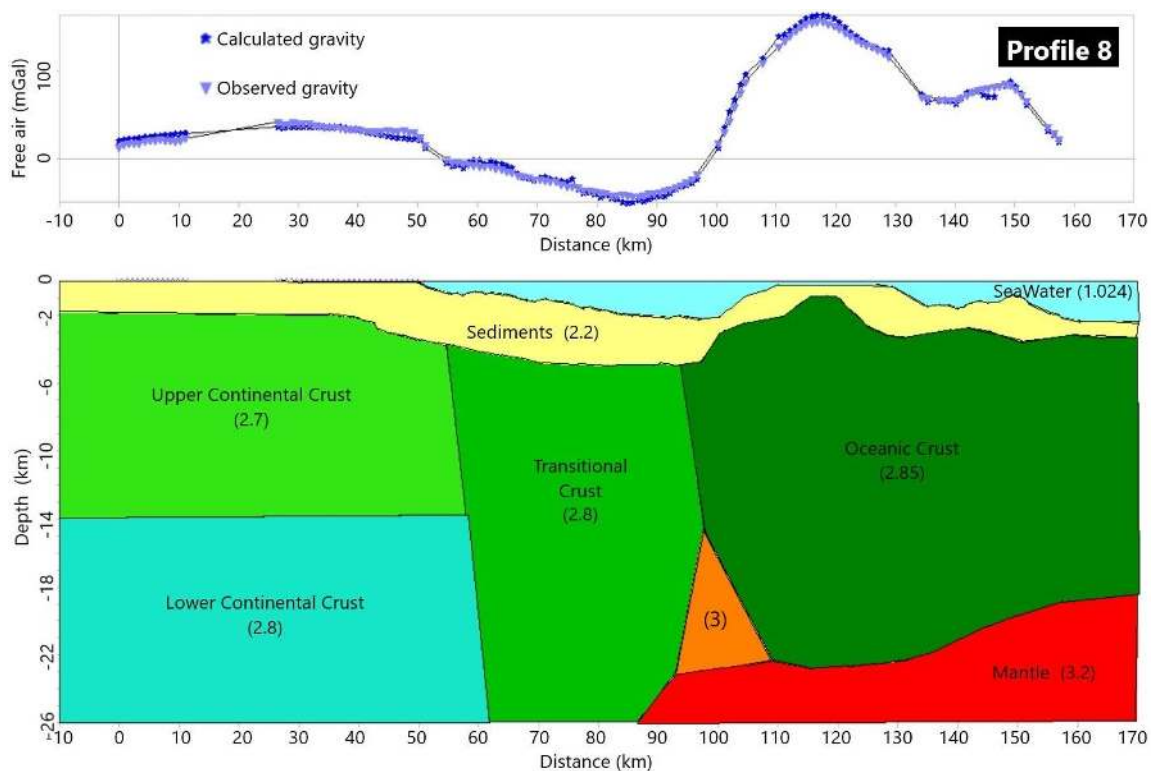


**Figure 48:** Gravimetric model of the profile 8 (S-N) with 2.5x vertical exaggeration. Densities in  $\text{g/cm}^3$ . The density is  $3.2 \text{ g/cm}^3$  below 26 km depth.

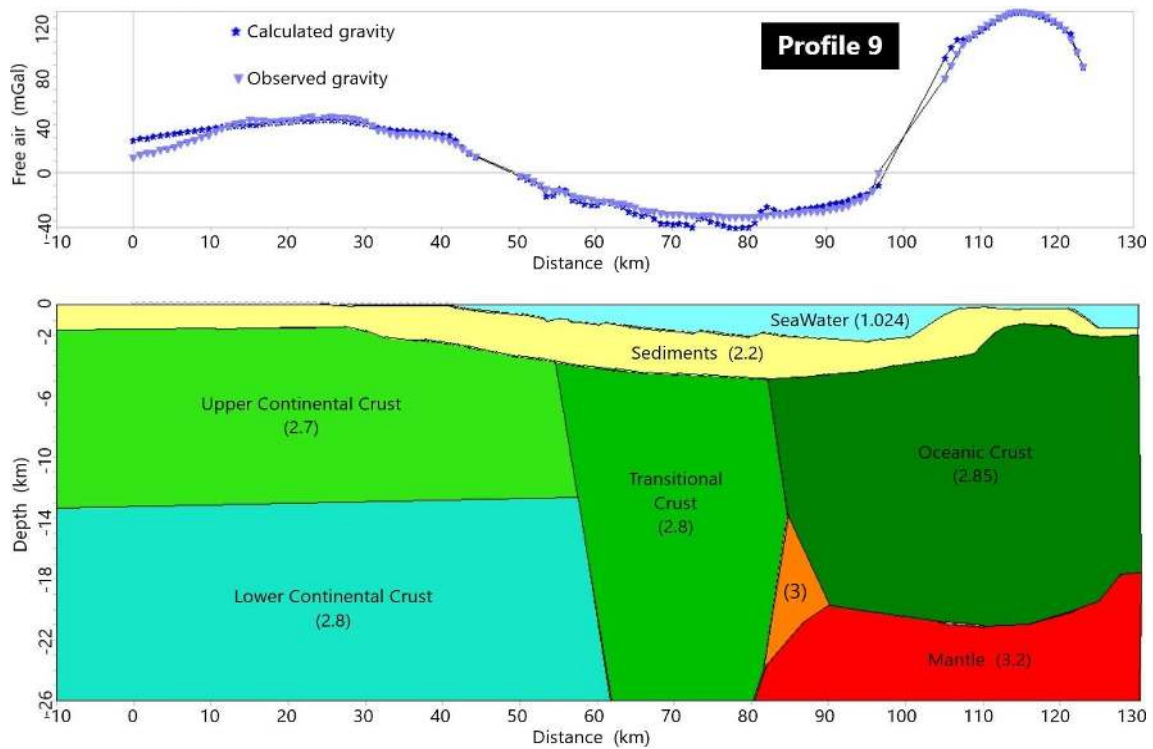


**Figure 49:** Gravimetric model of the profile 9 (S-N) with 1.9x vertical exaggeration. Densities in  $\text{g/cm}^3$ . The density is  $3.2 \text{ g/cm}^3$  below 26 km depth.

### 5.1.2 The basement and the Mohorovičić surfaces according to the gravity model

The seven profiles modelled with the free-air gravity anomaly of the Ceará Plateau (figures 43-49) are interpolated to create some maps (figures 50-53). The surfaces of the basement, and the Mohorovičić discontinuity are presented in figures 50 and 52, respectively. The sediment thickness calculated with the basement and the bathymetry is presented in figure 51. The crustal thickness calculated with the Mohorovičić discontinuity and the bathymetry is presented in figure 53. The location of the COB and the transitional crustal boundary are presented in the figures as red and yellow lines, respectively.

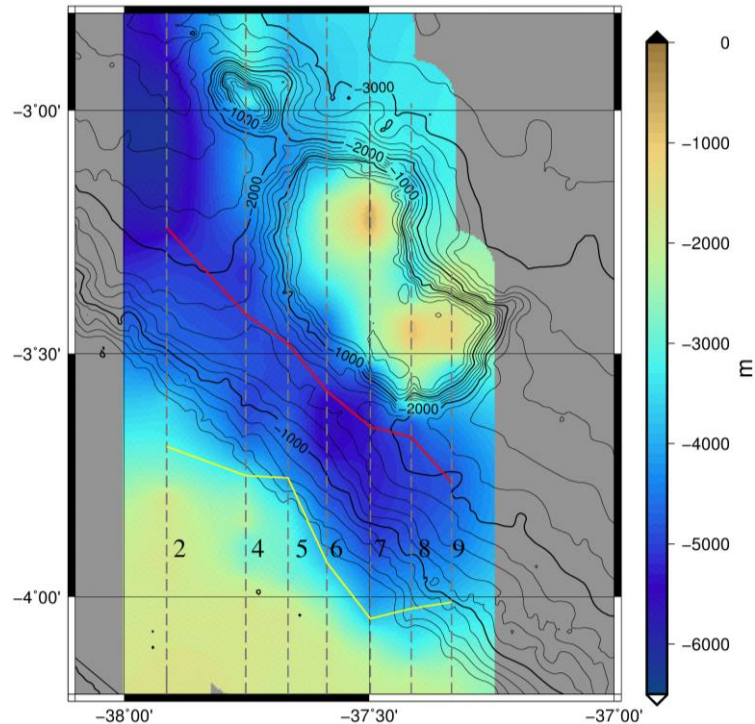


**Figure 50:** Basement of the Ceará Plateau area from the gravity 2D model. The red and the yellow lines are the COB and the limit between the thinned continental crust and the transitional crust, respectively. Grid interval of 15 seconds (approximately 450 m). Bathymetric contour each 500 m.

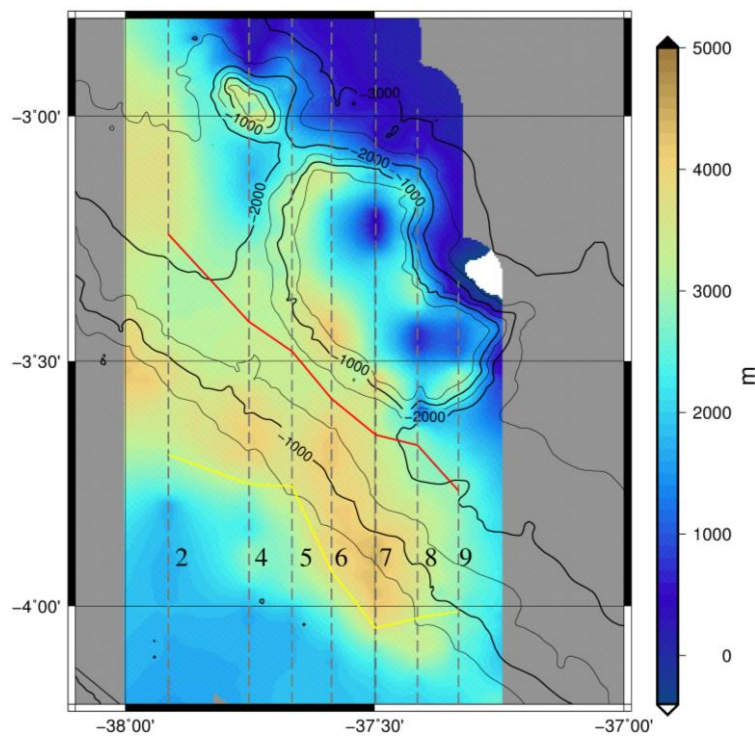


**Figure 51:** Sediment thickness of the Ceará Plateau area from the gravity 2D model. The red and the yellow lines are the COB and the limit between the thinned continental crust and the transitional crust, respectively. Grid interval of 15 seconds (approximately 450 m). Bathymetric contour each 500 m.



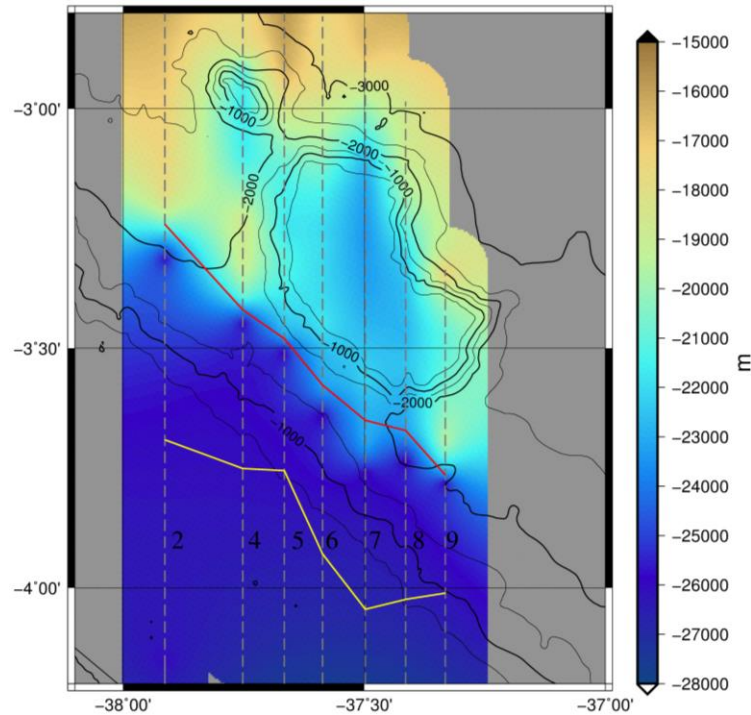


**Figure 52:** Mohorovičić discontinuity of the Ceará Plateau area from the gravity 2D model. The red and the yellow lines are the COB and the limit between the thinned continental crust and the transitional crust, respectively. Grid interval of 15 seconds (approximately 450 m). Bathymetric contour each 500 m.

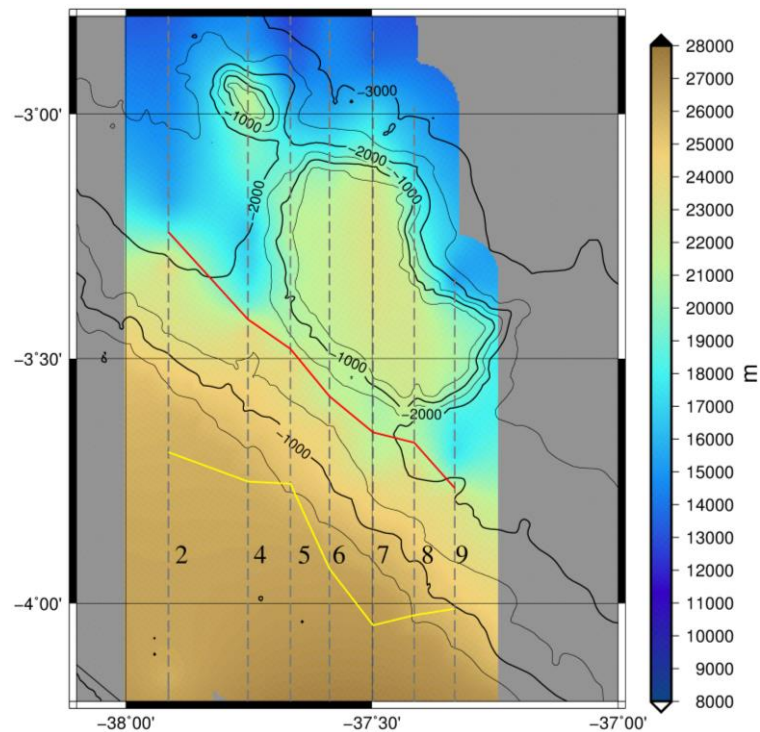


**Figure 53:** Crust thickness of the Ceará Plateau area from the gravity 2D model. The red and the yellow lines are the COB and the limit between the thinned continental crust and the transitional crust, respectively. Grid interval of 15 seconds (approximately 450 m). Bathymetric contour each 500 m.

## 5.2 Analysis of the magnetic data

### 5.2.1 The magnetic model

The result of the modelling presented in 4.3.5 is in figure 54 as a residual anomaly map. The residual anomaly amplitude is higher than the magnetic anomaly. It implies that the modelling is not reflecting the real situation.

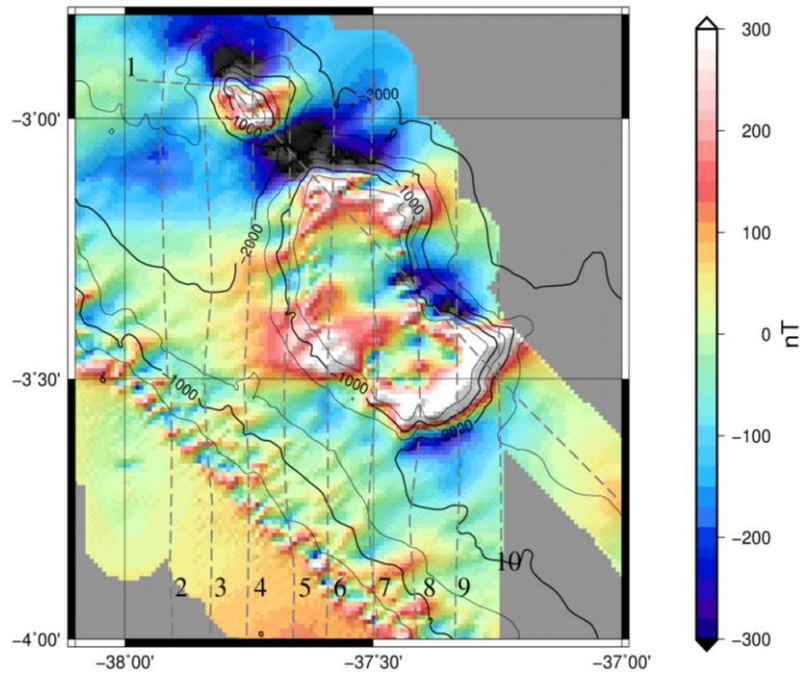


**Figure 54:** Residual anomaly map: the magnetic anomaly (figure 20) minus the theoretical magnetic anomaly (figure 42). Grid interval of 30 seconds (approximately 900 m). Bathymetric contour each 500 m.

The sources of the magnetic anomalies seem to be correlated with the gravity anomalies. According to the gravity model (5.1) the surface of the basement is different from the bathymetry. In order to model the basement effect, which probably contributes more than the sedimentary layer to the magnetic anomaly, it is used the basement surface in the same procedure applied at the bathymetric surface. Constant layers with different thickness were tested, and the model results are compared with residual anomalies. The better thickness is of 2 km. Other model parameters are the same as discussed in 4.3.5. The results are presented in figures 55 and 56.

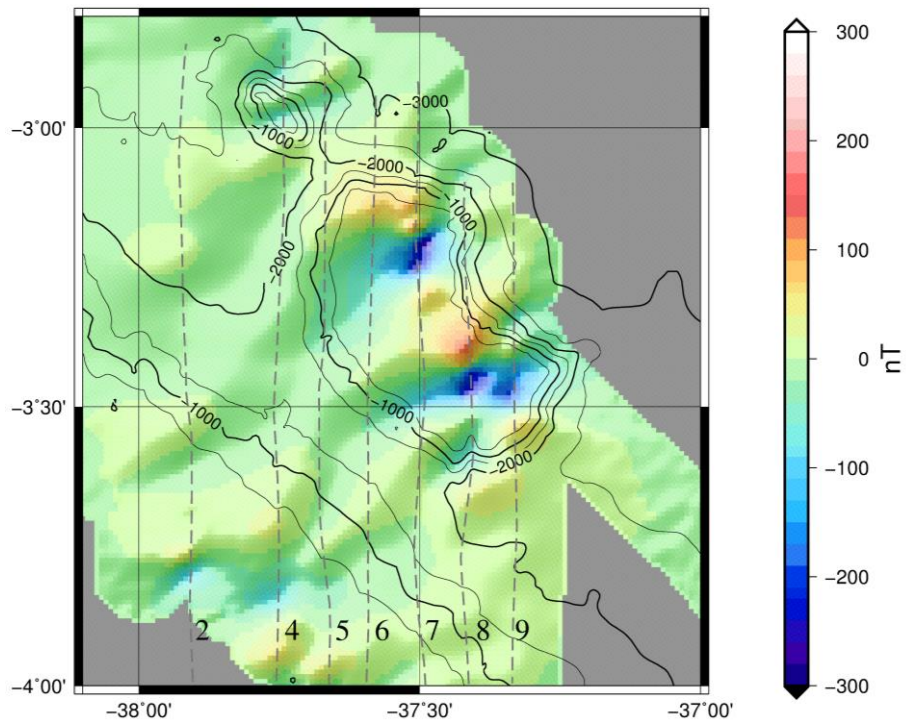


**Figure 55:** Modelled magnetic anomaly calculated with 2 km layer below the basement surface. Grid interval of 30 seconds (approximately 900 m). Bathymetric contour each 500 m.

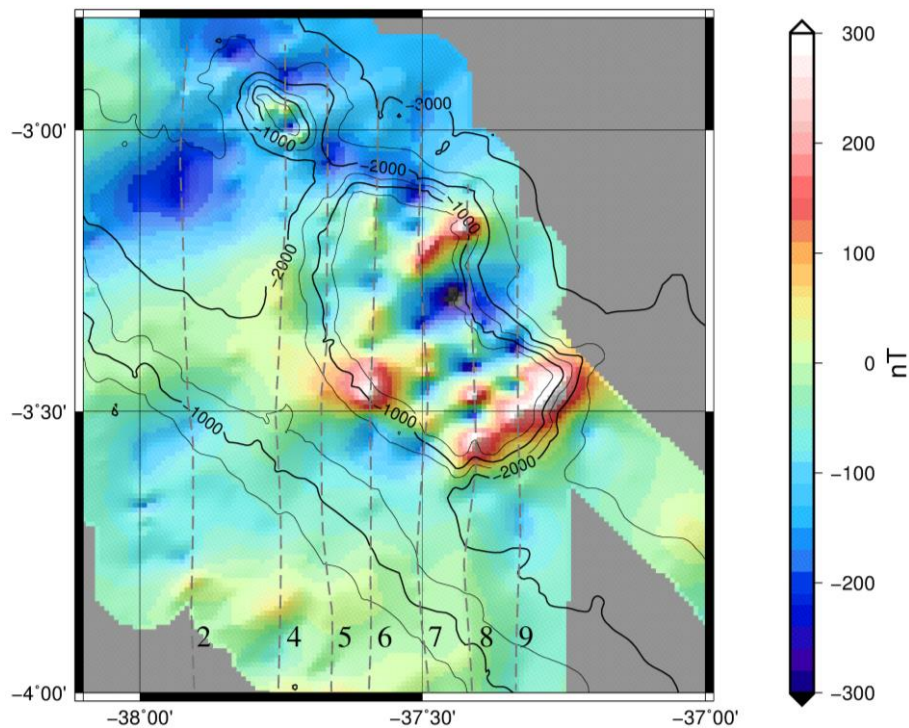


**Figure 56:** Magnetic residual anomaly map: the magnetic anomaly (figure 20) minus the modelled magnetic anomaly (figure 55). Grid interval of 30 seconds (approximately 900 m). Bathymetric contour each 500 m.



## 6. DISCUSSION

### 6.1 Comparison between the gravimetric and magnetic anomalies

#### 6.1.1 The gravity and magnetic anomalies source

The gravity anomaly, especially the Bouguer anomaly, highlights the lateral density variations. The maximum of the anomaly is related to a denser source.

The magnetic anomaly is related to variations in the susceptibility of the rock. As presented in figure 35, near to the Equator the magnetic anomalies are negative in the center of the source and positive in the North and South from the source. Then, the RTE magnetic anomaly indicates the center of the magnetized source as a low.

The gravimetric and the magnetic anomalies seem to have the same sources (figure 57). This implies that the geologic sources have high density and they are more magnetized compared to the surrounding rocks.

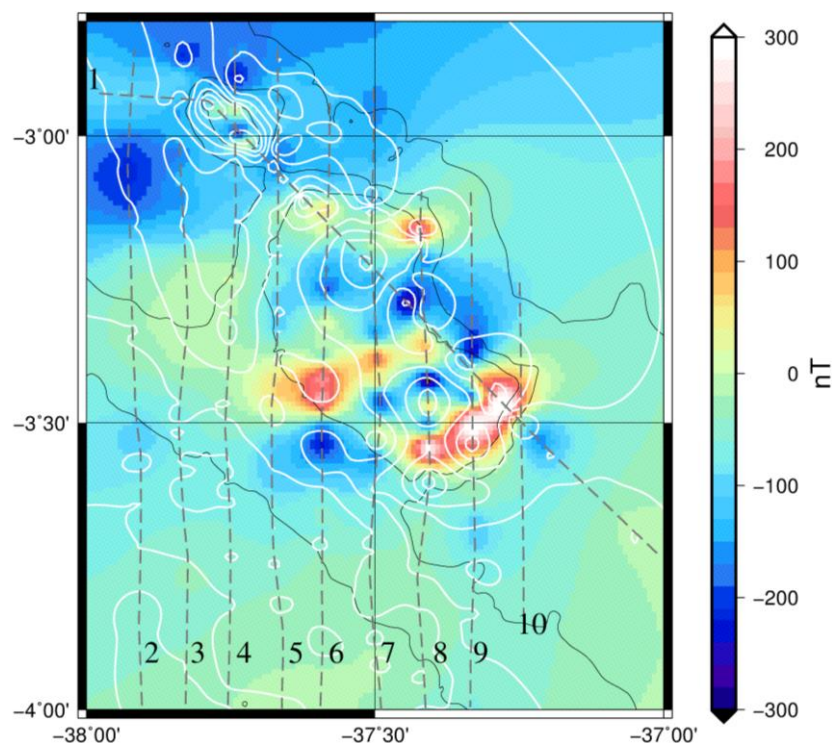


**Figure 57:** Comparison map: magnetic anomalies grid reduced to the Equator (figure 36c) and Bouguer residual anomalies (figure 28) contour in white lines. Grid interval of 20 seconds (approximately 620 m). Bathymetric contour each 1000 m.

### 6.1.2 The Bouguer anomaly and the TDR of the RTP

Among the techniques presented in 4.3.4 the TDR of the RTP resulted in a good correlation with the gravity anomalies (figure 58). The COB divides the TDR anomalies between an area with disturbed contours related to the oceanic crust and an undisturbed region where it is modelled as transitional crust, very deep in some places covered with huge amount of sediments. This specific region is so undisturbed that the TDR follows the track lines.

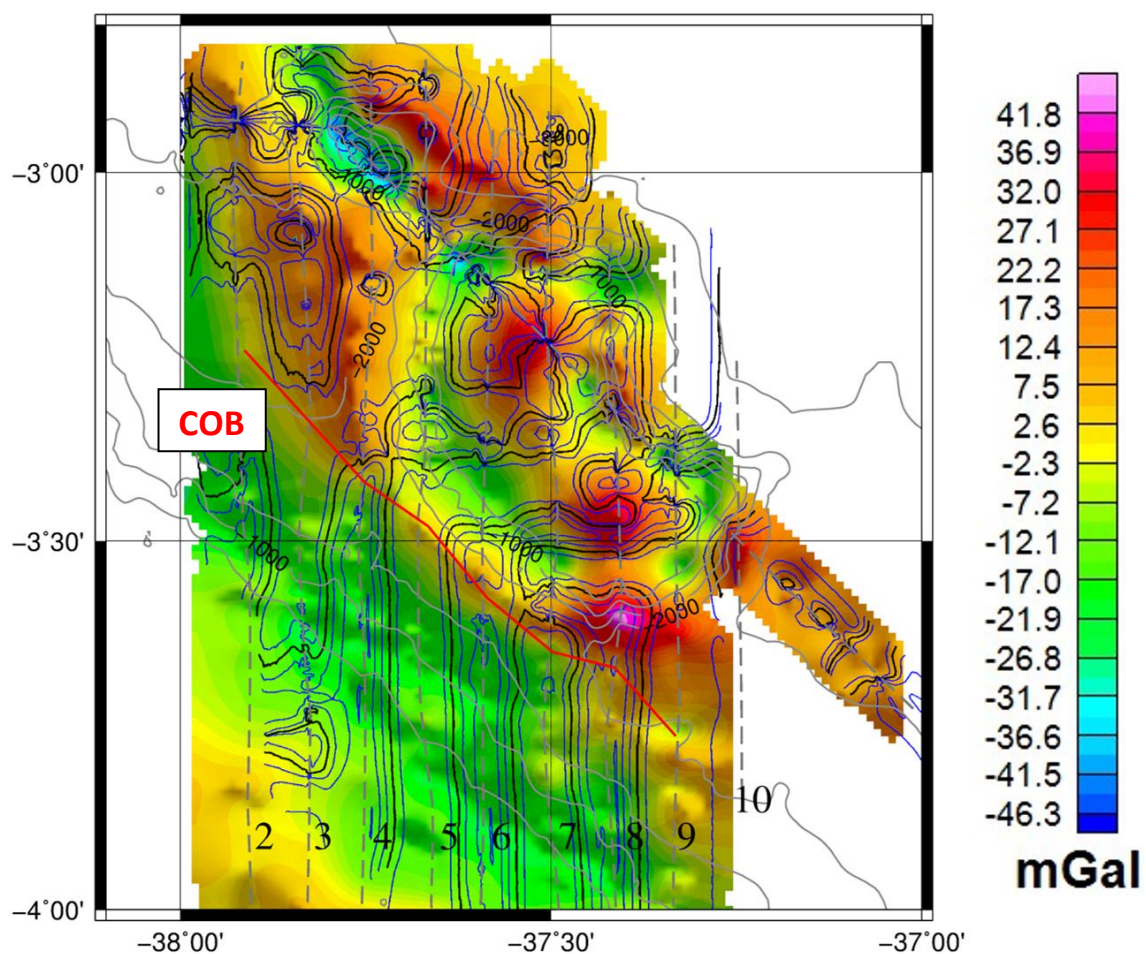


**Figure 58:** Bouguer residual anomaly map grid (figure 28) with the TDR of the RTP contour (figure 39). The TDR lines are disposed mostly around the high Bouguer residual anomalies, mainly the tilt angle zero (black lines), which indicates the sources boundary. The red line indicates the position of the COB. Grid interval of 30 seconds (approximately 900 m). Bathymetric contour each 500 m.

## **6.2 The gravity models**

### **6.2.1 The crustal model**

The models presented in 5.1, created through the free-air anomalies and based on the magnetic anomalies, seismic and core data, present the interpretation of the region where the Ceará Plateau is located. The models are related to the interpretation of the African Equatorial Margin crust, as presented by Mascle et al. (1998) and Jilinsk et al. (2013), where there is an almost abrupt contact between the continental and the oceanic crust. This crustal model, for both sides, is influenced by the transform phase of the Equatorial Margin.

The presence of a shallow mantle between the oceanic crust and the transitional crust is also a reflect of the Atlantic Ocean opening, related to the divergent phase of the margin formation (PÉRON-PINVIDIC et al., 2017).

### **6.2.2 The gravity modelling for continental crust instead of oceanic crust**

In order to analyze the gravity modellings adopted in this study, the profiles 2 and 7 are modelled replacing the oceanic crust ( $2.85 \text{ g/cm}^3$ ), with the continental transitional crust ( $2.8 \text{ g/cm}^3$ ). The results are presented in figures 59 and 60.

This approach is necessary to illustrate another possible modelling at the area and the limits of the potential data interpretation, especially with the few data available for research.

The continental transitional crust instead of oceanic crust is proved possible, but the profile 2 (figure 59) with 11 km thickness at the thinner region is a low value, indicative of a very stretched crust. There are no evidences to distinguish between this interpretation and the one presented in 5.1.

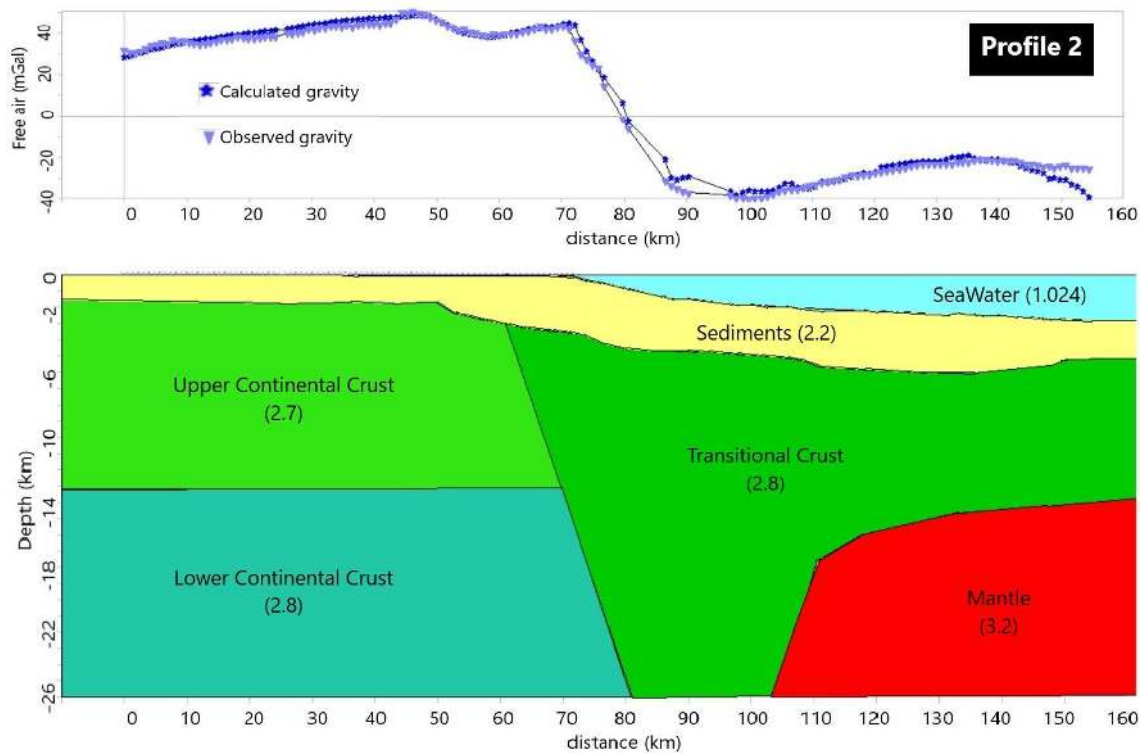


**Figure 59:** Gravimetric model of the profile 2 for only continental crust (S-N), with 2x vertical exaggeration. Densities in  $\text{g}/\text{cm}^3$ . The density is  $3.2 \text{ g}/\text{cm}^3$  below 26 km depth. Transitional crust with 11 km thickness at the thinner region.

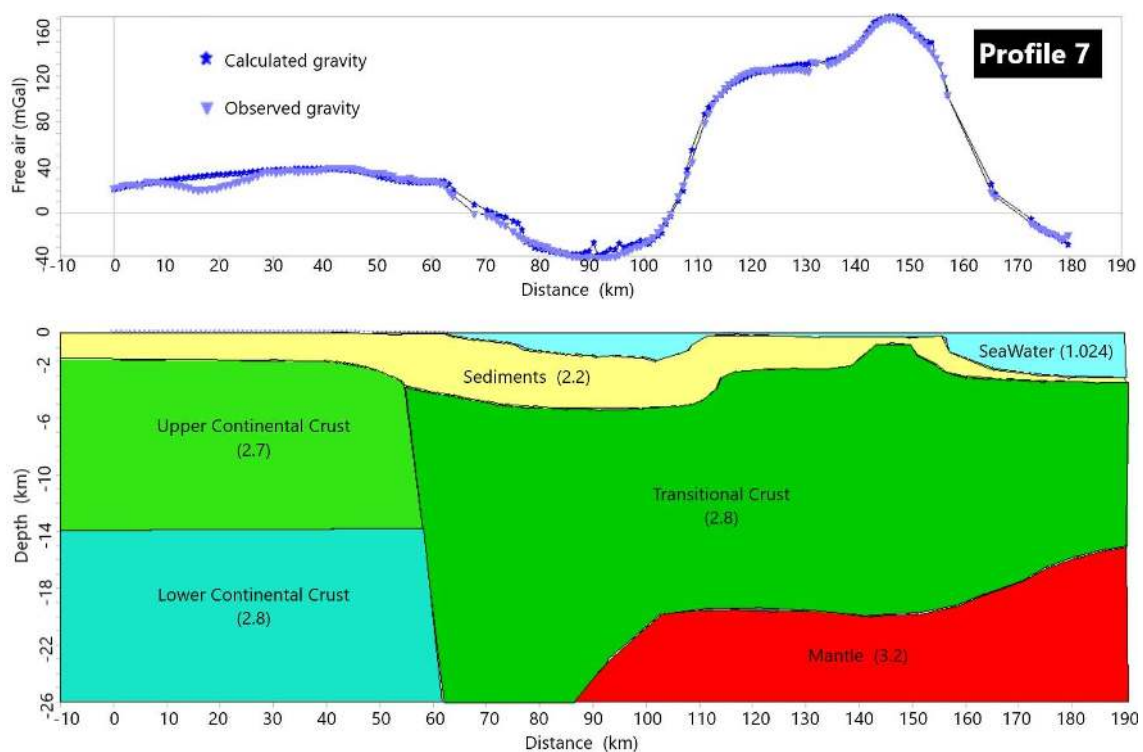


**Figure 60:** Gravimetric model of the profile 7 for only continental crust (S-N), with 2.8x vertical exaggeration. Densities in  $\text{g}/\text{cm}^3$ . The density is  $3.2 \text{ g}/\text{cm}^3$  below 26 km depth. Transitional crust with 11 km thickness at the thinner region, Ceará Plateau root with 20 km.

## **6.3 The COB and the transitional crust**

### **6.3.1 The Equant profiles compared to the predicted edge anomalies**

In the figure 58 the COB highlights a long wavelength Bouguer residual anomaly. The average anomaly difference, between the SW and NE, separated by the COB, is about 50 mGal. This anomaly is an indicative of lateral density differences, and this could represent the transition between the continental crust and the oceanic crust.

A method to demarcates the COB is the edge anomaly (RABINOWITZ and LABRECQUE, 1979). In this study, it is correlated the Bouguer residual anomaly with the estimated COB, as presented by Blaich et al. (2008; 2011). It is also noticed differences between the free-air and magnetic anomalies before and after the demarcation of the COB (figure 61).

The data do not cover the North of the Ceará Plateau. Then, it is not possible to compare the edge anomalies at this region.



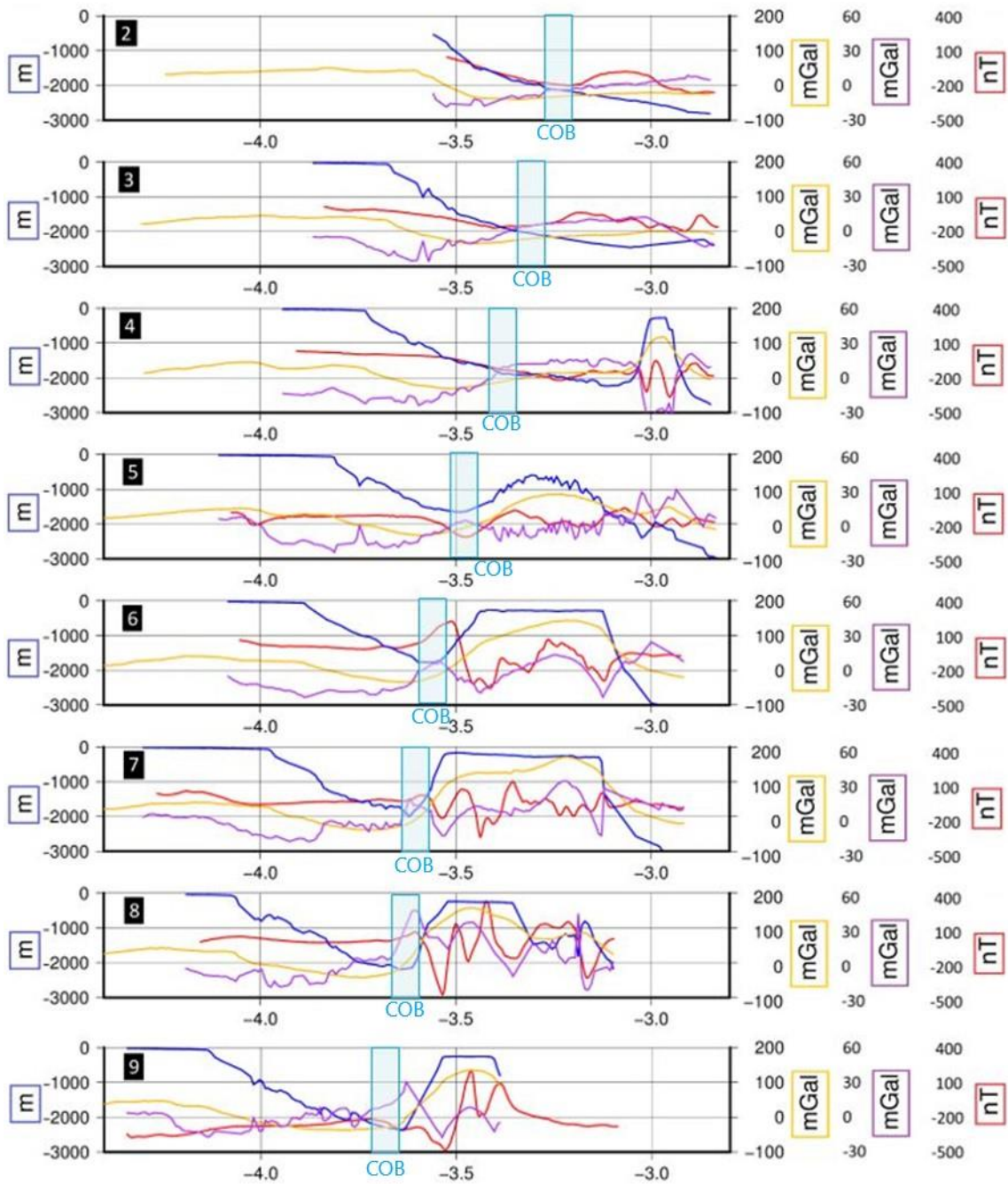


**Figure 61:** Profiles 2, 3, 4, 5, 6, 7, 8 and 9 from Equant I with the COB position (blue rectangles). Bathymetric (blue), free-air anomaly (yellow), Bouguer residual anomaly (purple), RTP (red) lines profiles (2-9).

### 6.3.2 The estimated position of the COB

As presented in 5.1 and discussed along this chapter, the COB is located between the continental shelf and the Ceará Plateau, although, this position was already predicted by Oliveira (2008) at north of the Plateau. He considered the EDC hypothesis for the area, and it could be a condition for the very thinned continental crust (figures 61 and 62).

Although, after Oliveira (2008), some seismic surveys were made available at the region. The interpretation of them (figures 21, 22, 23 and other available in: [http://www.brasil-rounds.gov.br/arquivos/Seminarios\\_r11/tec\\_ambiental/Bacia\\_Potiguar.pdf](http://www.brasil-rounds.gov.br/arquivos/Seminarios_r11/tec_ambiental/Bacia_Potiguar.pdf)) revealed a thick sediment layer above the Ceará Plateau, which was not considered in his models. Also, Oliveira (op. cit.) has not affirmed the position of the COB in his profiles, certainly because the few data available at that time. The geoid height and the surface wave tomography presented were not very accurate methods, in order to distinguish some kilometers (figure 5).

This study has used more detailed data for the oceanic area and the seismic lines. Although, the densities values and mostly of the parameters are based in the literature, which affords to the models more uncertainties.

It is estimated the COB position and the transitional crust, according to the gravity and the magnetic modelling, through some results:

- (1) The Bouguer residual anomaly indicative of a lateral density variation at the estimated COB (figures 58 and 61);
- (2) The Bouguer residual and magnetic anomalies associated with the COB position (figure 61);
- (3) The Bouguer residual, free-air and magnetic anomaly differences in the regions separated by the COB (figure 61);
- (4) The Magnetic anomaly high amplitudes compared to the continental shelf (figures 20). The ASA of the magnetic anomaly at the Ceará Plateau delimitation (figure 38), which defined the magnetic sources only at there. It is an



evidence that the magnetization of the basement above the plateau is higher than the basement on the continental shelf, since their depths are similar (figure 50);

(5) The very thin continental crust, on the order of 11 km, modelled with the transitional crust density used in this study (figure 59 and 60), possible but very unusual;

(6) To explain the formation of a continental basement, it would be necessary a fracture between it and the continental shelf, and the sediments in this area should be deformed during this period, which is not described in the seismic lines presented in this study (figures 21, 22 and 23). It would not be necessary a fracture if the Ceará Plateau was only formed by volcanic eruptions, but, with the data at this area, it is not possible to distinguish it yet.

Also, there are some indications that the Ceará Plateau area was overlapping the African Plate before the Atlantic Ocean started to open, according to the rotation poles estimated for these plates (RABINOWITZ and LABRECQUE, 1979; MATOS, 2000; MOULIN, 2003; SOARES JR, 2008). The stretching of the continental crust formed the thinned continental shelf, but it would be necessary too much stretching to form about 300 km of continental crust, if the Ceará Plateau is above the continental crust.

## **6.4 The magnetic models**

### **6.4.1 The magnetic modelling from the basement**

The magnetic modelling with the bathymetry was not satisfactory, then, as presented in 5.2.1, it was recalculated using the basement estimation (figure 50) with the gravity modelling. The result is comparable with the observed magnetic anomaly (figure 62), although, it is not a very good match (figure 56), which can be explicated by a high remanent magnetization in the rocks.

The differences between the modelled and the observed anomalies reveal that the subsurface has a more complex structure than the gravity modelling can

provide in this study, it is the reason the residual magnetic anomaly presented high amplitude anomalies (figure 56).

Due to the low resolution of the Equant I data it was not able to distinguish smaller structures, that are certainly present in this complex region.

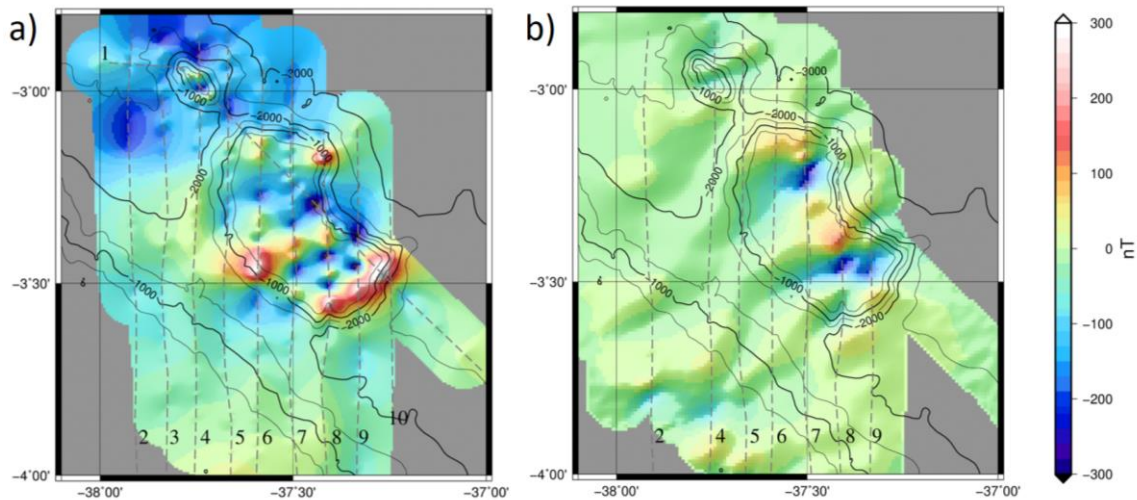


**Figure 62:** Magnetic anomalies comparison. a) Magnetic anomaly from Equant I data. b) Magnetic anomaly modelled with the basement.

### 6.5 Considerations about the Ceará Plateau formation

The results presented in this study indicated the COB location between the Ceará Plateau and the continental shelf, and a transitional crust is 40-50 km wide. Based on many studies (MAGALHÃES, 2015; NÓBREGA, 2008; LIGI et al., 2011; KEIR et al., 2013) the transitional crust is recognized as stretched continental crust and characterized by a large amount of igneous intrusions during the rifting phase. These intrusions are not limited to the marked area, but there it is more frequent. So, the width of the transitional crust represents an estimated region where the density of the crust is higher.

The three hypotheses presented in 3.1.3, 3.1.4 and 3.1.5 are valid to explain the models presented in this study. The source of the magmatism could be deep, according to the hotspot theory, shallow, according to the EDC theory, or from the tectonic dynamics of the FZ.

The Ceará Plateau formation is apparently connected with the seamounts on the east, including the Rocas Atoll and Fernando de Noronha Island, since they are at the oceanic crust and in the same line.

The age of the formation of the plateau is unknown, the huge amount of sediment (figure 51) seems to record a long period of time (JOVANE et al., 2016), but, there is no rock dating to sustain it yet.

## **6.6 The Iracema Guyot**

The Iracema Guyot is the smaller seamount Northwest the Ceará Plateau, with about 12 km wide. The profile 4 (figure 44) crosses the structure, but it is not according to the magnetic modelling, because the magnetic calculated anomaly amplitude is lower than the observed one (figure 62).

The Bouguer anomaly (figure 26) and the residual Bouguer anomaly (figure 28) presented this guyot as a low. It could be because a very punctual root or a seamount low-density material. In order to model it, using the same densities of the other profiles (table 3), the seamount is modelled as an almost sedimentary structure.

This structure could have had different volcanism episodes while sedimentation was taking place, resulting in magmatic rocks closer to the top of the guyot. This could result in a strong magnetic anomaly and a low Bouguer anomaly. However, there are no seismic profiles available crossing it to sustain or refuse this hypothesis.

## 7. CONCLUSIONS

The Ceará Plateau is located at the BEM, a very complex and poorly known region. This study aimed to comprehend better the area by correlating the physical properties, from gravity and magnetic data, with a geological model. Also, it was presented an extensive bibliographic review about the region.

It was presented: some corrections and filters, for both potential methods, used in the first evaluation of the data; several forward modelled profiles from the free-air anomaly; and some continuous magnetized layer models from the magnetic anomaly. The models have been produced with the aid of some interpreted seismic profiles and the published literature.

After the analyses and the modelling, it was constructed the basement surface between 800 m and 6000 m, approximately, and the Mohorovičić discontinuity surface about 22-23 km below the Ceará Plateau. Also, the sediment and the crust thickness were presented for the Ceará Plateau and its area.

The region of a transitional crust was estimated between a less altered continental crust and the oceanic crust, with an extension of 40-50 km. Also, a discussion about the COB position was performed. The lineament was delimited between the continental shelf and the Ceará Plateau, approximately 40 km from the continental shelf, placing the plateau at the oceanic crust. However, the interpretation is not conclusive in this point due to the few data.

In order to decrease ambiguity and enhance the interpretation, it is recommended for future works: direct measures for the density, seismic lines combined with gravity and magnetic data, and even other kind of information about the region, as tectonic and magmatic models for the BEM and its seamounts formation. Also, a more detailed gravity and magnetic survey including the North area of the Plateau. These certainly would enable a more conclusive model for the area.

## REFERENCES

- AGURTO-DETZEL, H.; ASSUMPCÃO, M.; BIANCHI, M.; PIRCHINER, M. Intraplate seismicity in mid-plate South America: correlations with geophysical lithospheric parameters. **Geol. Soc. Spec. Pub.**, v. 432, p. 73–90, 2015. DOI: 10.1144/sp432.5.
- AIRY, G. B. On the computation of the effect of the attraction of mountain-masses, as disturbing the apparent astronomical latitude of stations in geodetic surveys. **Philos. Trans. R. Soc. London**, v. 145, p. 101–104, 1855. DOI: 10.1098/rstl.1855.0003.
- ALMEIDA, F. F. M. Ilhas oceânicas brasileiras e suas relações com a Tectônica Atlântica. **Terræ Didática**, v. 2, n. 1, p. 3–18, 2006. DOI: 10.20396/td.v2i1.8637462.
- ALMEIDA, N. M.; VITAL, H.; GOMES, M. P. Morphology of submarine canyons along the continental margin of the Potiguar Basin, NE Brazil. **Mar. Pet. Geol.**, v. 68, p. 307–324, 2015. DOI: 10.1016/j.marpetgeo.2015.08.035.
- ANDERSON, D. L. The plastic layer of the Earth's Mantle. **Sci. Am.**, v. 207, n. 1, p. 52–59, 1962. DOI: 10.1038/scientificamerican0762-52.
- ASSUMPCÃO, M.; FENG, M.; TASSARA, A.; JULIA, J. Models of crustal thickness for South America from seismic refraction, receiver functions and surface wave tomography. **Tectonophysics**, v. 609, p. 82–96, 2013. DOI: 10.1016/j.tecto.2012.11.014.
- AZEVEDO, R. P. Interpretação geodinâmica da evolução Mesozoica da Bacia de Barreirinhas. In: 34 CONGRESSO BRASILEIRO DE GEOLOGIA, 34., 1986, Goiânia. **Resumos ...** Goiânia: SBG, 1986. v. 3, p. 1115–1130.
- AZEVEDO, R. P. **Tectonic evolution of Brazilian Equatorial Continental Margin Basins**. 1991. PhD (Thesis) - Royal School of Mines Imperial College, London.
- BARMIN, M. P.; RITZWOLLER, M. H.; LEVSHIN, A. L. A fast and reliable method for surface wave tomography. **Pure Appl. Geophys.**, v. 158, n. 8, p. 1351–1375, 2001. DOI: 10.1007/pl00001225.
- BASILE, C.; BRUN, J.P.; MASCLE, J. Structure et formation de la marge transformante de Côte d'Ivoire-Ghana: apports de la sismique réflexion et de la odélisation analogique. **Bull. Soc. Géol. France**, v. 163, p. 207–216, 1992.
- BASILE, C.; MAILLARD, A.; PATRIAT, M.; GAULLIER, V.; LONCKE, L.; ROEST, W.; MERCIER DE LEPINAYD, M.; PATTIER, F. Structure and evolution of the demerara plateau, offshore French Guiana: rifting, tectonic inversion and post-rift tilting at transform–divergent margins intersection. **Tectonophysics**, v. 591, p. 16–29, 2013. DOI: 10.1016/j.tecto.2012.01.010.

- BASILE, C.; MASCLE, J.; GUIRAUD, R. Phanerozoic geological evolution of the Equatorial Atlantic. **J. Af. Earth Sci.**, v. 43, n. 1/3, p. 275–282, 2005. DOI: 10.1016/j.jafrearsci.2005.07.011.
- BASILE, C.; MASCLE, J.; POPOFF, M.; BOUILLIN, J.P.; MASCLE, G. The Côte d'Ivoire-Ghana transform margin: a marginal ridge structure deduced from seismic data. **Tectonophysics**, v. 222, p. 1–19, 1993. DOI: 10.1016/0040-1951(93)90186-n.
- BERTANI, R. T.; COSTA, I. G.; MATOS, R. M. D. Evolução tectono-sedimentar, estilo estrutural e hábitat do petróleo na Bacia Potiguar. In: RAJA GABAGLIA, G. P., MILANI, E. J. (Coord.) **Origem e evolução de bacias sedimentares**. Rio de Janeiro: Petrobras. SEREC.CENSUD, 1990. p. 291–310.
- BLAICH, O. A.; FALEIDE, J. I.; TSIKALAS, F. Crustal breakup and continent-ocean transition at South Atlantic conjugate margins. **J. Geophys. Res.: Solid Earth**, v. 116, n. B1, 2011.
- BLAICH, O. A.; TSIKALAS, F.; FALEIDE, J. I. Northeastern Brazilian margin: Regional tectonic evolution based on integrated analysis of seismic reflection and potential field data and modelling. **Tectonophysics**, v. 458, n. 1, p. 51-67, 2008.
- BLAKELY, R. **Potential Theory in Gravity and Magnetic Applications**, 2. ed. Cambridge: Cambridge University Press, 1996.
- BONATTI, E. Origin of the offsets of the Mid-Atlantic in fractures zones. **J. Geol.**, v. 81, n. 2, p. 144–156, 1973. DOI: 10.1086/627831.
- BONATTI, E.; HONNOREZ, J. Sections of the Earth's crust in the equatorial Atlantic. **J. Geophys. Res.**, v. 8, n. 23, p. 4104–4116, 1976. DOI: 10.1029/jb081i023p04104.
- BONATTI, E.; LIGI, M.; GASPERINI, L.; PEYVE, A.; RAZNITSIN, Y.; CHEN, Y. J. Transform migration and vertical tectonics at the Romanche fracture zone, Equatorial Atlantic. **J. Geophys. Res.**, v. 99, n. B11, p. 21779–21802, 1994. DOI: 10.1029/94jb01178.
- BRITO NEVES, B. B.; FUCK, R. A.; CORDANI, U. G.; THOMAZ FILHO, A. Influence of basement structures on the evolution of the major sedimentary basins of Brazil: a case of tectonic heritage. **J. Geodyn.**, v. 1, n. 3/5, p. 495–510, 1984. DOI: 10.1016/0264-3707(84)90021-8.
- CAMPOS, T. F. C.; VIRGENS NETO, J.; AMORIM, V. A.; HARTMANN, L. A.; PETTA R. A. Modificações metassomáticas das rochas milonitizadas do complexo ultramáfico do Arquipélago de São Pedro e São Paulo, Atlântico Equatorial. **Geochim. Bras.**, v. 17, n. 2, p. 81–90, 2003.
- CANDE, S. C.; KENT, D. V. Revised calibration of the magnetic polarity time scale for the Late Cretaceous and Cenozoic. **J. Geophys. Res.**, v. 100, p. 6093–6095, 1995. DOI: 10.1029/94jb03098.

- CASTRO, D. L. **Interpretação quantitativa de anomalias gravimétricas ar-livre da Margem Continental Norte Brasileira, Setor Nordeste.** 1990. Thesis (Master) – Instituto de Geociências, Universidade Federal do Rio Grande do Norte, Natal.
- CASTRO, D. L.; BEZERRA, F. H. R. Fault evolution in the Potiguar rift termination, Equatorial Margin of Brazil. **Solid Earth**, v. 6, n. 1, p. 185–196, 2015. DOI: 10.5194/se-6-185-2015.
- CASTRO, D. L.; BEZERRA F. H. R.; SOUZA, M. O. L.; FUCK, R. A. Influence of Neoproterozoic tectonic fabric on the origin of the Potiguar Basin, northeastern Brazil and its links with West Africa based on gravity and magnetic data. **J. Geodyn.**, v. 54, p. 29–42, 2012. DOI: 10.1016/j.jog.2011.09.002.
- CASTRO, F. D.; COSTA, L. P.; SANTOS, N. B.; SILVA, C. R. O. S. Aspectos geomorfológicos, geológicos e oceanográficos da margem continental potiguar: uma fração do Brasil carente em informação. In: CONGRESSO DE PESQUISA E INOVAÇÃO DA REDE NORTE NORDESTE DE EDUCAÇÃO TECNOLÓGICA, 5., 2010, Macéio. **Anais ...** Maceió: CONNEPI, 2010.
- CHANG, H. K.; KOWSMANN, R. O.; FIGUEIREDO, A. M. F.; BENDER, A. A. Tectonics and stratigraphy of the East Brazil Rift system: an overview. **Tectonophysics**, v. 213, n. 1/2, p. 97–138, 1992. DOI: 10.1016/0040-1951(92)90253-3.
- CHASE, C. G. Tectonic history of the Fiji Plateau. **Geol. Soc. Am. Bull.**, v. 82, n. 11, p. 3087–3110, 1971. DOI: 10.1130/0016-7606(1971)82[3087:thotfp]2.0.co;2.
- COFFIN, M. F.; ELDHOLM, O. Large igneous provinces: crustal structure, dimensions, and external consequences. **Rev. Geophys.**, v. 32, n. 1, p. 1–36, 1994. DOI: 10.1029/93rg02508.
- COFFIN, M. F.; MUNSCHY, M.; COLWELL, J. B.; SCHLICH, R.; HUGH, L., DAVIES, H. L.; LI, Z. Seismic stratigraphy of the Raggatt Basin, southern Kerguelen Plateau: tectonic and paleoceanographic implications. **Geol. Soc. Am. Bull.**, v. 102, n. 5, p. 563–579, 1990. DOI: 10.1130/0016-7606(1990)102<0563:ssotrb>2.3.co;2.
- CONSTANTINO, R.; MOLINA, E. C. Basement structures in Santos Basin (Brazil) from satellite altimetry and marine geophysics. **Rev. Bras. Geofís.**, v. 33, n. 1, p. 29–43, 2015. DOI: 10.22564/rbgf.v33i1.599.
- COURTILLOT, V.; DAVAILLE, A.; BESSE, J.; STOCK, J. Three distinct types of hotspots in the Earth's mantle. **Earth Planet. Sci. Lett.**, v. 205, n. 3–4, p. 295–308, 2003. DOI: 10.1016/s0012-821x(02)01048-8.
- DAVIES, G. F. Ocean bathymetry and mantle convection. Part 1: Large-scale flow and hotspots. **J. Geophys. Res.**, v. 93, n. B9, p. 10467–10480, 1988. DOI: 10.1029/jb093ib09p10467.



DEHLINGER, P. **Marine Gravity**. The Netherlands: Elsevier Scientific Publishing Company, 1978. Elsevier Oceanography Series, v. 22. ISBN: 0444416803.

DONNELLY, T. W. Late Cretaceous basalts from the Caribbean, a possible flood basalt province of vast size. In: EOS TRANSACTIONS - AGU, 54., 1973, Washington D. C.: AGU, 1973, p. 1004.

DEMIN, A.; PICCIRILIO, E. M.; MARZOLI, A.; BELLINI, G.; RENNE, P. R.; ERNESTO, M.; MARQUES, L. The Central Atlantic Magmatic Province (CAMP) in Brazil: Petrology, Geochemistry,  $^{40}\text{Ar}/^{39}\text{Ar}$  ages, paleomagnetism and geodynamic implications. In: HAMES, W. E., MCHONE, J. G., RENNE, P. R., AND RUPPEL, C. (Ed.). **The Central Atlantic Magmatic Province: Insights from fragments of Pangea**. Washington D. C.: AGU, 2003. p. 91–128. (Geophysical Monograph, 136). DOI: 10.1029/136gm06.

EVANS, P.; CROMPTON, W. Geological factors in gravity interpretation illustrated by evidence from India and Burma. **Quarterly Journal of the Geological Society**, v. 102, n. 1-4, p. 211-249, 1946.

FAINSTEIN, R.; MILLIMAN, J. D. Structure and origin of three continental margin plateaus, Northeast Brazil. **AAPG Bulletin**, v. 63, n. 2, p. 218–237, 1979. DOI: 10.1306/c1ea55da-16c9-11d7-8645000102c1865d.

FERREIRA, F. J. F.; SOUZA, J.; BONGIOLO, A. B. S.; CASTRO, L. G. Enhancement of the total horizontal gradient of magnetic anomalies using the tilt angle. **Geophysics**, v. 78, n. 3, p. J33–J41, 2013. DOI: 10.1190/geo2011-0441.1.

FERREIRA, J. M.; OLIVEIRA, R. T.; TAKEYA, M. K.; ASSUMPÇÃO, M. Superposition of local and regional stresses in NE Brazil: evidence from focal mechanisms around the Potiguar marginal basin. **Geophys. J. Int.**, v. 134, n. 2, p. 341–355, 1998. DOI: 10.1046/j.1365-246x.1998.00563.x.

FORBES, J. M. 1981. The equatorial electrojet. **Rev. Geophys.**, v. 19, n. 3, p. 469–504. DOI: 10.1029/rg019i003p00469.

FOULGER, G. R. **Plates vs Plumes: a geological controversy**. Chichester, UK: Wiley-Blackwell, 2010. 340 p. ISBN: 978-1-4051-6148-0.

GEE, J. S.; KENT, D. V. Source of oceanic magnetic anomalies and the geomagnetic polarity timescale, In: KONO, M., **Treatise on geophysics**. The Netherlands: Elsevier, 2007. v. 5, p. 455–507. DOI: 10.1016/b978-044452748-6/00097-3.

GENTE, P.; DYMENT, J.; MAIA, M.; GOSLIN, J. Interaction between the Mid-Atlantic Ridge and the Azores hot spot during the last 85 Myr: emplacement and rifting of the hot spot-derived plateaus. **Geochem. Geophys. Geosyst.**, v. 4, n. 10, p. 1-23, 2003. DOI: 10.1029/2003gc000527.

GORINI, M. A. The tectonic fabric of the Equatorial Atlantic and adjoining continental margins. GULF of Guinea to northeastern. In: ASMUS H. E. (Ed.)

**Estruturas e tectonismo da margem continental brasileira e suas implicações nos processos sedimentares e na avaliação do potencial de recursos minerais.**

Rio de Janeiro: Série Projeto REMAC, 1981. n. 9, p. 11–116.

GORINI, M. A. **The tectonic fabric of the Equatorial Atlantic and adjoining continental margins: Gulf of Guinea to Northeastern Brazil.** 1977. 365 p. PhD (Thesis), Columbia University.

GUIRAUD, R.; MAURIN, J.-CH. Early Cretaceous rift of western and Central Africa: an overview. In: ZIEGLER, P. A. (Ed.), **Geodynamics of Rifting, v. II. Case History Studies on Rifts: North and South America and Africa.** Tectonophysics, v. 213, n. 1/2, p. 153–168, 1992. DOI: 10.1016/b978-0-444-89912-5.50035-1.

HAMILTON, E. L. Sound velocity, elasticity and related properties of marine sediments. **Geophysics**, v. 36, n. 2, p. 266–284, 1971. DOI: 10.1190/1.1440168.

HAMZA, V. M.; CARDOSO, R. R.; PONTE NETO, C. F. Spherical harmonic analysis of earth's conductive heat flow. **Int. J. Earth Sci.**, v. 97, n. 2, p. 205–226, 2008. DOI: 10.1007/s00531-007-0254-3.

HAQ, B. U.; AL-QAHTANI, A. M. Phanerozoic cycles of sea-level change on the Arabian Platform. **GeoArabia**, v. 10, n. 2, p. 127–160, 2005.

HAQ, B. U.; HARDENBOL, J.; VAIL, P. R. Chronology of fluctuating Sea Levels since the Triassic. **Science**, v. 235, n. 4793, p. 1156–1167, 1987. DOI: 10.1126/science.235.4793.1156.

HERNÁNDEZ-MOLINA, F. J.; LARTER, R. D.; REBESCO, M.; MALDONADO, A. Miocene reversal of bottom water flow along the Pacific Margin of the Antarctic Peninsula: Stratigraphic evidence from a contourite sedimentary tail. **Mar. Geol.**, v. 228, p. 93–116, 2006. DOI: 10.1016/j.margeo.2005.12.010.

HINZE, W. J.; VON FRESE, R. R. B.; SAAD, A. H. **Gravity and Magnetic Exploration: principles, practices, and applications.** New York: Cambridge University Press, 2013. DOI: 10.1017/CBO9780511843129.

International Hydrographic Organization; Intergovernmental Oceanographic Commission. **Standardization of undersea feature names: guidelines proposal from terminology**, 4th ed. [S.l.] : IHO , 2008, Monaco, p. 32.

JACOBSEN, H. A case for upward continuation as a standard separation filter for potential-field maps. **Geophysics**, v. 52, n. 8, p. 1138–1148, 1987. DOI: 10.1190/1.1442378.

JILINSKI, P.; MEJU, M. A.; FONTES, S. L. Demarcation of continental-oceanic transition zone using angular differences between gradients of geophysical fields. **Geophys. J. Int.**, v. 195, n. 1, p. 276–281, 2013. DOI: 10.1093/gji/ggt216.

JOHNSON, H. P.; KENT, D. V.; TIVEY, M. A.; GEE, J. S.; LARSON, R. S.; EMBLEY, R. W. Conference on the magnetization of the Oceanic Crust Steers

- Future Research. In: EOS TRANSECTIONS AGU, 1997, Washington D. C.: AGU, 1997, v. 78, n. 19, p. 199–200. DOI: 10.1029/97eo00133.
- JONES, C. H. **Updaters for GravMag**. 2012. Available in: <<http://cires.colorado.edu/people/jones.craig/GSSH/updaters/GravMag.html>>. Accessed on: June 1, 2016.
- JOVANE, L.; FIGUEIREDO, J. J. P.; ALVES, D. P. V.; IACOPINI, D.; GIORGIONI, M.; VANNUCCHI, P.; MOURA, D. S.; BEZERRA F. H. R.; VITAL, H.; RIOS, I. L. A.; MOLINA, E. C. Seismostratigraphy of the Ceará Plateau: Clues to Decipher the Cenozoic Evolution of Brazilian Equatorial Margin. **Front. Earth Sci.**, v. 4, n. 90, p. 1–14, 2016. DOI:10.3389/feart.2016.00090.
- JUAREZ, M. T.; TAUXE, L.; GEE, J. S.; PICK, T. The intensity of the Earth's magnetic field over the past 160 million years. **Nature**, v. 394, n. 6696, p. 878–881, 1998. DOI: 10.1038/29746.
- KEIR, D.; BASTOW, I. D.; PAGLI, C.; CHAMBERS, E. L. The development of extension and magmatism in the Red Sea rift of Afar. **Tectonophysics**, v. 607, p. 98–114, 2013. DOI: 10.1016/j.tecto.2012.10.015.
- KING, S. D. Hotspots and edge-driven convection. **Geology**, v. 35, n. 3, p. 223–226, 2007. DOI: 10.1130/g23291a.1.
- KING, S. D.; ANDERSON, D. L. An alternative mechanism of flood basalt formation. **Earth Planet. Sci. Lett.**, v. 136, n. 3–4, p. 269–279, 1995. DOI: 10.1016/0012-821x(95)00205-q.
- KING, S. D.; ANDERSON, D. L. Edge-driven convection. **Earth Planet. Sci. Lett.**, v. 160, n. 3, p. 289–296, 1998. DOI: 10.1016/s0012-821x(98)00089-2.
- KOIZUMI, K.; ISHIWATARI, A. Oceanic plateau accretion inferred from late paleozoic greenstones in the Jurassic Tamba accretionary complex, southwest Japan. **The Island arc**, v. 15, n. 1, p. 58–83, 2006. DOI: 10.1111/j.1440-1738.2006.00518.x.
- KOPPERS, A. A. P.; YAMAZAKI, T.; GELDMACHER, J. Louisville Seamount Trail: implications for geodynamic mantle flow models and the geochemical evolution of primary hotspots. **IODP Sci. Prosp.**, v. 330, 2010. DOI:10.2204/iodp.sp.330.2010.
- LIGI, M.; BONATTI, E.; TONTINI, F. C.; CIPRIANI, A.; COCCHI, L.; SCHETTINO, A.; RASUL, N. Initial burst of oceanic crust accretion in the Red Sea due to edge-driven mantle convection. **Geology**, v. 39, n. 11, p. 1019–1022, 2011. DOI: 10.1130/g32243.1.
- LIMA, C.; NASCIMENTO, E.; ASSUMPÇÃO, M. Stress orientations in Brazilian sedimentary basins from breakout analysis – implications for force models in the South American plate. **Geophys. J. Int.**, v. 130, n. 1, p. 112–124, 1997. DOI: 10.1111/j.1365-246x.1997.tb00991.x.

MACDONALD, D.; GOMEZ-PEREZ, I.; FRANZESE, J.; SAPALLETTI, L.; LAWVER, L.; GAHAGAN, L.; DANZIEL, I.; THOMAS, C.; TREWIN, N.; HOLE, M.; PATON, D. Mesozoic break-up of SW Gondwana: implications for regional hydrocarbon potential of the southern South Atlantic. **Mar. Pet. Geol.**, v. 20, n. 3–4, p. 287–308, 2003. DOI: 10.1016/S0264-8172(03)00045-X.

MAGALHÃES, J. R. G. **Compartimentação tectono-sedimentar da Bacia da Paraíba, a partir da integração de métodos potenciais e interpretação sísmica de dados offshore.** 2015. 86 f. Thesis (Master) – Centro de Tecnologia e Geociências, Universidade Federal de Pernambuco, Recife.

MAIA, M.; DYMENT, J.; JOUANNETAUD, D. Constraints on age and construction process of the foundation chain submarine volcanoes from magnetic modeling. **Earth Planet. Sci. Lett.**, v. 235, n. 1/2, p. 183–199, 2005. DOI: 10.1016/j.epsl.2005.02.044.

MAIA, M.; SICHEL, S.; BRIAIS, A.; BRUNELLI, D.; LIGI, M.; FERREIRA, N.; CAMPOS, T.; MOUGEL, B.; BREHME, I.; HÉMOND, C.; MOTOKI, A.; MOURA, D.; SCALABRIN, C.; PESSANHA, I.; ALVES, E.; AYRES, A.; OLIVEIRA, P. Extreme mantle uplift and exhumation along a transpressive transform fault. **Nature Geoscience**, v. 9, n. 8, p. 619–623, 2016. DOI: 10.1038/ngeo2759.

MARQUES, M. S. P. **Avaliação de dados de altimetria do satélite GEOSAT a partir de comparação com dados do levantamento gravimétrico marinho Equant.** 1992. Thesis (Master) – Instituto de Geociências, Universidade Federal do Pará, Belém.

MARTINS, G.; OLIVEIRA, E. P.; LAFON, J. The algodões amphibolite–tonalite gneiss sequence, borborema province, NE Brazil: geochemical and geochronological evidence for palaeoproterozoic accretion of oceanic plateau/back-arc basalts and adakitic plutons. **Gondwana Res.**, v. 15, n. 1, p. 71–85, 2009. DOI: 10.1016/j.gr.2008.06.002.

MASCLE, J.; BLAREZ, E. Evidence for transform margin evolution from the Ivory Coast-Ghana continental margin. **Nature**, v. 326, n. 6111, p. 378–381, 1978. DOI: 10.1038/326378a0.

MASCLE, J.; BLAREZ, E.; MARINHO, M. The shallow structures of the Guinea and Ivory Coast-Ghana transform margins: their bearing on the Equatorial Atlantic Mesozoic evolution. **Tectonophysics**, v. 155, p. 193–209, 1988. DOI: 10.1016/0040-1951(88)90266-1.

MASCLE, J.; LOHMANN, G. P.; CLIFT, P. D.; SHIPBOARD SCIENTIFIC PARTY. Introduction. **Proc. ODP, Init. Repts.**, n. 159, p. 516, 1996. DOI: 10.2973/odp.proc.ir.159.1996.

- MASCLE, J.; LOHMANN, G.P.; MOULLADE, M. (Ed.). Côte D'Ivoire-Ghana Transform Margin Sites 959-962. **Proc. ODP, Sci. Results**, n. 159, 1998. DOI: 10.2973/odp.proc.sr.159.1998.
- MATOS, R. M. D. Tectonic Evolution of the Equatorial South Atlantic. In: MOHRIAK, W.; TAIWANI, M.(Ed.). **Atlantic rifts and continental margins**. Washington, D.C.: American Geophysical Union, 2000. p. 331–354 (Geophysical monograph, 115). DOI: 10.1029/gm115p0331.
- MATOS, R. M. D. History of the northeast Brazilian rift system: kinematic implications for the break-up between Brazil and West Africa. In: CAMERON, N. R.; BATE, R. H.; CLURE, V. S. (Ed.) **The Oil and Gas Habitats of the South Atlantic**. Geological Society, London, Special Publications, v. 153, n. 1, p. 55–73, 1999. DOI: 10.1144/gsl.sp.1999.153.01.04.
- MATOS, R. M. D. The northeast Brazilian rift system, **Tectonics**, v. 11, n. 4, p. 766–791, 1992. DOI: 10.1029/91tc03092.
- MAUS, S.; BARCKHAUSEN, U.; BERKENBOSCH, H.; BOURNAS, N.; BROZENA, J.; CHILDERS, V.; DOSTALER, F.; FAIRHEAD, J. D.; FINN, C.; VON FRESE, R. R. B.; GAINA, C.; GOLYNSKY, S.; KUCKS, R.; LUHR, H.; MILLIGAN, P.; MOGREN, S.; MULLER, R. D.; OLESEN, O.; PILKINGTON, M.; SALTUS, R.; SCHRECKENBERGER, B.; THÉBAULT, E.; CARATORI TONTINI, F. EMAG2: A 2 –arc min resolution Earth Magnetic Anomaly Grid compiled from satellite, airborne, and marine magnetic measurements. **Geochem. Geophys. Geosyst.**, v. 10, n. 8, p. 1–12, 2009. DOI: 10.1029/2009GC002471.
- MCHONE, J. G. Non-plume magmatism and tectonics during the opening of the central Atlantic Ocean. **Tectonophysics**, v. 316, n. 3–4, p. 287–296, 2000. DOI: 10.1016/s0040-1951(99)00260-7.
- MEIRELES, A. J. A. M.; ARRUDA, M. G. C.; GORAYEB, A.; THIERS, PAULO. R. L. Integração dos indicadores geoambientais de flutuações do nível relativo do mar e de mudanças climáticas no litoral cearense. **Mercator: Revista de Geografia da UFC**, v. 4, n. 8, 2005.
- MILLER, H. G.; SINGH, V. Potential field tilt – a new concept for location of potential field sources. **J. Applied Geophys.**, v. 32, n. 2/3, p. 213–217, 1994. DOI: 10.1016/0926-9851(94)90022-1.
- MILLER, K. G. Sea level change, last 250 million years. In: GORNITZ, V. (Ed.). **Encyclopedia of Paleoclimatology and ancient environments**. The Netherlands: Springer, 2009. XXVIII. 1049 p. ISBN: 978-1-4020-4551-6. DOI: 10.1007/978-1-4020-4411-3\_206.
- MILLER, K. G.; KOMINZ, M. A.; BROWNING, J. V.; WRIGHT, J. D.; MOUNTAIN, G. S.; KATZ, M. E.; SUGARMAN, P. J.; CRAMER, B. S.; CHRISTIE-BLICK, N.; PEKAR, S. F. The Phanerozoic record of the Global Sea-

- Level change. **Science**, v. 313, p. 1293–1298, 2005. DOI: 10.1126/science.1116412.
- MIZUSAKI, A. M. P.; THOMAZ-FILHO, A.; MILANI, E. J.; CÉSERO, P. Mesozoic and Cenozoic igneous activity and its tectonic control in northeastern Brazil. **J. South Am. Earth Sci.**, v. 15, n. 2, p. 183–198, 2002. DOI: 10.1016/s0895-9811(02)00014-7.
- MOHRIAK, W. U.; BASSETTO, M.; VIEIRA, I. S. Crustal architecture and tectonic evolution of the Sergipe-Alagoas and Jacuibe basins, offshore Northeastern Brazil. **Tectonophysics**, v. 288, n. 1–4, p. 199–220, 1998.
- MOHRIAK, W. U.; ROSENDAHL, B. R. Transform zones in the South Atlantic rifted continental margins. In: STORTI, F.; HOLDSWORTH, R. E.; SALVINI, F. (Eds.). **Intraplate strike-slip deformation belts**. Geological Society, London, Special Publication, 210, p. 211–228, 2003. DOI: 10.1144/gsl.sp.2003.210.01.13.
- MOLINA, E. C. **Ajustamento e integração de dados gravimétricos e de altimetria por satélite na representação do campo de gravidade no Atlântico Sul**. 1996. 137 f. PhD Thesis – Instituto de Astronomia, Geofísica e Ciências Atmosféricas, Universidade de São Paulo.
- MOONEY, W. D. Crust and lithospheric structure - Global crustal structure. Chapter 11. In: DZIEWONSKI, A.; ROMANOWICZ, B.; SCHUBERT, G. **Treatise on geophysics: Seismology and structure of the Earth**, v. 1. The Netherlands: Elsevier Science, 2007. Chap. 11. 858 p. ISBN 9780444519283.
- MORGAN, W. J. Convection plumes in the lower mantle. **Nature**, v. 230, n. 5288, p. 42–43, 1971. DOI : 10.1038/230042a0.
- MORGAN, W. J. Hotspots tracks and the Early Rifting of the Atlantic. **Tectonophysics**, v. 94, n. 1–4, p. 123–139, 1983. DOI: 10.1016/0040-1951(83)90013-6.
- MORLEY, L. W.; LAROCHELLE, A. Paleomagnetism as a means of dating geological events. **Geochron. Can. (Royal Society of Canada) Spec. Publ.**, v. 8, p. 39–50, 1964.
- MOULIN, M. **Étude géologique et géophysique des marges continentales passives: exemple du Zaire et de l'Angola**. 2003. 360 p. PhD Thesis - Université de Bretagne Occidentale, Brest.
- MÜLLER, R.D.; QIN, X.; SANDWELL, DT; DUTKIEWICZ A.; WILLIAMS SE.; FLAMENT N.; MAUS, S.; SETON, M. The GPlates Portal: Cloud-Based Interactive 3D Visualization of Global Geophysical and Geological Data in a Web Browser. **PLoS ONE**, v. 11, n.3, p. e0150883, 2016. DOI: 10.1371/journal.pone.0150883.
- MÜLLER, R. D.; SDROLIAS, M.; GAINA, C.; ROEST, W. R. Age, spreading rates and spreading symmetry of the world's ocean crust. **Geochem. Geophys. Geosyst.**, v. 9, n. 4, 2008. DOI:10.1029/2007GC001743.

- NABIGHIAN, M. N. The analytic signal of two-dimensional magnetic bodies with polygonal cross-section: Its properties and use for automated anomaly interpretation. **Geophysics**, v. 37, n. 3, p. 507–517, 1972. DOI: 10.1190/1.1440276.
- NESS, G. E.; DAUPHIN, J. P.; COUCH, R.; MACARIO, A.; BOA HORA, M. P.; LATGÉ, M. A.; BRAGA, L. F. Project equant a gravity and magnetics study of the northern continental margin of Brazil. In: INTERNATIONAL CONGRESS OF THE BRAZILIAN GEOPHYSICAL SOCIETY - Symposium on Marine Geophysics in Atlantic Type Oceans, 1., 1989, Rio de Janeiro. **Resumos Expandidos**. Rio de Janeiro: 1989, p. 821–824.
- NÓBREGA, M. A.; SA, J. M.; BEZERRA, F. H. R.; HADLER NETO, J. C.; IUNES, P. J.; OLIVEIRA, S. G.; SAENZ, C. A. T.; LIMA FILHO, F. P. The use of apatite fission track thermochronology to constrain fault movements and sedimentary basin evolution in northeastern Brazil, **Radiat. Meas.**, v. 39, n. 6, p. 627–633, 2005. DOI: 10.1016/j.radmeas.2004.12.006.
- NÓBREGA, M. **Mapeamento de estruturas do embasamento e seus limites crustais no Atlântico Equatorial, adjacente à margem brasileira**. 2011. 81 p. Thesis (Master). – Instituto de Geociências, Universidade Federal Fluminense, Niterói.
- OKAY, A. I. Was the late Triassic orogeny in Turkey caused by the collision of an oceanic plateau? **Geological Society, London, Spec. Publ.**, v. 173, p. 25–41, 2000. DOI: 10.1144/gsl.sp.2000.173.01.02.
- OLIVEIRA, P. H. S.; FERREIRA, J. M.; BEZERRA, F. H. R.; ASSUMPÇÃO, M.; NASCIMENTO, A. F.; SOUSA, M. O. L.; MENEZES, E. A. S. Influence of the continental margin on the stress field and seismicity in the intraplate Acaraú Seismic Zone, NE Brazil. **Geophys. J. Int.**, v. 202, n. 3, p. 1453–1462, 2015. DOI: 10.1093/gji/ggv211.
- OLIVEIRA, R. G. **Arcabouço geofísico, isostasia e causas do magmatismo cenozoico da Província Borborema e de sua Margem continental (Nordeste do Brasil)**. 2008. 411 p. PhD Thesis – Centro de Ciências Exatas e da Terra, Universidade Federal do Rio Grande do Norte, Natal.
- OLIVEIRA, P. R. A. **Morfologia e Sedimentologia do Extremo Leste da Plataforma Continental ao Largo do Estado do Ceará – Área Fortim a Icapuí**. 2007. 85 p. Monography (Undergraduation) – Universidade Federal do Ceará, Fortaleza.
- OLIVEIRA, S. P.; FERREIRA, F. J.; SOUZA, J. EdgeDetectPFI: An algorithm for automatic edge detection in potential field anomaly images—application to dike-like magnetic structures. **Comput. Geosci.**, v. 103, p. 80–91, 2017. DOI: 10.1016/j.cageo.2017.02.006.



- OLSON, C. J.; BECKER, J. J.; SANDWELL, D. T. A new global bathymetry map at 15 arcsecond resolution for resolving seafloor fabric: SRTM15\_PLUS. In: AGU Fall Meeting Abstracts. 2014.
- PAVLIS, N. K.; HOLMES, S. A.; KENYON, S. C.; FACTOR, J. K. An Earth Gravitational Model to Degree 2160: EGM2008. In: EGU General Assembly. Vienna, Austria, 2008.
- PEDLEY, R. C.; BUSBY, J. P.; DABEK, Z. K. GRAVMAG user manual—interactive 2.5 D gravity and magnetic modelling. **British Geological Survey, Technical Report WK/93/26/R**, v. 73, 1993.
- PÉRON-PINVIDIC, G.; MANATSCHAL, G.; MASINI, E.; SUTRA, E.; FLAMENT, J. M.; HAUPERT, I.; UNTERNEHR, P. Unravelling the along-strike variability of the Angola–Gabon rifted margin: a mapping approach. **Geological Society, London, Spec. Publ.**, v. 438, n. 1, p. 49–76, 2017. DOI: 10.1144/sp438.1.
- PESSOA NETO, O. C.; SOARES, U. M.; SILVA, J. G. F.; ROESNER, E. H.; FLORENCIO, C. P.; SOUZA, C. A. V. Bacia Potiguar. **Bol. Geoci. Petrob.**, v. 15, n. 2, p. 357–369, 2007.
- PRATT, J. H. On the Attraction of the Himalaya Mountains, and of the Elevated Region beyond Them, upon the Plumb-Line in India. **Proc. R. Soc. Lond.**, v. 7, p. 175–182, 1854. DOI: 10.1098/rspl.1854.0046.
- RABINOWITZ, P. D.; LABRECQUE, J. The Mesozoic South Atlantic Ocean and evolution of its continental margins. **J. Geophys. Res.: Solid Earth**, v. 84, n. B11, p. 5973–6002, 1979.
- RIVALENTI, G.; MAZZUCHELLI, M.; GIRARDI, V. A. V.; VANNUCCI, R.; BARBIERI, M. A.; ZANCETTI, A.; GOLDSTEIN, S. L. Composition and processes of the mantle lithosphere in northeastern Brazil and Fernando de Noronha: Evidence from mantle xenoliths. **Contrib. Mineral. Petrol.**, v. 138, n. 4, p. 308–325, 2000. DOI: 10.1007/s004100050565.
- ROEST, W. R.; VERHOEF, J.; PILKINGTON, M. Magnetic interpretation using the 3-D analytic signal. **Geophysics**, v. 57, n. 1, p. 116–125, 1992. DOI: 10.1190/1.1443174.
- RUDNICK, R. L. Making continental crust. **Nature**, v. 378, n. 6557, p. 571–578, 1995. DOI: 10.1038/378571a0.
- SANDWELL, D. T.; MÜLLER, R. D.; SMITH, W. H. F.; GARCIA, E.; FRANCIS, R. New global marine gravity model from CryoSat-2 and Jason-1 reveals buried tectonic structure. **Science**, v. 346, n. 6205, p. 65–67, 2014. DOI: 10.1126/science.1258213.
- SANDWELL D. T.; SMITH W. H. F. Marine Gravity from Geosat and ERS-1 Satellite Altimetry. **J. Geophys. Res.**, v. 102, n. B5, p.10039–10054, 1997. DOI: 10.1029/96jb03223.

- SIBUET J-C.; MASCLE, J. Plate kinematic implications of Atlantic Equatorial Fracture Zone Trends. **J. Geophys. Res.**, v. 83, n. B7, p. 3401–3421, 1978. DOI: 10.1029/jb083ib07p03401.
- SICHEL, S. E.; HEKINIAN, R.; JUTEAU, T.; GARCIA, E.; SICHLER, B.; UBINTSEV, G. Mergulhos em Submersível no Atlântico Equatorial. **Ver. Bras. Geociênc.**, v. 1, n. 1, p. 1–33, 2001.
- SILVA, J. B. C. **Métodos potenciais. Gravimetria.** Belém: CPRM. v. 151, 1986.
- SILVEIRA, J. D. Morfologia do litoral. In: AZEVEDO, A. (Ed.). **Brasil: a Terra e o homem.** São Paulo: Companhia Editora Nacional, 1964. v.1, p. 253–305.
- SLEEP, N. Hotspots and mantle plumes: Some phenomenology. **J. Geophys. Res.**, v. 95, n. B5, p. 6715–6736, 1990. DOI: 10.1029/jb095ib05p06715.
- SOARES JR, A. V.; COSTA, J. B. S.; HASUI, Y. Evolução da Margem Atlântica Equatorial do Brasil: Três fases distensivas. **Geociências UNESP**, v. 27, n. 4, p. 427–437, 2008.
- SOARES JR, A. V.; HASUI, Y.; COSTA, J. B. S.; MACHADO, F. B. Evolução do rifteamento e paleogeografia da Margem Atlântica Equatorial do Brasil: Triássico ao Holoceno. **Geociências UNESP**, v. 30, n. 4, p. 669–692, 2011.
- SOUTO FILHO, J. D.; CORREA, A. C. F.; SANTOS NETO, E. V.; TRINDADE, L. A. F. Alagamar-Açu petroleum system, onshore Potiguar Basin, Brazil: A numerical approach for secondary migration. In: MELLO, M. R.; KATZ, B. J. (Ed.). **Petroleum systems of South Atlantic margins.** Tulsa: American Association of Petroleum Geologists, 2000. p. 151–158. (AAPG Memoir, v. 73).
- SOUZA, J.; FERREIRA, F. J. On the use of derivatives for interpreting magnetic anomalies due to dyke-like bodies: qualitative and quantitative analysis. In: INTERNATIONAL GEOPHYSICAL CONFERENCE AND OIL & GAS EXHIBITION, Istanbul 2012. **Abstract ...** Tulsa: SEG, 2012. p. 1–4.
- SOUZA, J. D.; FERREIRA, F. J. On the use of derivatives for interpreting magnetic anomalies due to dyke-like bodies II: application to synthetic and field data. In: SEG Technical Program Expanded Abstracts 2013, p. 1121–1125. Society of Exploration Geophysicists, 2013.
- SOUZA, J.; FERREIRA, F. J. The application of the Signum transform to the interpretation of magnetic anomalies due to prismatic bodies. In: International Geophysical Conference and Exhibition, 24., Perth. **Abstracts ...** [Sydney]: Australian Society of Exploration Geophysicists, 2015: p. 1–5.
- SOUZA, C. R.; SUGUIO, K.; OLIVEIRA, A. M.; OLIVEIRA, P. E. **Quaternário do Brasil.** Ribeirão Preto, Brasil: Holos Editora, 2005.
- SOUZA, S. M. Atualização da litoestratigrafia da Bacia Potiguar. In: Congresso Brasileiro de Geologia, 32., 1982, Salvador. **Anais...** Salvador: SBG, 1982. v. 5, p. 2392–2406.

- STEIN, C. A.; CLOETINGH, S.; WORTEL, R. Seasat-derived gravity constraints on stress and deformation in the Northeastern Indian Ocean. **Geophys. Res. Lett.**, v. 16, n. 8, p. 823–826, 1989. DOI: 10.1029/gl016i008p00823.
- STEINBERGER, B. Plumes in a convecting mantle: Models and observations for individual hotspots. **J. Geophys. Res.**, v. 105, p. 11127–11152, 2000. DOI: 10.1029/1999jb900398.
- SYMONDS, P. A.; PLANKE, S.; FREY, O.; SKOGSEID, J. Volcanic evolution of the Western Australian Continental Margin and Its Implications for Basin Development. In: PURCELL, P.G.; PURCELL, R.R. **The sedimentary Basins of Western Australia**. Perth: Petroleum Exploration Society of Australia, 1998. p. 33–54.
- SZATMARI, P.; FRANÇOLIN, J. B. L.; ZANOTTO, O.; WOLFF, S. Evolução tectônica da margem equatorial brasileira. **Rev. Bras. Geocienc.**, v. 17, p. 180–188, 1987.
- TABOSA, W. F. **Morfologia, hidrodinâmica e sedimentologia da plataforma continental Brasileira adjacente a São Bento do Norte e Caiçara do Norte – RN/NE – Brasil**. 2006. 112 p. PhD Thesis – Centro de Ciências Exatas e da Terra, Universidade Federal do Rio Grande do Norte, Natal.
- TALWANI, M.; WORZEL, J. L.; LANDISMAN, M. Rapid gravity computations for two-dimensional bodies with application to the Mendocino Submarine Fracture Zone. **J. Geophys. Res.**, v. 64, n. 1, p. 49–59, 1959. DOI: 10.1029/jz064i001p00049.
- TAYLOR, B. The single largest oceanic plateau: Ontong Java–Manihiki–Hikurangi. **Earth Planet. Sci. Lett.**, v. 241, p. 372–380, 2006. DOI: 10.1016/j.epsl.2005.11.049.
- THARIMENA, S.; RYCHERT, C.; HARMON, N. A unified continental thickness from seismology and diamonds suggests a melt-defined plate. **Science**, v. 357, n. 6351, 580–583, 2017. DOI: 10.1126/science.aan0741.
- THÉBAULT, E.; FINLAY, C. C.; BEGGAN, C. D.; ALKEN, P.; AUBERT, J.; BARROIS, O.; BERTRAND, F.; BONDAR, T.; BONESS, A.; BROCCO, L.; CANET, E.; CHAMBODUT, A.; CHULLIAT, A.; COÏSSON, P.; CIVET, F.; DU, A.; FOURNIER, A.; FRATTER, I.; GILLET, N.; HAMILTON, B.; HAMOUDI, M.; HULOT, G.; JAGER, T.; KORTE, M.; KUANG, W.; LALANNE, X.; LANGLAIS, B.; LÉGER, J.; LESUR, V.; LOWES, F. J.; MACMILLAN, S.; MANDEA, M.; MANOJ, C.; MAUS, S.; OLSEN, N.; PETROV, V.; RIDLEY, V.; ROTHER, M.; SABAKA, T. J.; SATURINO, D.; SCHACHTSCHNEIDER, R.; SIROL, O.; TANGBORN, A.; THOMSON, A.; TOFFNER-CLAUSEN, L.; VIGNERON, P.; WARDINSKI, I.; ZVEREVA, T. International Geomagnetic Reference Field: the 12th generation. **Earth, Planets Space**, v. 67, n. 1, 79, 2015. DOI: 10.1186/s40623-015-0228-9.

USSAMI, N. **Apostila do curso de gravimetria e geomagnetismo no IAG – USP**, 2008.

VENING-MEINESZ, F. A. Gravity over the Hawaiian archipelago and over the Madeira area. **Proceedings of the Netherlands Acad. Wetensch.**, v. 44, p. 1–12, 1941.

VINE, F. J.; MATTHEWS, D. H. Magnetic anomalies over oceanic ridges. **Nature**, v. 199, p. 947–949, 1963. DOI: 10.1038/199947a0.

VITAL, H.; ESTEVES, L. S.; ARAÚJO, T. C. M. PATCHINEELAM, S. M. Oceanografia geológica e geofísica da plataforma continental brasileira. In: SOUZA, C. R. G., SUGUIO, K., OLIVEIRA, A. M. S., OLIVEIRA, P. E. **Quaternário do Brasil**. São Paulo: USP, 2005. Chap. 8. p. 153–173.

VOGT, P. R. Bermuda and Appalachian-Labrador rises: Common non-hotspot processes? **Geology**, v. 19, n. 1, p. 41–44, 1991. DOI: 10.1130/0091-7613(1991)019<0041:baalrc>2.3.co;2.

WATTS A. B. **Isostasy and flexure of the lithosphere**. Cambridge: Cambridge University Press, 2001. 457 p.

WATTS, A. B.; MOORE, J. D. P. Flexural isostasy: constraints from gravity and topography power spectra. **J. Geophys. Res.- Solid Earth**, v. 122, p. 8417–8430, 2017. DOI: 10.1002/2017JB014571.

WESSEL, P.; SMITH, W. H. F. New, Improved Version of the Generic Mapping Tools Released. **Eos Transactions AGU**, v. 79, n. 47, p. 579, 1998. DOI: 10.1029/98EO00426.

WHALEN, L.; GAZEL, E.; VIDITO, C.; PUFFER, J.; BIZIMIS, M.; HENIKA, W.; CADDICK, M. J. Supercontinental inheritance and its influence on supercontinental breakup: The Central Atlantic Magmatic Province and the break up of Pangea. **Geochem. Geophys. Geosyst.**, v. 16, n. 10, p. 3532–3554, 2015. DOI:10.1002/2015GC005885.

WILSON, J. T. A possible origin of the Hawaiian Islands. **Can. J. Phys.**, v. 41, p. 863–870, 1963. DOI: 10.1139/p63-094.

ZALAN, P.V. **Tectonics and sedimentation of the PiauíCamocim sub-basin, Ceará Basin, offshore northeastern Brazil**. 1984. 133 p. PhD Thesis – Colorado School of Mines, Colorado.

ZEMBRUSCKI, S. G. Geomorfologia da margem continental sul brasileira e das bacias oceânicas adjacentes. In: Série Projeto Reconhecimento Global da Margem Continental Brasileira. Rio de Janeiro: PETROBRAS/CENPES/DINTEP, 1979. v. 7. p. 129–177. (Projeto REMAC, v.7).